UNIVERSITÀ DEGLI STUDI DI MILANO

Scuola di Dottorato in Fisica, Astrofisica e Fisica Applicata
Dipartimento di Fisica

Corso di Dottorato in Fisica, Astrofisica e Fisica Applicata
Ciclo XXX

Simulation of antihydrogen production in AEGIS

Settore Scientifico Disciplinare FIS/03

Supervisore: Professor Fabrizio CASTELLI

Co-Supervisore: Professor Marco GIAMMARCHI

Coordinatore: Professor Francesco RAGUSA

Tesi di Dottorato di:
Michele SACERDOTI

Anno Accademico 2016/2017

Commission of the final examination:

Chairman:
Alberto Rotondi, Dipartimento di Fisica, Università di Pavia

External Member:
Franco Prati, Dipartimento di Scienza e Alta Tecnologia, Università degli Studi dell'Insubria

Internal Member (Ph D. Supervisor):
Fabrizio Castelli, Dipartimento di Fisica, Università degli Studi di Milano

Final examination:

Date 25/1/2018

Università degli Studi di Milano, Dipartimento di Fisica, Via Celoria 16, Milano, Italy

A mio Padre

Fatti non foste a viver come bruti,
ma per seguir virtute e conoscenza.
(Dante Alighieri, la Divina Commedia, canto XXVI)

Contents

Appendices   112

List of Figures

List of Tables

Introduction

Motivation

The gravitational acceleration of antimatter produced by a body made of ordinary matter has never been measured. As Einstein General Relativity was conceived before the discovery of antimatter in cosmic rays, the validity of the Weak Equivalence Principle is questioned for antimatter in a matter field.

Not only for this reason, antimatter is a hot topic in contemporary physics, owing to its important role in our understanding of fundamental interactions. For example, precision spectroscopy measurements on antimatter are considered an important test of the validity of the CPT theorem. At CERN six rival experiments are racing to understand the nature and the properties of antimatter [81].

Among these, the experiment AEGIS (Antimatter Experiment: Gravity, Interferometry, Spectroscopy) [82] [30] has the primary scientific goal of performing the first measurement of gravity acceleration of antihydrogen with a precision of percent level. AEGIS is currently underway at the Antiproton Decelerator at CERN, Geneva.

The experiment is very challenging because this measurement requires very stringent conditions to create a beam of antihydrogen atoms which will be directed to a suitable measurement apparatus to see its gravitational behavior.

The present Thesis concerns the work performed with numerical simulations to study the behavior of the main part of the experiment, the production of antihydrogen, to check whether the measurement is feasible and suggest possible modifications to increase the number of antihydrogen atoms which are produced.

Thesis overview

Main results

Driven by the motivations described above, the present Thesis is devoted to the simulation of the layout of the experiment as presented in the proposal of 2007 [30] and as built at CERN until now.

Alternative layouts have been also simulated to try to increase the number of the antihydrogen atoms.

The results have been presented to the Collaboration in meetings and reports and have been cross checked by other researchers in the collaboration who have also produced reports and published an article. The results partly coincide and partly differ from the work of the other researchers.

The results of the thesis are produced by a Monte Carlo calculation written in Fortran 90 and C++, using routines of the ODEINT library for numerically solving ordinary differential equations. The calculation is based on a semiclassical treatment of the reaction that produces antihydrogen. The other researchers have followed similar simulation methods.

An active discussion on the significance of the differences are actually under way, also with the help of theoretical considerations.

The importance of the work of the Thesis to reach the goal of AEGIS is clear. Without a result of the measurement of gravitation of antihydrogen to some degree of precision before the end of 2018 other experiments could reach the goal before AEGIS.

The result of the thesis is that the only way to produce a sufficient number of antihydrogen atoms to measure their gravitation acceleration is to use a vertical silicon transmission target. The reflection target of the initial AEGIS proposal doesn't seem to produce enough atoms for the measurement.

A carbon-supported transmission target has been studied by the AEGIS collaboration and the results published in [76]. A self-standing transmission target is being studied [78]. It should allow a lower positrons implantation energy, a higher percentage of produced o-PS and less emitted positrons and electrons.

Organizational note

The present Thesis consists of fourteen Chapters and an Appendix. Here is a brief description.

Chapter 1: Physics motivation and previous experiments: I describe the theoretical framework of the experiments that have been proposed as well as arguments against antigravity.

Chapter 2: The AEGIS experiment: I describe the AEGIS experiment from the antiprotons and positrons production to the gravity measurement with the Moiré deflectometer.

Chapter 3: The Thesis work: I give a list of the activities I have done between 2009 and 2017.

Chapter 4: Simulation of the production of antihydrogen with the basic layout: I describe the simulation of the experiment with the layout that has been considered initially in first Aegis proposal [30].

Chapter 5: Simulation of the production of antihydrogen with the introduction of reflectors of various shapes for guiding the cloud of Ps atoms towards the trapped antiprotons: I simulate the modified layout of the experiment with reflectors to increase the production of antihydrogen.

Chapter 6: Simulation of the production of antihydrogen with the introduction of an ellipsoidal reflector before laser excitation for guiding the cloud of Ps atoms towards the trapped antiprotons: Another possible enhancement is described and simulated to avoid the problems with the previous reflectors.

Chapter 7: Simulation of the creation, propagation and detection of Ps in the positronium chamber of AEGIS: I describe a modification of the Montecarlo program to simulate a side experiment in the positronium chamber of AEGIS.

Chapter 8: Simulation of the production of antihydrogen with the introduction of a focusing electric field on the cloud of Rydberg Ps, thanks to their high polarizability and the Stark acceleration: An electric field is simulated to focus Ps on the antiproton cloud hence increasing the number of produced antihydrogen atoms.

Chapter 9: Simulation of the production of antihydrogen with a Ps transmission target in different positions: An alternative target is simulated which generates positronium on the opposite side of the implantation of positrons.

Chapter 10: Verification of the calculations of the Genova group: Genova group has made a simulation of the experiment and I have verified it with my program.

Chapter 11: Simulation of the production of antihydrogen with a Ps transmission target in vertical position on axis: A proposal of a vertical transmission target has been simulated, which seems to be the best layout for the experiment.

Chapter 12: Simulation of the production of antihydrogen taking into account the 1T magnetic field: To complete the simulation I have taken into account the magnetic field in the antihydrogen production area, ignored in the previous simulations.

Chapter 13: Calculation of the cross section of the charge exchange reaction without and with the 1T magnetic field: I have calculated the cross section of the reaction to compare it with the one I had used before, which was derived from the initial AEGIS proposal. I have also obtained the distributions of the principal and azimuthal quantum number, the velocity and canonical angular momentum of antihydrogen and the impact parameter of the Ps.

Chapter 14: Simulation of the production of antihydrogen taking into account the new cross section calculation: I have used the new cross section to evaluate the number of antihydrogen atoms produced in the various layouts and compare them with the results of chapter 12.

Chapter 15: Conclusions: I have drawn some conclusions on the work that I have done and on my current and future activities in the AEGIS experiment.

Appendix: Description of the Monte Carlo program and the CTMC program

Physics motivation and previous experiments

1.1 Physics motivation

The first goal of AEGIS (Antimatter Experiment: Gravity, Interferometry, Spectroscopy) experiment [30] is to measure the gravitation acceleration of antimatter in a matter field.

CPT invariance dictates that antimatter gravitational behavior in an antimatter field should be the same as the matter gravitational behavior in a matter field but the case of antimatter in a matter field is not constrained.

The Weak Equivalence Principle (WEP) states that "if any uncharged test body is placed at an initial event in spacetime and given an initial velocity there, then its subsequent trajectory will be independent of its internal structure and composition" [3]. So an antimatter body should behave as a matter body in the Earth gravitation. However WEP is a foundation of General Relativity that does not imply the existence of antimatter.

The suggestion that some kind of an antigravity force exists was considered by Maxwell for the same law of distance between gravitation and electric forces but was ruled out because in gravitation bodies have only one sign and the force between them is only attractive [4]. The modern idea of "antigravity" is a consequence of General Relativity combined with Quantum Mechanics [2].

The Weak Equivalence Principle states that the inertial mass is equal to the gravitational mass,

$$m_i = m_G \tag{1.1}$$

The inertial mass is the kinematic factor in Newton's law of force

$$F = m_i\, a \tag{1.2}$$

The gravitational mass has the role of a "charge" in Newton's law of gravitation

$$F = -G\, m_G\, m'_G\, /r^2 \tag{1.3}$$

Now, even though the CPT Theorem tells us that the inertial mass of a particle is equal to the inertial part of the antiparticle

$$m_i = \bar{m}_i \tag{1.4}$$

this does not imply that

$$m_G = m_i = \bar{m}_i \overset{?}{=} \bar{m}_G \tag{1.5}$$

So $m_G \neq \bar{m}_G$ does not mean that CPT is violated.

If an apple falls towards the earth in a certain way, CPT only dictates that an antiapple falls towards an antiearth in the same way but says nothing about how an antiapple falls towards an earth [5].

Models have been developed to quantize and unify gravity with the other forces of nature. A feature of these models is that the normal spin-two graviton can have two partners: a spin-one (gravivector) and a spin-zero (graviscalar). These partners are massive and so the interaction has a finite range and has coupling strengths similar to gravity which can depend from the composition.

The most important work on this subject was done by Sherk [6, 7, 8, 9] who realized the theoretical and experimental implications of the two partners of the graviton but many other authors have worked in this field.

In these theories the simplest potential between two point masses m_1 and m_2 is of the form [10, 11, 12]

$$V = -\left(\frac{G\,m_1\,m_2}{r\,\gamma_1\,\gamma_2}\right)\left([2(u_1.u_2)^2 - 1] \mp \sum q_{v1}\,q_{v2}\,(u_1.u_2)\,e^{-r/v} + \sum q_{s1}\,q_{s2}\,e^{-r/s}\right),$$
(1.6)

where u_i is the normalized (with respect to c) four-velocity

$$u_i = \gamma_i(1, \beta_i).$$
(1.7)

In equation 1.6 the first term arises from normal graviton exchange. v and s are the ranges of the gravivector and the graviscalar. The summation signs indicate that there could be many partners of each spin, each with its own charge and range. The sign in front of the vector exchange term reflects the fact that the force is repulsive between matter and matter (like charges) but attractive between matter and antimatter (opposite charges). The scalar force is always attractive. q_v and q_s are the vector and scalar charges per unit mass and are dependent on the composition, such as would be the case if it were different baryon number or lepton number per unit atomic mass.

The force associated with the scalar partner is always attractive. This depends from the fact that there is an even-spin exchange as in normal tensor gravity with spin 2. The scalar could couple with the trace of the energy-momentum tensor or the square of the electromagnetic field tensor.

Passing to the static limit and assuming there is only one vector and one scalar partner of the graviton, the static potential is

$$V = -G\,m_1\,m_2\,(1 \mp a\,e^{-r/v} + b\,e^{-r/s})/r,$$
(1.8)

where a and b represent the products of the vector and scalar charges of the two particles. The signs have been arranged so that both $a, b \geq 0$.

Equation 1.8 derives from a general property of field theory. If there is a charge force mediated by an integer-spin boson of mass M, the static potential and the force will be of the Yukawa form.

$$V = -K\,\alpha\,e^{-r/\lambda}/r,$$
(1.9)

$$F = -K\,\alpha(1 + r/\lambda)\,e^{-r/\lambda}/r^2,$$
(1.10)

$$\lambda = \hbar/Mc$$
(1.11)

where

$$K = G\,m_1\,m_2 \tag{1.12}$$

For each force, *a* and *b* represent the coupling strength relative to *G*, while *v* and *s* the relative range.

Experiments on interactions between matter and matter bodies will be sensitive to the difference of the two terms in *a* and *b*, i.e. to $|\,a - b\,|$. Limits on this difference will not necessarily be applicable to antimatter-matter experiments, for which the sign of *a* changes, and which are thus sensitive to $|\,a + b\,|$.

Limits on the range of the scalar and vector forces have been obtained by Eötvös-style experiments [13] . Scalar and vector couplings also appear in the context of relativistic theories of gravity based on modified Newtonian gravity [14, 15] which attempt to provide an alternative to dark matter, while new scalar fields coupling to matter with gravitational strength appear in the context of chameleon field theories [16].

Models have investigated the possibility of different baryonic and fermionic contributions to the gravitational field [17, 18], which would imply a differential interaction between matter and antimatter.

Assuming an approximate simmetry between the two partners, $a \sim b$ and $v \sim s$. Equation 1.6 shows that the various interactions have different velocity dependences, so that a rapidly rotating object can reach the point where the total energy becomes positive. Such a system would be unstable if the constants a and b were too large. Reference [19], based on the stability of the 1.588 ms pulsar, has obtained the limits:

$$a \sim b \leq 70, \; v, s \gg 4\,km \qquad a \sim b \ll 100, \; v, s = 4\,km \tag{1.13}$$

In quantum gravity theories, under the static potential regime of equation 1.8, antimatter always falls at the same rate or faster than matter towards the earth. It never goes up or slower than matter. It is interesting to verify experimentally these previsions.

1.2 Previous proposed and current experiments

1.2.1 The Fairbanks experiments

In 1957 Fairbank and his student Witteborn began a program to compare the gravitational acceleration of electrons and positrons[20]. The experiment consisted in analyzing the time of flight distribution of electrons and positrons that were freely falling inside a vertical metal drift tube. The tube was constructed so that stray electric and magnetic field gradient were reduced to less 10^{-11} V/m. This was needed because the force of gravity is very small, for electrons

$$m_e g/e = 5.6 \times 10^{-11} V/m \tag{1.14}$$

As the experiment was in preparation Schiff and Barnhill observed that the electrons inside the metal of the drift tube would sag under gravity, until the gravitational force was balanced by the electrostatic force of compression. The force would create an electric field inside the drift tube that would exactly cancel the acceleration due to gravity on the electron. If M, Q and m_e, e are the mass and charge of the particle being measured and of the electron, the effective gravitational acceleration that should be measured is:

$$g_{eff} = g[1 - (m_e Q/Me)] \tag{1.15}$$

For the electron one should measure zero and Fairbank and Witteborn found [20] that $g_{eff} < 0.09g$.

Later two other questions of principle concerning the experiment were raised.

Dessler, Michel, Rorschach and Trammel [21] observed that also the ions should sag in the drift tube and this would produce an effect 2000 times greater and of opposite sign. This effect should depend from the temperature of the tube.

The second question of principle concerned the "patch effect", fields that are produced from irregularities in the surface and crystalline structure of a conductor. Fairbanks and Witteborn measured a low field and suggested that the stray fields from this second source were shielded at low temperatures.

The experiment was abandoned because they could not produce the necessary supply of low-energy positrons. In 1988 Fairbank reconsidered a measurement of the gravitational acceleration of the positrons [22] but he died in 1989.

1.2.2   The antiproton gravity experiment

In 1982 Goldman and Nieto proposed to measure the gravity of antiproton [23]. The proposal evolved in 1986 in a collaboration to do the experiment at LEAR at CERN [24] which was never completed (see figure 1.1).

The following description of the experiment is derived from [2].

A 2 MeV beam from LEAR containing approximately 10^9 antiprotons in a 250 ns bunch would be directed to a degrading foil, which would be at the entrance of an electromagnetic Penning trap, 50 cm long. The degraded beam would be allowed in the trap while it has a voltage of 50 kV at the endcap opposite the entrance. About 10^8 antiprotons would be captured in the trap by pulsing the voltage on the entrance cap from ground up to 50 kV before the antiprotons return back to the entrance. Electron cooling would then bring the antiprotons to room temperature.

After transferring the antiprotons to a smaller Penning trap, the antiprotons would be cooled to a few K by resistive cooling. After transfer of the antiprotons to a third "launching" trap the voltage holding the antiprotons in the trap would be lowered, allowing approximately 100 particles at a time to be released into a vertical drift tube, to observe their free upstream motion. This tube, of approximately 50-100 cm in length, would shield antiprotons against stray electric fields and would have a surface designed to reduce the patch effect. The tube would be surrounded by a superconducting magnet to produce a guide field.

The field would be uniform to better than a part in 10^5, so that the force on the antiproton due to the interaction of a magnetic field gradient on the effective magnetic moment of the antiproton would be small compared to the force of gravity.

The gravity measurement would be done as follows. The antiprotons would be released by dropping the voltage in the trap endcaps at time t=0. The antiprotons would go into the drift tube with various energies. Those with large kinetic energy would quickly race through the drift tube of effective length L and be detected at the top of the tube with a microchannel plate. As time goes on, the antiprotons with smaller and smaller initial kinetic energy would arrive. Finally, the last antiproton with just enough energy to make it up the drift tube against the force of gravity would arrive al time $t = \tau$.

The value of the gravitational acceleration in the antiproton is then given by

$$\tau = [2L/g(\bar{p})]^{1/2} = 0.452s(L/m)^{1/2}[g(p)/g(\bar{p})]^{1/2}. \tag{1.16}$$

where L is the effective length of the drift tube. Launched hundred at a time to reduce the mutual Coulomb forces among them, the antiprotons would eventually build up a time-of-flight spectrum, the end point of this spectrum would yield the value of $g(\bar{p})$.
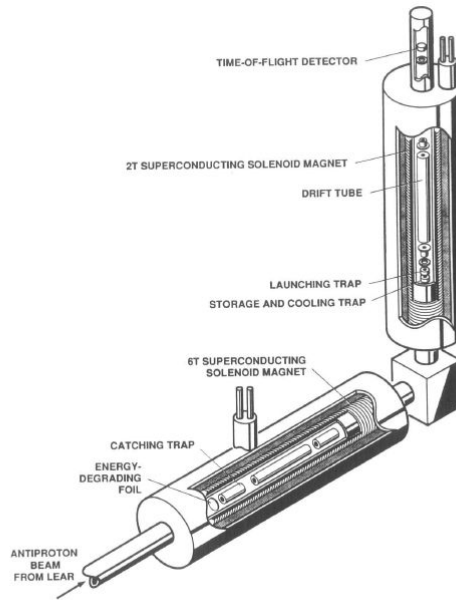
Fig. 1. Schematic diagram of the antiproton gravity experiment. Taken, with modification, from [Dye89].

Figure 1.1: Schematic diagram of the antiproton gravity experiment

The experiment would use negative H^- ions as a calibration, as they have the same inertial mass (up to a part in a thousand), the same charge and almost the same effective magnetic moment as the antiproton, and thus affording a precise measurement of the ratio $g(\bar{p})/g(H^-)$.

The experiment was started in Los Alamos National laboratories but the cancellation of LEAR in 1996 at CERN and its substitution with the Antiproton Decelerator led to the convergence of the PS200 collaboration in a wider international group with the goal of creating antihydrogen with the ATHENA experiment. Antihydrogen, being neutral, is not subject to stray fields.

1.2.3 The ALPHA experiment

The ALPHA experiment uses the antiprotons of the Antiproton Decelerator at CERN to produce antihydrogen [81]. They are mixed with positrons in a magnetic trap and some antihydrogen atoms are produced by three-body collision processes. The trap confines those anti-atoms whose magnetic moment $\mu_{\bar{H}}$ is aligned such that they are attracted to the minimum in the trap magnetic field **B**, and whose kinetic energy is below the trap well depth, $\mu_{\bar{H}}(|\mathbf{B}|_{Wall} - |\mathbf{B}|_{Center})$. In ALPHA (see figure 1.2) this magnetic minimum is created by an octupole magnet that produces transverse fields of magnitude 1.54 T at the trap wall at $R_{Wall} = 22.3$ mm and two mirror coils that produce axial fields of 1 T at their centres. The mirror coil centres are offset by ± 138mm from the trap centre. These fields are superimposed on a uniform axial field of 1 T produced by an external solenoid.

In the last phase of the experiment anti-atoms are released from the minimum-B trap by turning off the octupole and mirror fields. The escaping anti-atoms are then detected when they annihilate on the trap wall; a silicon-based annihilation vertex imaging detector records the times (binned to 0.1 ms) and locations (azimuthal FWHM of 8 mm) of
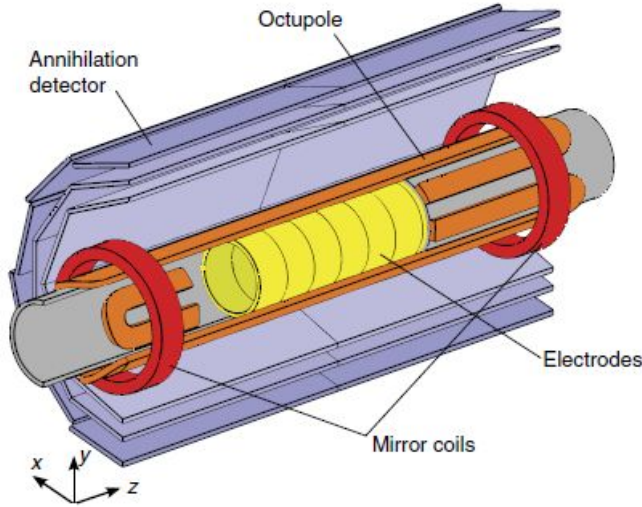
Figure 1.2: ALPHA Experimental schematics of the antihydrogen production and trapping region from Figure 1 [81]

these annihilations.

The ALPHA collaboration has developed a method that yields directly measured limits on the ratio of the gravitational to inertial mass of antimatter, accomplished essentially by searching for the free fall (or rise) of 434 ground-state antihydrogen atoms. The results set statistical bounds on the value of $F = M_g/M$, the ratio of the gravitational mass M_g to the inertial mass M of antihydrogen. M is assumed numerically equal to the mass of hydrogen.

In the absence of systematic errors, F has been found to be < 75 at a statistical significance level of 5%; worst-case systematic errors increase this limit to $F < 110$. A similar search places somewhat tighter bounds on a negative F, that is, on antigravity, with $F > -65$.

Limits are far from the F =1 regime where one could test for small deviations from the weak equivalence principle, but the methodology, coupled with planned and ongoing improvements to the ALPHA apparatus, should allow to improve the measurement substantially.

1.3   Arguments against antigravity

Three classic arguments have been raised against "antigravity" but they do not apply with similar force to modern ideas stimulated by quantum gravity [2].

P. Morrison [26] pointed out that, if one had "antigravity", a matter-antimatter pair on the earth's surface could be raised adiabatically to a height L with no loss of energy. Then the photonic energy obtained from the pair's annihilation would be blue-shifted in going back to the earth's surface. When the energy of the photon would be reconverted into a pair, the pair would have acquired kinetic energy and thus energy would not be conserved.

Schiff, shortly thereafter, asked whether the contribution of "antigravity" from positrons

in the vacuum polarisation diagrams of atoms would have been evident in the Eötvös experiment [27, 28]. His conclusion was that the effect would have been so huge that "antigravity" could be ruled out.

Good [29] observed that if there were "antigravity", then the K_L, which is a linear combination of the K_0 and the $\bar{K}_0$, would regenerate into the K_S. This is because the K_0 and the $\bar{K}_0$ would undergo different phase shifts from the "antigravity" gravitational potential.

Goldman and Nieto have demonstrated in [2] that the three arguments can not rule out a difference between the gravitational acceleration of antimatter and that of matter towards the earth due to gravitovector and gravitoscalar contributions.

The AEGIS experiment

The AEGIS experimental layout has been described in the June 8, 2007 proposal [30] and in [83] and was summarized in 2012 in an article by the Collaboration [31]. In subsequent years the layout has been modified and different articles have been published on specific parts.

In the following pages the apparatus will be described especially for the parts that have been simulated in this thesis.

2.1 Overall layout

The goal of the apparatus is the production of a beam of anti-hydrogen atoms launched horizontally to measure its gravitational acceleration through the observation of the trajectory. A gravity measurement with a percent level relative precision should be achieved by observing the vertical displacement of the shadow image produced by the passage of an $\bar{H}$ beam through a moiré deflectometer, a device similar to a particle counterpart of a grating wave interferometer.

This measurement requires pulsed production of $\bar{H}$ atoms in order to measure the time of flight of each atom. Furthermore, the ensemble of formed atoms needs to be cold in order to minimize the beam divergence once they are accelerated and thus the required measurement time to obtain a statistically significant result.

The essential steps are the following (see figure 2.1):

- Production of positrons (e+) from a Surko-type source and accumulator.

- Capture and accumulation of $\bar{p}$ from the Antiproton Decelerator (AD) in a cylindrical Penning trap.

- Cooling of the $\bar{p}$ to sub-K temperatures.

- Production of positronium (Ps) by bombardment of a cryogenic nanoporous material (called positronium converter) with an intense e+ pulse.

- Excitation of the Ps to a Rydberg state with principal quantum number $n \approx 20$.

- Formation of $\bar{H}$ by charge exchange between Rydberg Ps and cold $\bar{p}$.

- Pulsed formation of an $\bar{H}$ beam by Stark acceleration with inhomogeneous electric fields.

- Determination of g in a two-grating moiré deflectometer coupled with a position-sensitive detector.
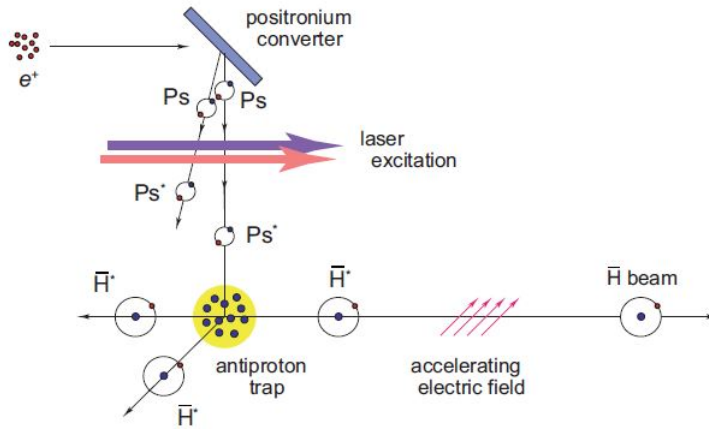
Figure 2.1: AEGIS method for the production of a pulsed beam of cold $\bar{H}$ atoms from [31]

The experimental apparatus which realizes the different steps consists of:

- a positron source (50 mCi) and accumulator,

- a high-field magnet (5T) housing trapping electrodes,

- a separate highly homogeneous magnet (1T) which houses the antihydrogen production and beam formation structures.

- a moiré deflectometer consisting of two 150-mm gratings placed at 1 m and 1.5 m from the antihydrogen formation point, along with a high-resolution antihydrogen detector at 2 m.

- a laser system that implements a Ps excitation to a Rydberg state passing through an intermediate state (n = 3).

2.2   Antiproton Decelerator AD and ELENA

AEGIS uses the antiprotons produced by the Antiproton Decelerator (AD) of CERN. The antiprotons are used by other experiments as well: ALPHA, ASACUSA, ATRAP in the same building.

Antiprotons are produced by a proton beam that comes from the Proton Syncrotron (PS) of CERN, which is fired into a block of Ir at 26 GeV/c. The antiprotons, which emerge from the block at different energies and angles together with other secondary particles, are focused before they reach the AD and only the ones with the right energy are injected and stored in it.

The AD is an oval-shaped ring with a circumference of 188 m composed of bending and focussing magnets that keep the antiprotons on the same track, while strong electric fields slow them down (see figure 2.2).The spread in energy of the antiprotons and their deviation from their track is reduced by a technique known as "cooling". Antiprotons are subjected to several cycles of cooling and deceleration until they are slowed down to
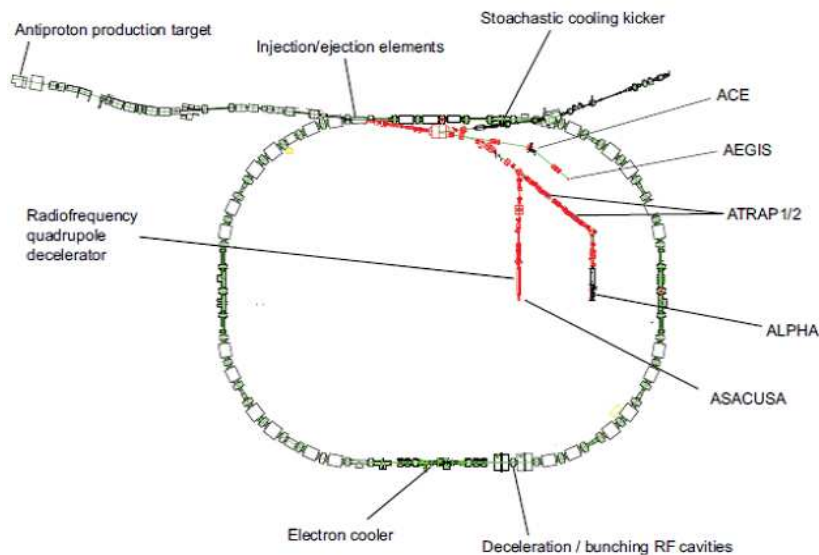
Figure 2.2: Schematic diagram of Antiproton Decelerator (AD) and the position of experimental installations in 2012

around a tenth of the speed of light. They are then ready to be ejected into the antimatter experiments [32].

At the end of a 100-s cycle a 200-ns-long beam containing approximately 3×10^7 $\bar{p}$ of energy 5.3 MeV are ejected from AD.

In 2018 a new more efficient decelerator, Extra Low ENergy Antiproton ring (ELENA), will enhance the AD decelerating antiprotons to 100 keV, and the various experiments will use the new source of antiprotons at various dates.

This synchrotron, with a circumference of 30 metres inside the AD, will slow the antiprotons even more, reducing their energy by a factor of 50, from 5.3 MeV to just 0.1 MeV. An electron cooling system will increase the beam density. The number of antiprotons that can be trapped will be increased by a factor of 10 to 100, improving the efficiency of the experiments.

2.3   Antiproton capture and accumulation

Antiprotons are extracted from AD at 5.3 MeV/c and are further degraded passing through an aluminium foil with tunable thickness to an energy of 9 keV. Then they are conveyed in the first trap system.

A magnetic field of 5 T gives the radial confinement while a series of electrodes with 15 mm radius generate an electric field for axial confinement. The goal is to accumulate 0.1 % of the incoming $\sim 3 \times 10^4$ antiprotons with a broad energy distribution. It is achieved with a depth of the trapping potential up to 20 keV.

The trapped antiprotons are cooled by interaction with electrons emitted by an electron gun, around 10^9 particles. Although the electrons are heated by this process, they efficiently cool themselves by emission of cyclotron radiation in the 5 tesla magnetic field
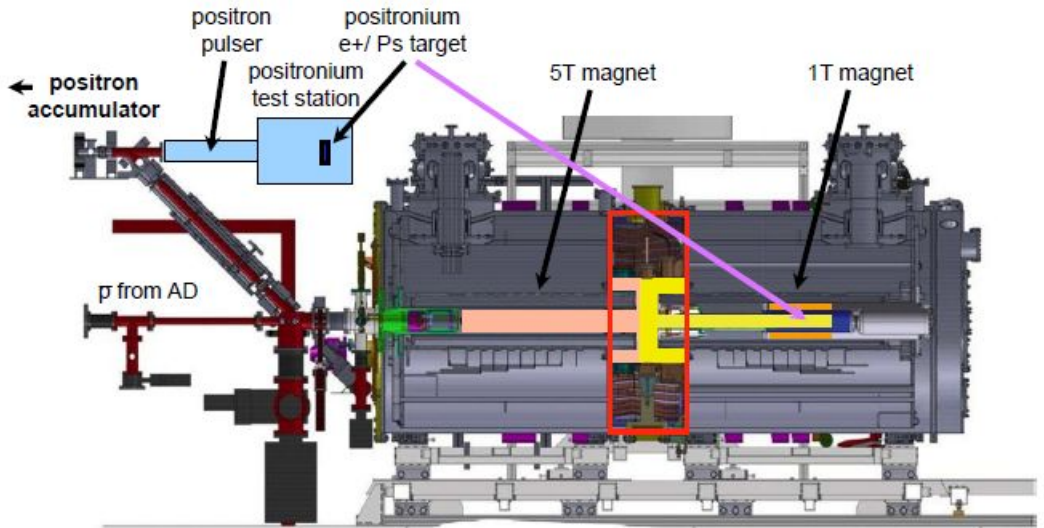
Figure 2.3: General drawing of the AEGIS experiment with the two magnets

with a time constant of about 0.4 sec. Ideally, the two species of particles will reach a final equilibrium temperature equal to that of the environment of about 1K or less.

The cooling process can be described by a simple model with two differential equations [84] [30]; their solution shows that 10^4 antiprotons having energies in the keV range can be cooled down to less than a few eV within a few tenths of a second if they overlap completely with an electron cloud of density around $10^7 - 10^8\ cm^{-3}$. The cooling process is not exponential and its rate increases very rapidly as the antiproton energy decreases. The rotating wall cooling is also used.

The duty cycle of the AD ($\sim 100s$) determines the overall accumulation rate of antiprotons, the stacking of several pulses should be necessary to reach 10^5 trapped antiprotons. This trapping rate should increase approximately by two orders of magnitude once the ELENA decelerator is operational.

The final cooling of the antiprotons will take advantage of a dilution refrigerator and of a resistive active-feedback cooling system. The final design specifications call for 10^5 $\bar{p}$ cooled down to $\sim 100mK$, which corresponds to a velocity of about 50 m/s . Cold $\bar{p}$ are important to maximize the flux of $\bar{H}$ and measure $\bar{g}$.

After catching and manipulation in the 5 T magnet, antiprotons are transferred ballistically to the 1 tesla magnet system which is composed of four electrodes regions with different characteristics (see figure 2.4). The first part features electrodes with r = 22 mm used as catching traps for particles coming from the 5 T system. This trap then splits into two smaller radius sections (5 mm each). The "upper" section is used for positrons, while the "lower" on-axis trap – equipped with low noise electronics - is used to store and cool antiprotons down to the lowest possible temperature.

Sympathetic cooling with (laser cooled) C_2 ions is being considered for the final stage
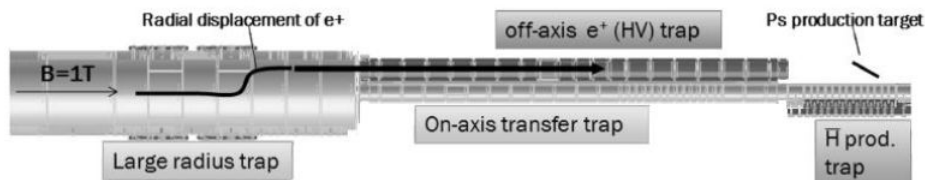
Figure 2.4: The trap system located inside the 1 tesla region. The on-axis trap manipulates antiprotons and stores them. Positrons are sent off-axis to reach the production target.

of the antiproton preparation in the 1T region [33, 34]. The design of the injection region of the apparatus (upstream of the 5 T magnet) incorporates the option for injecting negative ions from an external source, for which space has been reserved on the upstream side of the apparatus. Similarly, the design of the electrodes holding antiprotons, as well as of the central region between the 1 T and the 5 T magnets, incorporates the option for injecting the required laser light to optically cool any negative ions, if an appropriate species can be identified.

2.4 Positron and positronium production

Positrons are produced in AEGIS by means of a 50 mCi Na-22 source. A solid rare-gas (Neon) moderator is used together with a Surko-style [35] differentially pumped trap system. Moderators are usually grown at a temperature of 7 K with ultra-pure neon admitted at a pressure of 10^{-4} mbar for a few minutes. The trap system culminates in a positron accumulator (see the top left of Figure 2.3) having the capability of stacking about 10^8 positrons during 200 s. This accumulation time is matched to the antiproton accumulation time discussed above.

Positrons can be directed via an accelerator/buncher to a dedicated chamber for study of Ps spectroscopy or they can be sent to the main magnets of the experiment, as shown in Figure 2.3. When positrons are injected in the main trap system (see Figure 2.4), they can be manipulated, accumulated and sent off-axis via the excitation of the diocotron motion [36] to reach the converter of the experiment.

Ps will be obtained in AEGIS by sending a pulse of positrons on a suitable target acting as positronium converter with high efficiency. Ps formation in porous materials [37] by electron capture is particularly suitable. Ps exists and can be formed in two states: the short-living para-positronium (p-PS) with spin=0 (mean lifetime is 0.125 ns), and the long-living ortho-positronium (o-Ps) with spin=1 (mean lifetime is 142 ns). Ps is synthesized in the material bulk, or can be formed at the surface of the pore. Anyway, only the long-living o-Ps can diffuse into a pore and, if the pores are connected to the surface of the material, the Ps can escape from the target toward the surrounding vacuum by following the pore channels and colliding with the pore walls, thermalizing in the process. The energy spectrum of the emitted Ps depends on the energy of the Ps entering the pore, on the number of collisions with a pore surface and on the mean energy loss for each collision. The depth in the bulk where Ps is formed depends on the e+ implantation energy (around 10 keV)) and with an appropriate choice of material (such as Xerogel [41]) or design (such as in [42]) of the pore geometry and of the implantation energy, the
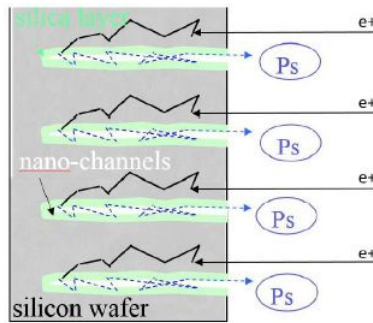
Figure 2.5: Ps production in nano-channels in a Silica-based nano-porous target

energy spectrum of the emitted Ps should match the required values.

Because of the desirability of low temperature antihydrogen and of minimizing the distance between the target and the ultra-cold antiprotons, the target will be enclosed in the sub-K antihydrogen production region, and will thus itself lie at cryogenic temperatures.

A quantum mechanical treatment (Ps scattering on phonons in potential wells) is required to predict the thermalization of positronium in nanopores at low temperature. Brusa et al [38] and Crivelli et al [39] have shown that the minimum temperature that Ps atoms reach in a potential well (nanopore) is determined by the well (pore) dimensions: for pore dimensions smaller than a few nanometers single-phonon scattering does not allow to reach the ground state. Increasing the diameter of the nanochannels decreases the minimum accessible temperature: in nanostructures of 20 nm, it is around 7 K. On the other hand, an increase in the diameter of nanochannels is expected to extend the thermalization time of ortho-positronium (o-Ps) due to a reduction in the collisional frequency with the pore walls [38]. It is thus necessary to optimize the nanochannel dimensions to reach the optimal o-Ps temperature that maximizes the antihydrogen formation rate (see Figure 2.5)

Up to 40% of the injected positrons produce o-Ps; at the appropriate injection energies (several keV), about 20% of the Ps diffuse out of the target for a total of 3% of thermalized o-Ps at room temperature [40, 42]. These expected 10^7 thermalized o-Ps emitted from the target are currently assumed to be emitted isotropically. However, quantum effects within the narrow pores produce a lower bound on the minimal temperature in the transverse plane to the pore axis, while the component parallel to the axis is unbounded, resulting in anisotropic cooling.

The velocity component perpendicular to the pore axis is thus expected to dominate over the parallel component [38], which would lead to preferential directional emission.

2.5 Laser excitation of Ps

Antihydrogen production by charge exchange between positronium atoms and antiprotons requires efficient excitation of positronium atoms up to high-n levels (Rydberg levels), as explained later. A strategy based on a pulsed two-step incoherent optical excitation $1 \rightarrow 3 \rightarrow n$ [43] was envisaged. The required two laser have been constructed by Milan University and INFN and are optimized with positronium produced both inside
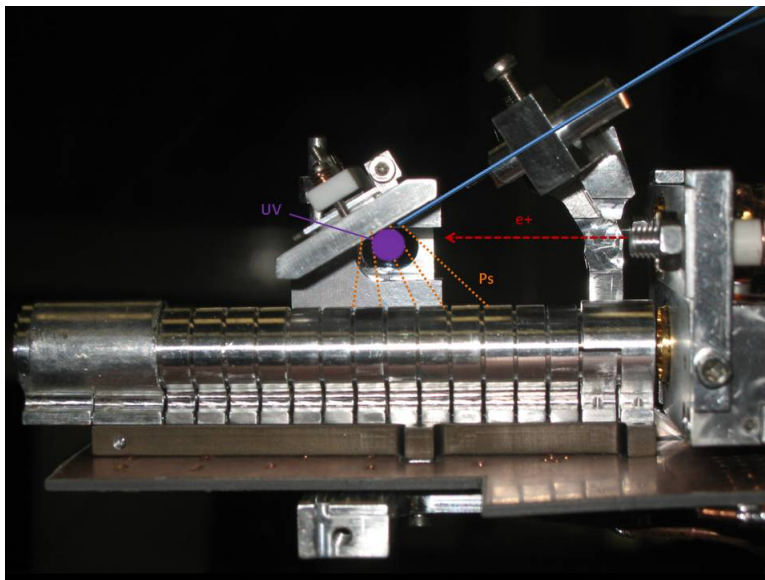
Figure 2.6: picture of the target at the top with the incoming positrons, the laser beam, the outgoing Ps and the antiproton trap in the 1T region at the bottom

the AEGIS magnet as well as on an external test platform (bread box).

The rationale for choosing this scheme, rather than the alternative $1 \rightarrow 2 \rightarrow n$ scheme is:

- the n = 3 state has a longer lifetime of 10.5 ns than the n = 2 state (with 3 ns),

- the laser energy per pulse required to saturate the transitions is lower, an important consideration when losses into the cryogenic environment of the experiment must be minimized and

- calculations of the excitation efficiency [44] indicate a higher value when passing through the n = 3 level.

The Ps atoms are emitted from a cryogenic surface, although their temperature should be substantially higher. The aim is an effective temperature of 100 K, corresponding to a velocity of approximately 3×10^4 m s^{-1}. The Ps atoms move in a magnetic field of 1 T. In these conditions the combination of the Doppler, motional Stark and quadratic Zeeman effects results in a high broadening of the excitation transition frequencies, up to 1 THz for Rydberg transitions, making the excitation process substantially less selective than in the usual case of Rydberg spectroscopy. Furthermore, the laser pulse length is required to be of few ns, and to have maximal overlap with an expanding cloud with an initial transverse area of approximately 6 mm^2. The requirements on the energy and bandwidth of the excitation lasers have suggested the use of the optical parametric generation and amplification technologies for generating both wavelengths.

The laser system is composed of two subsystems: one for the generation of 205 nm radiation for the $1 \rightarrow 3$ transition, and the other for the generation of 1650 nm radiation for the $3 \rightarrow$ Rydberg transition. Both are driven by a Qswitched Nd:YAG laser delivering a maximum of 650 mJ in 4-6 ns pulses. The spectral width of the first laser pulse

is tailored to match the broadening of the first transition, which is determined by the Doppler width of the emitted o-Ps cloud (32 GHz at 100 K). Differently, the width of the second transition (of the order of THz or more) is dominated by the motional Stark effect inducing strong mixing of the Rydberg sublevels. In this case there is no stringent request on the spectral width of the second laser pulse for saturating the transition [44].

The laser systems have enough power to guarantee a 30% transition efficiency, close to the theoretical limit of 33%. The system can cover a frequency band wide enough to excite different Rydberg levels (from n = 16 to the ionization limit), and exceeds the saturation power by more than a factor of 10 for both transitions, maintaining a great flexibility for the choice of the best strategy for obtaining a large number of antihydrogen atoms.

2.6   Formation of antihydrogen

Antihydrogen atoms are formed by the charge exchange process

$$\bar{p} + Ps^* \rightarrow \bar{H}^* + e^- \tag{2.1}$$

The cross section for this process has been evaluated through Classical Trajectory Monte Carlo (CTMC) simulations for the experiment proposal [30], which indicate a strong dependence of the cross section on the principal quantum number of the Rydberg positronium, and on the relative velocity of the antiprotons and of the Ps* (or more precisely, on the ratio k_v of the relative velocity between the positronium and the antiproton, v_r, and the Rydberg positronium internal motion, v_{orb}, i.e. the relative orbital velocity between the positron and the electron).

Figure 2 shows the production cross section as a function of the Ps* principal quantum number n, with the orbital angular quantum number l_{Ps*} randomly chosen between 0 and $n_{Ps} - 1$ and $l_{Ps*} = 2$, in the reference case without magnetic field. $l_{Ps*} = 2$ is the forecasted quantum number l of Ps* after the laser excitation. The cross section is proportional to n^4 and for n=20 is about $10^{-10} cm^2$. Secondly, the quantum state of the $\bar{H}$ will be (to some extent) related to the Ps excited state and the final temperature of the antiatom will be mostly determined by the temperature of the $\bar{p}$ before the production reaction.

Part of this Thesis is devoted to the calculation of the cross section in the magnetic field of 1 T which is created in this zone of the experiment to axially confine $\bar{p}$.

The emission velocity of Ps from a nanoporous target is determined by the target temperature, the interaction time of the Ps inside the target (which is itself a function of the injection energy of the positrons into the target and the topology of the target material), and by the pore size. The first two aspects have been investigated in [45] which shows that for specific target compositions, the velocity distribution of o-Ps emitted from the target surface shows evidence of (partial) thermalization. Of particular interest in the case of AEGIS is the behavior at cryogenic temperatures. Studies [40] have shown that the temperatures both of the thermalized component, but also of the only partially thermalized component of o-Ps, follow a decrease in the target temperature (figure 2.8). A lower bound on the o-Ps temperature is given by the dimensions of the pores [38]. While it is difficult to determine precisely the degree to which the two parameters affecting the Rydberg antihydrogen production rate can be optimized, an estimate can be obtained by assuming that the currently observed fraction of Ps* with a velocity component between 5 and 15 kms^{-1} (in which the CTMC-derived cross section is approximately constant and of the order of 10^{-9} cm^2)) is maintained also at cryogenic temperatures.

The number of antihydrogen atoms that should be generated to measure the gravity acceleration is around 1 per second, or 200 per 200 s accumulation cycle. As there were
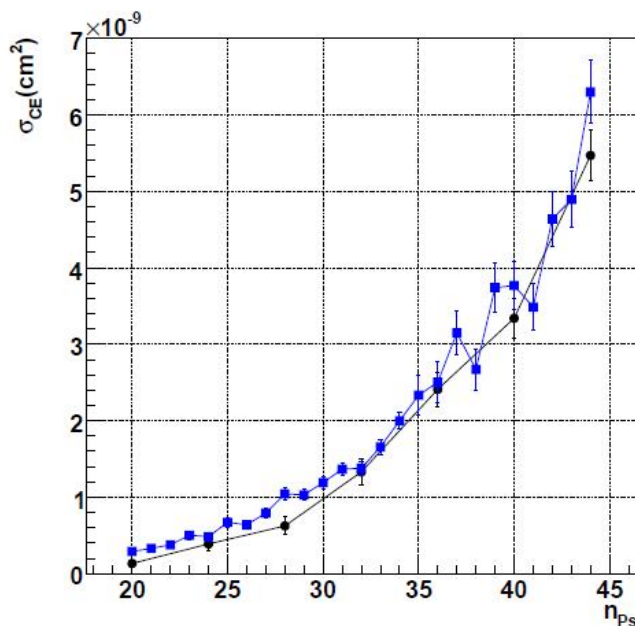
Figure 2.7: Cross section for the formation of Rydberg antihydrogen through the charge exchange process $\bar{p} + Ps^* \rightarrow \bar{H}^* + e^-$ as a function of n_{Ps} (the Ps* principal quantum number) for Ps* with a velocity ratio k_v of 1, and two assumptions on l_{Ps*} : squares refer to l_{Ps*} randomly chosen between 0 and $n_{Ps} - 1$ while circles correspond to $l_{Ps*} = 2$ without magnetic field [30].
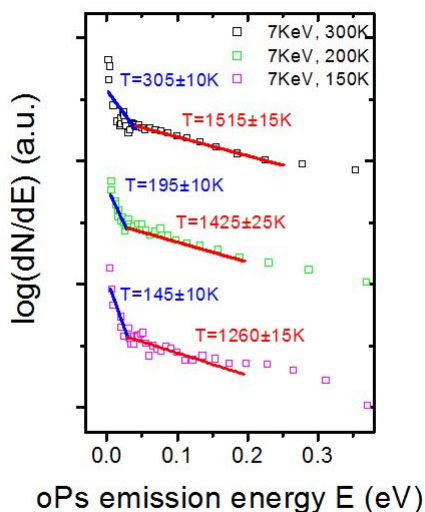
Figure 2.8: o-Ps energy spectra for different Ps production target temperatures (from [40]).
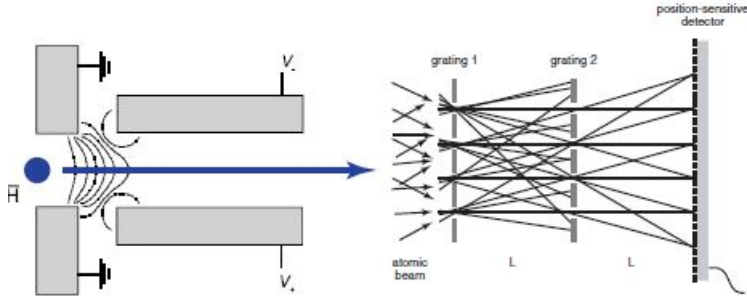
Figure 2.9: (Left) Sketch of the electrode configuration to accelerate $\bar{H}$. (Right) Sketch of the principle of the moiré deflectomer technique with two identical gratings and a position-sensitive detector.[31]

doubts that this number included in the proposal could be reached, the work of this Thesis has been devoted to simulate the process to verify it and, if the outcome was insufficient, suggest enhancements of the layout of AEGIS to increase it.

The distance between the target and the antiproton cloud, around 1.5 cm (see Figure 2.6), is critical for geometric reasons as well as the percentage of Ps* that can enter the antiprotons accumulation trap through the free space between the electrodes. An insufficient number of produced antihydrogen atoms would make impossible the accumulation of data in the following stage.

2.7   Acceleration of antiydrogen

The Rydberg antihydrogen atoms will be axially accelerated through their coupling to an externally applied pulsed electric-field gradient (Stark acceleration), applying techniques proposed for and demonstrated with Rydberg hydrogen atoms [48], wherein atoms moving with an initial velocity of $\approx 700ms^{-1}$ are stopped in a few μs over a distance of 2 mm. In the case of AEGIS, the inhomogeneous electric field is applied by appropriately polarizing the electrodes that initially confine the ultra-cold antiprotons immediately after the pulsed formation of antihydrogen (Figure 2.9). Although the quantum numbers of the Ps* used to form Rydberg antihydrogen are fairly well determined by the laser excitations (although the magnetic sublevels are randomly populated), the charge exchange process will populate a range of (n, m, l) antihydrogen states.

It should also be pointed out that these are no longer good quantum numbers in the $E \times B$ fields that appear at the moment of applying an electric-field gradient. Therefore, in our simulations we prefer to use the (n, k) quantum numbers, where $k = n_1 - n_2$, and n_1 and n_2 are the parabolic quantum numbers [85] obeying $n = n_1 + n_2 + |m| + 1$, and alternative to the usual formulation based on spherical quantum numbers (n; l; m). For atoms in electric fields, k is a good quantum number, and the simulations should remain valid as long as the magnetic field (B = 0.5–1 T) is relatively weak. These simulations allow us to evaluate the spread in velocity of the produced antihydrogen atoms, and to track these atoms through the 1 T magnet to the entrance of the moiré deflectometer. By ensuring that the electric-field gradient used to accelerate the produced Rydberg antihydrogen atoms is axial, no significant change in their radial velocity distribution is expected. The divergence of the antihydrogen beam is thus defined by the longitudinal velocity (given by the Stark acceleration field strength and duration as well as the orig-

inal velocity distribution) and the transverse velocity (given by the temperature of the antiprotons prior to formation of antihydrogen). The accelerating electric field will be applied for a time of the order of 70 μs. From simulations we expect an uncertainty of 10 μs on the beam starting time.

2.8   Antihydrogen beam through the moiré deflectometer

Some proposals of detecting the deflection of a beam of particles lie on the idea of using their matter wave nature through interferometers with high sensitivity, like those of the Mach-Zehnder type or employing the Talbot configuration. In spite of its high sensitivity, a matter wave interferometer of the Mach–Zehnder type is poorly suited to first measurements with antihydrogen, mostly due to the very stringent limits it places on the beam divergence, but also due to expected decoherence effects through interactions between (anti-)matter waves and material gratings. On the other side, a Talbot interferometer is less sensible to beam divergence, but requires unrealistic conditions on grating slits and distances to assure working on a diffraction regime [86].

Therefore AEGIS relies on a classical device called moiré deflectometer which can be considered as a particle counterpart of a grating wave interferometer.

A moirè deflectometer has been successfully used in an experiment where the gravitational acceleration of a beam of argon atoms traveling at an average velocity of 750 m s^{-1} was measured to a relative precision of 2×10^{-4} [49].

The horizontally accelerated antihydrogen atoms (v $\approx$ 500 ms^{-1}) propagate through the apparatus in the form of a broad beam until they enter the deflectometer, in which their free fall is measured. The deflectometer itself consists of two gratings and a third plane which records the impacting atoms (Figure 2.9). The position of the deflectometer is shown in Figure 2.10.

The two gratings of a deflectometer function as a shadow mask, projecting a periodic pattern onto the third plane that corresponds to the gap and inter-gap geometry. This periodic structure along the vertical (y) coordinate has a period equal to the grating period, 80 μm in AEGIS. Antihydrogen atoms that do not pass through a grating gap annihilate, producing pions. Antihydrogen atoms that do pass through the gaps in the two planes will follow parabolic trajectories whose sagitta depends on the amount of time spent in the deflectometer, on average 2 ms, during which time the atom falls by 10 μm (for a grating distance of 40 cm).

The periodic pattern (i.e. the antihydrogen impact points) is thus shifted downward, with respect to the horizontal line, by an amount that depends on the velocity of the atoms. The vertical shift of the pattern turn out to be $\delta_y = gt^{-2}$ [49], where t is the time of flight between the two gratings.

The figure of merit is the fraction of accelerated antihydrogen atoms that reach and traverse the full moiré deflectometer to impact the downstream high-resolution antihydrogen detector. This fraction is determined by the solid angle subtended by the detector, the divergence of the antihydrogen beam and the grating open fraction. As the transverse component of the velocity distribution is defined by the antiproton temperature, it is desirable that this temperature be the lowest possible.

As the velocity scales with $T^{1/2}$, while the solid angle scales as $(v_r/v_z)^2$, where v_r and v_z are the radial and axial velocity components, an increase by a factor of 10 of the temperature decreases the flux of antihydrogen atoms reaching the detector by the same factor. This purely geometrically defined flux is reduced by the open fraction of the two gratings of the deflectometer itself: the contrast of the periodic impact pattern in
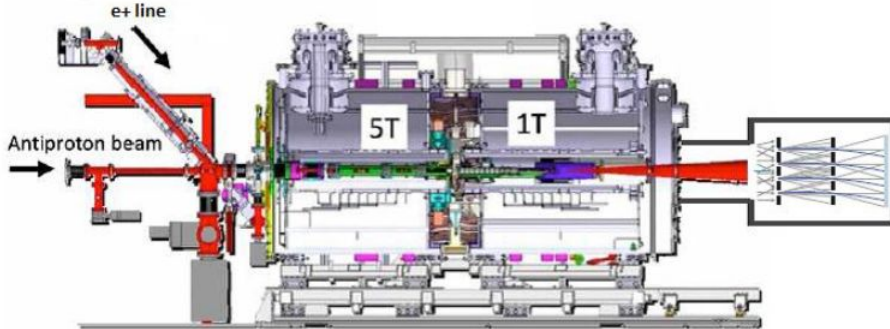
Figure 2.10: Position of the moiré deflectometer in the AEGIS apparatus on the right.

the plane of the detector is maximal in the case of an open fraction of 30%, resulting in a factor of 10 reduction in the flux. AEGIS simulations have shown that in order to achieve a 1% measurement of g, 10^5 antihydrogen atoms with an initial temperature distribution (prior to acceleration) of 100 mK are required (a factor of 10 more for 1 K antiprotons).

Assuming the production rate of 1 atom per second, and assuming that cooling of the antiprotons can be carried out during one AD duty cycle of 100 s, this corresponds to 10^4–10^5 AD cycles, i.e. several weeks to several months of experimental operation. Over such time scales, stability considerations are important; the precise relative alignments of the gratings and the antihydrogen detector will be monitored through a series of optical interferometers directly incorporated into these structures, allowing an offline correction of all measurements. On the other hand, the measurement of g is insensitive to variations in the flux of antihydrogen atoms. The value of g is extracted from the primary observables (time of flight t and vertical displacement of the fringe pattern δ_y, which can be transformed into a phase when normalized to the periodicity of the grating, as in figure 2.11). A quadratic fit to the plot of phase versus time of flight yields the local gravitational acceleration g.

As the length of experimental operation is so long, the production rate of antihydrogen is extremely important for the results of the experiment. This Thesis goal is to verify whether this rate is achievable.

The current AEGIS design calls for such a setup with a sophisticated detector that can record the annihilation position of impinging anti-atoms with a vertical resolution of about 2 μm. The detector will consist of a combination of complementary technologies, including a nuclear photographic emulsion and a silicon strip or pixel detector. Both types of systems have been extensively tested in the AEGIS setup and found to have the required position resolution and detection efficiency for an antihydrogen gravity measurement [50, 51].

2.9   Proof of principle of the moiré deflectometer

A prototype device of the moiré deflectomer has been tested with antiprotons [80].

It was formed by two parallel gratings and an emulsion detector, the distance between the gratings was 25 mm while the detector was placed 25 mm from the second
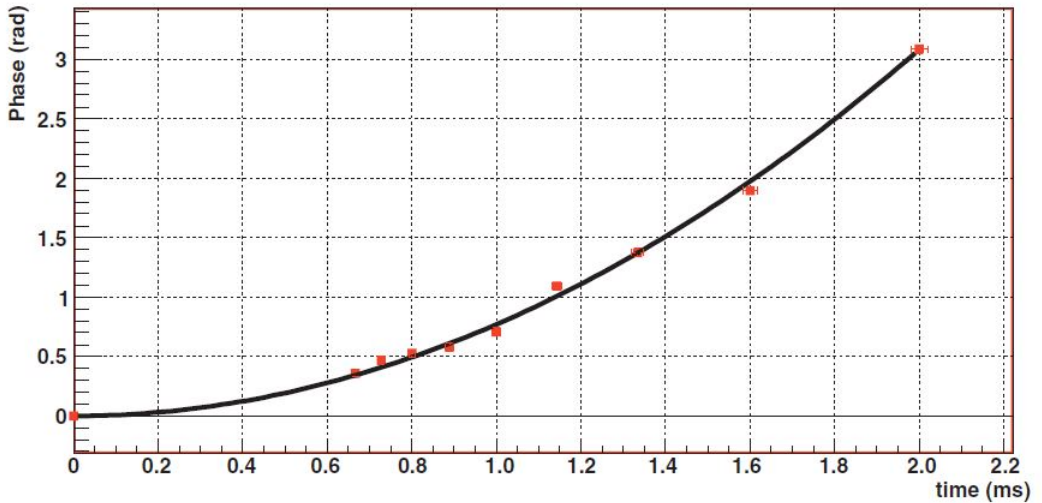
Figure 2.11: Phase shift as a function of the antihydrogen time of flight t between two gratings. Each point corresponds to 10^3 simulated antihydrogen atoms. A total of 10^5 atoms was generated and propagated through the Stark accelerator and moiré interferometer. An impact vertex resolution of 10 μm was assumed. The precision in the determination of the phase at each point is influenced both by statistics and systematic effects; the error on each point is estimated $\approx$0.05 rad. A quadratic fit to the plot of phase versus time of flight yields the local gravitational acceleration g.[31]

grating and had a resolution of 2 μm. The slits had a thickness of 100 μm, a width of 12 μm and a periodicity of 40 μm, granting a classical regime when compared to the de Broglie wavelength of the antiprotons ($8.8 \ 10^{-8} \mu m$).

A divergent beam of antiprotons with mean energy 106 keV was passed through the deflectometer producing a fringe pattern on the detector; it was expected that the presence of a force would shift the pattern. A comparison with a interference pattern produced by light has been carried out. An additional transmission grating was put in direct contact with the emulsion and illuminated with antiprotons and with light to have a reference for alignment.

The results showed an upward shift in the moiré pattern with respect to the interference pattern due to the light, given by $\Delta y = F\tau^2/m$, where F is the force perpendicular to the slits, τ is the time of flight between the two gratings and m is the antiproton mass. A shift $\Delta y = 9.8\mu m \pm 0.9\mu m (stat.) \pm 6.4\mu m (syst.)$ (Figure 2.12), corresponds to a force acting on antiprotons of $530 \pm 50aN(stat) \pm 350aN(syst)$.

The moiré deflectometer and the emulsion detector were mounted at the end of the 1T magnet in a dedicated vacuum chamber, so that the force was identified with a Lorentz force due to the fringe magnetic field of the trapping region (see Figure 2.10). A magnetic field component perpendicular to the grating period and the antiproton direction of $B \sim 7.4G$ was estimated, compatible with the magnetic field $\sim 10G$ measured at the position of the deflectometer.

The fringe pattern of antihydrogen due to gravity is expected to be comparable to the one observed in the case of antiprotons. The gravitational force acting on antihydrogen is expected to be about ten orders of magnitude smaller than the sensitivity level reached with the prototype device, but the resolution of the setup will be improved by scaling
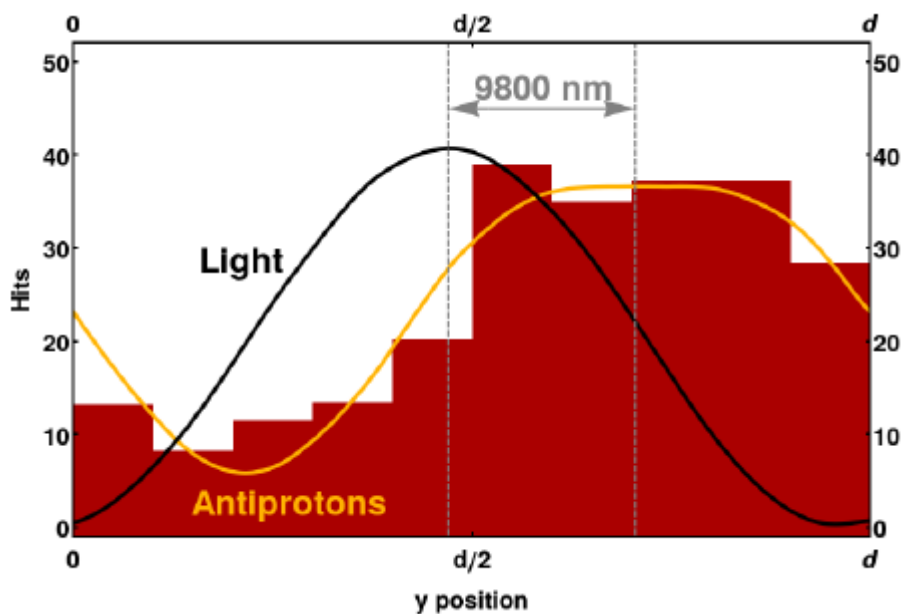
Figure 2.12: Light and antiproton patterns showing the observed shift of antiprotons through the moiré deflectometer. Reproduced from [80]

up the deflectometer with a distance between gratings ~ 1 m. Furthermore, the velocity of antihydrogen should be much smaller than the velocity of the antiprotons used in the test ($\sim 500ms^{-1}$). An improvement of about eleven orders of magnitude sensitivity, eight orders for the slower velocity and three for the length of the deflectometer, can be expected in relation to the prototype.

The Thesis work

The thesis work has closely followed the phases of construction of the experiment in order to simulate the various parts from the design phase to the assembling.

The simulation has always regarded the antihydrogen production phase from the Ps creation in the target to the mixing of Ps with antiprotons, which is the most critical part.

As the physical layout was changed from design to construction also the simulation was changed. The data were modified according to the dimensions of different parts of the experiment in order to have the most realistic simulations in relation to the real situation.

The results of the simulation were sent to the collaboration with various reports and discussed at meetings. Sometimes the results have been confirmed by other teams with independent calculations.

As the simulations produced unsatisfactory results in terms of antihydrogen atoms produced per cycle of 200 s possible modifications to the experiment have been suggested and simulated. Some have been discarded as unfeasible, others are still under study.

The work has started in 2009 before the beginning of my Phd course in 2014 when I became part of the Aegis team as "Laureato frequentatore" of Milan University. So the work of this thesis spans from 2009 to now, even if the intensity of the activity has increased during the period of the Phd course and has come to a final conclusion.

The principal activities have been the following:

- simulation of the production of antihydrogen with the basic layout

- simulation of the production of antihydrogen with the introduction of reflectors of various shapes for efficient guiding of the cloud of Ps atoms towards the trapped antiprotons

- simulation of the production of antihydrogen with the introduction of an ellipsoidal reflector before laser excitation for guiding the cloud of Ps atoms towards the trapped antiprotons

- simulation of the creation, propagation and detection of Ps in the positronium chamber of Aegis

- simulation of the production of antihydrogen with the introduction of a focusing electric field on the cloud of Rydberg Ps, thanks to their high polarizability and the Stark acceleration

- simulation of the production of antihydrogen with a Ps transmission target in different positions

- verification of the calculations of the Genova group on the production of antihydrogen

- simulation of the production of antihydrogen with a Ps transmission target in vertical position on axis

- simulation of the production of antihydrogen taking into account the 1T magnetic field

- calculation of the cross section of the charge exchange reaction without and with the 1T magnetic field

- simulation of the production of antihydrogen taking into account the new cross section calculation

Simulation of the production of antihydrogen with the basic layout

I did the first simulation of the production of antihydrogen with a Monte Carlo program in 2009-2010 when the experiment was in the design phase under the supervision of Prof. Marco Giammarchi, who was coordinating the Milan AEGIS group.

The report was sent to the collaboration on February 2, 2010 with the title: *"A simulation program for the production of antihydrogen in the AEGIS experiment"*[52].

The program simulated the creation of ortho-positronium atoms from a suitable target and their excitation by a laser beam, following them until they reached the antiproton cloud. Each Ps was followed in his trajectory with the step of 1 ns. The possible ionization between Rydberg atoms was taken into account as well as laser efficiency and life time of excited states.
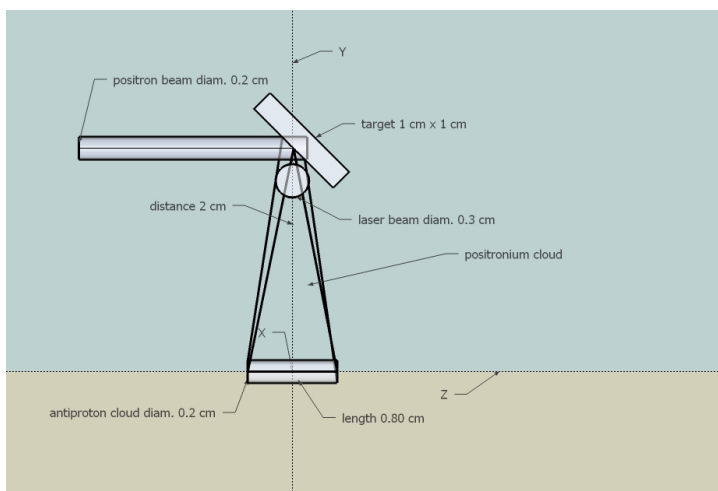
Figure 4.1: Layout of the antihydrogen formation part of AEGIS. See text for a detailed description.

The simulation was run with the following geometrical data, as represented in Figure 4.1:

- the positron beam had a diameter of 0.2 cm,

- the target was a square with a side of 1 cm, slanted at 45 degrees with respect to the positron beam,

- the antiproton cloud was 0.8 cm long with a diameter of 0.2 cm and was centered under the target at a distance of 2 cm,

- the laser beam had a diameter of 0.3 cm, its center was located on the vertical axis between the center of the target and the center of the antiproton cloud, with a distance of 0.05 cm between the border of the beam and the surface of the target, in order not to damage it.
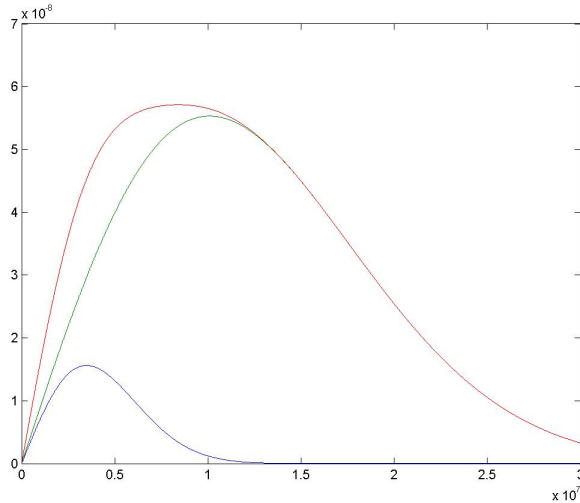
Figure 4.2: Positronium velocity distribution of [40] in cm/s in red as the sum of 145K distribution in blue and 1260K distribution in green, referred in following chapters as "Trento" velocity

The physical data were the following:

- 1 million Ps atoms generated from the target,

- flat distribution of the emission time of Ps from the target in an interval of 20 ns (duration of the positron bunch),

- uniform distribution of the emission direction of Ps over half of the solid angle,

- Gaussian distribution of the emission point of Ps from the target in the area covered by the incoming positrons, with the maximum in the center of the target and $\sigma = 0.05cm$,

- velocity distribution of the Ps taken from the data of [40] for a target temperature of 150K (see Figure 2.8),

- laser impulse 5 ns long, with a starting time optimized for maximum production of antihydrogen given the velocity distribution (50 ns after the beginning of the positron bunch),

- laser efficiency 20%,

- excitation level of Ps n=25, l=2 with a decay time of 16.5 μs,

- ionization probability computed with Robicheaux formula for the self-ionization of Rydberg atoms due to their mutual interaction [59],

- velocity limit of Ps with n=25 to produce antihydrogen $0.87 \times 10^7 cm/s = c/(137 \times n)$.

I assumed for simplicity infinite cross section for $v < 0.87 \times 10^7 cm/s$ and 0 otherwise. This matching of velocities is important for antihydrogen formation. The velocity distribution was taken from [40]. In that research, a silicon target with nanochannels obtained by electrochemical etching was used and the o-Ps energy distribution with a positron implantation energy of 7 keV and a target temperature of 150K was measured.

The energy distribution was transformed in a velocity distribution, considering that 9% of Ps had a temperature of 145K and 91% had a temperature of 1260K (see Figure 4.2)

The ionization probability of Rydberg Ps was taken into account computing for every nanosecond the *time to come together T* according to [59]:

$$T = 20\mu s \times \sqrt{M(amu) R_0^5(\mu m)} / n^2 \qquad (4.1)$$

where M is the mass of the Ps , R_0 is the distance between two Ps atoms and n is the level of the Ps.

The laser beam was turned on 50 nanoseconds after the beginning of the positron bunch for 5 ns.

The results are in table 4.1.

Ps from target	1,000,000
Ps hit by the laser beam	113,572
Ps that geometrically can hit the antiproton cloud	6,471
- which are excited by the laser beam	404
- which arrive to the antiproton cloud	393
- which have a velocity below the limit	269

Table 4.1: Results of the simulation with the basic layout

Figure 4.3 shows the decision tree of the results.

There has been no decay for ionization because, when the laser is turned on (50 ns), the density of the Ps cloud is low enough not to create the phenomenon. If the laser beam was nearer to the centre of the target, the time would be shorter and the number of excited Ps atoms decayed for ionization larger.

When the laser beam is turned on the thermalized Ps can reach it while the fast Ps are already far away. This is the reason why most of the Ps that hit the antiproton cloud have a low velocity and can create antihydrogen.

If the delay is reduced the number of Ps that hit the antiproton cloud is increased but their velocity is too high to create antihydrogen. The table 4.2 contains the different simulation results.

The Figures 4.4 and 4.5 represent the velocity distribution of the Ps hit by the laser beam after 50 ns (113,572) and of the excited Ps when they arrive at the antiproton cloud (393). The velocity limit is shown.

This simulation gave an indication of the number of Ps arriving at the antiproton cloud with a velocity that would allow the production of antihydrogen but didn't give
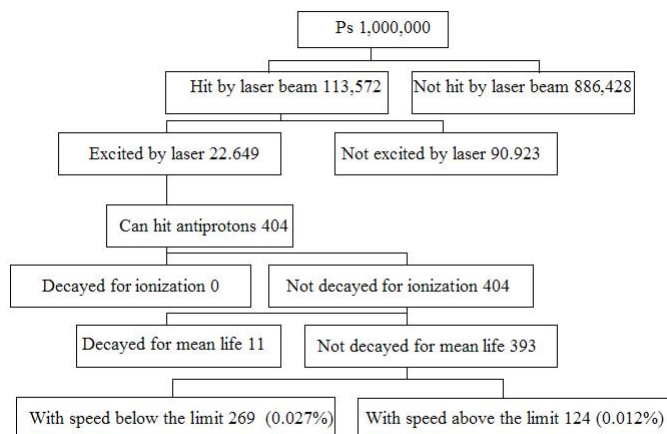
Figure 4.3: Schema of the results of the simulation

Laser delay in ns	30	40	50	60
Ps hit by laser	162,701	145,158	113,572	87,450
Excited Ps that arrive to the antiproton cloud	733	577	393	278
Excited Ps that arrive to the antiproton cloud with velocity below the limit	173	269	269	259

Table 4.2: Results for different delays

the number of antihydrogen atoms because the cross section of the charge exchange reaction was not included. All the other processes though were simulated.

It was clear that the solid angle of the antiproton cloud seen from the target at the distance of 2 cm limited the number of Ps exiting from the target that would cross the antiprotons and produce antihydrogen. As the distribution of the direction of Ps from the target was unknown, it was assumed flat.
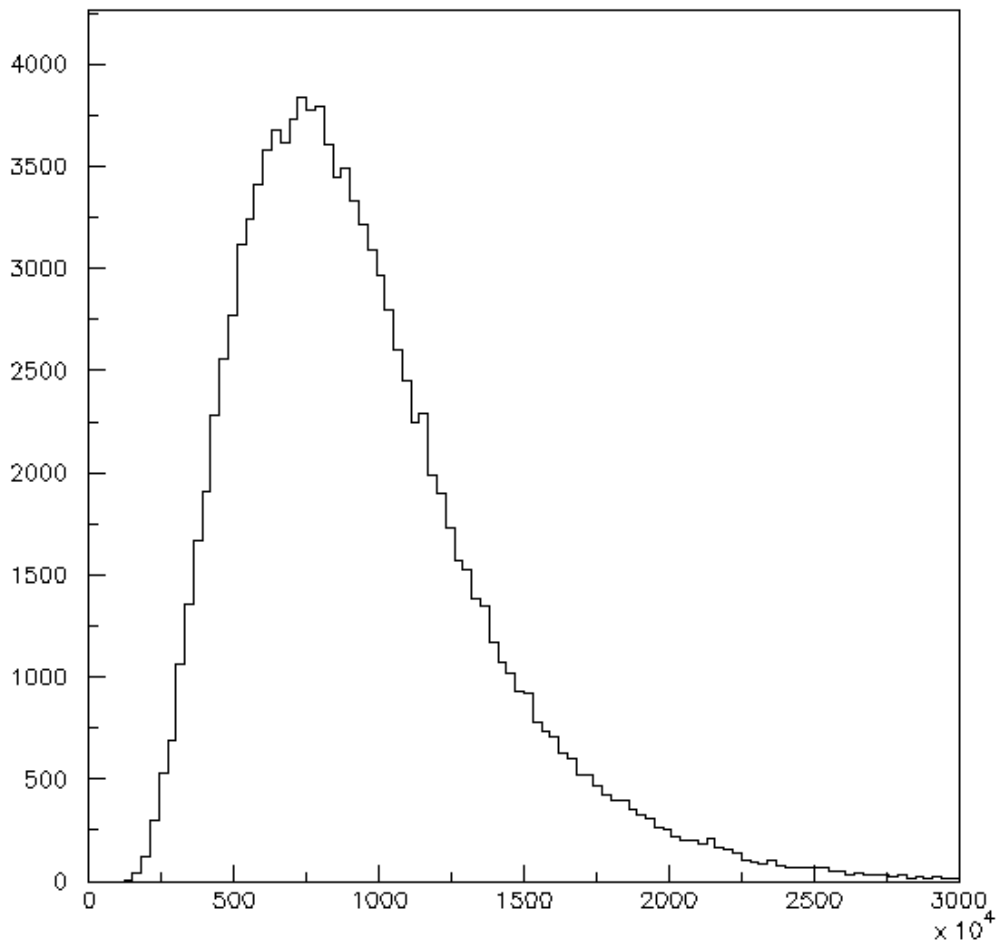
Figure 4.4: Velocity distribution
of Ps hit by the laser beam in
cm/s
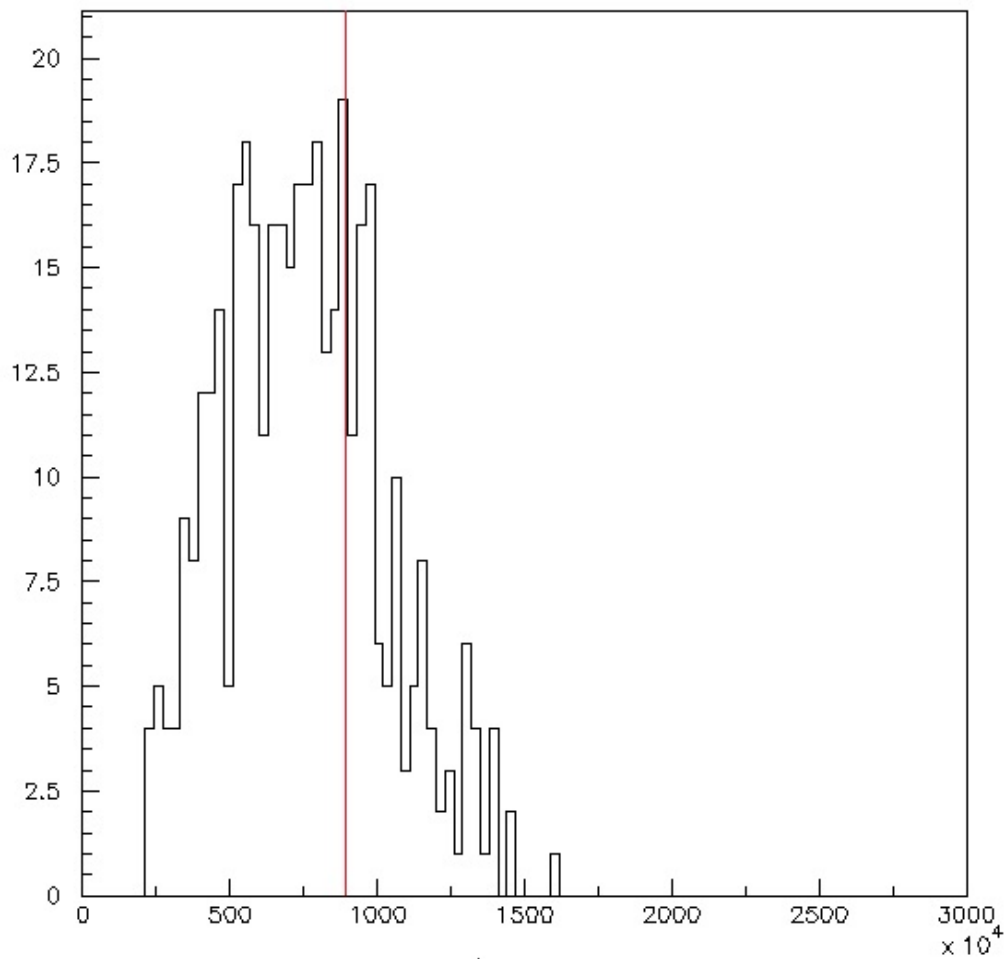
Figure 4.5: Velocity distribution of excited Ps in cm/s when they arrive at the antiproton cloud, the red line represents the velocity limit

Simulation of the production of antihydrogen with the introduction of reflectors of various shapes for guiding the cloud of Ps atoms towards the trapped antiprotons

The first simulation gave an unfavorable result for the experiment because the number of the excited Ps arriving to the antiproton cloud was insufficient to produce the needed number of antihydrogen atoms. Their number had to be multiplied by 10 considering that the number of Ps produced by the target should be 10 million, but we also have to consider the average cross section calculated in the AEGIS proposal for Ps with n=25 which amounts to $10^{-9}cm^2$, while in the trap we have 10^5 antiprotons (see Figure 5.1). So the approximate number of antihydrogen atoms produced in a cycle of 200 s would be around 2, instead of the 200 needed to measure the gravity acceleration.

It was suggested that I could add to the design of AEGIS some reflectors for moving Ps atoms, trying to improve the geometrical limiting factor and increase the number of Ps that would reach the antiproton cloud. The reflectors were considered like mirrors with no loss of the number of reflected particles. A velocity limit of $4.4 \times 10^4 m/s$ was introduced on the best result with the parabolic and ellipsoidal reflectors considering that only slow Ps would be reflected while fast ones would be ionized.

The result of the simulation was presented to a collaboration meeting on April 8, 2011.

Two reflectors were considered in the AEGIS design: one around the target with a spherical or ellipsoidal shape and one parabolical under the antiproton cloud.

Figures 5.2,5.3,5.4,5.5 represent the two layouts on two perpendicular sections y-z and x-y.

The ellipsoid should have a focus in the target center and one in the antiproton cloud center to use the geometrical properties of its shape. The spherical reflector had a radius of 0.7 cm, the parabolic reflector was parallel to the axis of the antiproton trap, according to the formula $y = 1.1 \times x^2 - 0.4\,cm$ in order to fit in the Penning trap radius of 0.6 cm.

Moreover the distance between the center of the trap and the center of the antiproton cloud was reduced from 2 to 1.5 cm to increase the number of Ps that would reach the antiproton cloud.

Table 5.1 shows the number of antihydrogen atoms produced for 1 million Ps created by the target. One can see the efficiency of the ellipsoidal and parabolic reflectors in directing the Ps to the antiproton cloud and the increase factor of the generated antihydrogen atoms from the 0.086 atoms without reflectors. For 10 million Ps 13 atoms would be produced with the limit on the velocity, but still not enough for the gravity measurement.
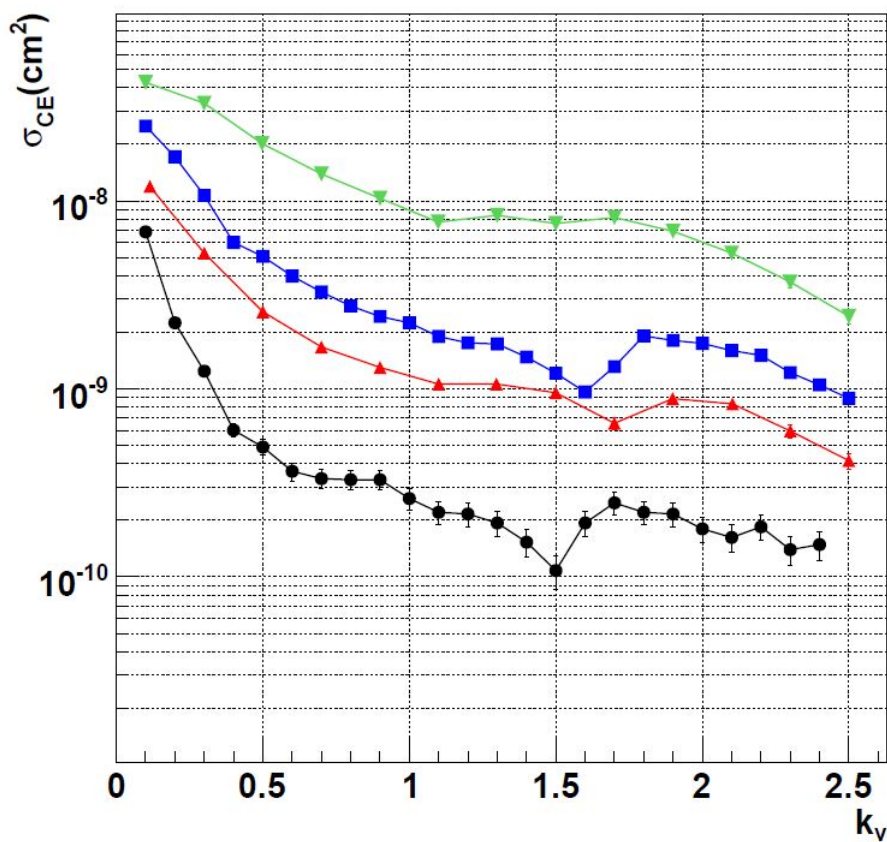
Figure 5.1: In this plot the charge exchange process 2.1 cross section as a function of k_v for different values of n_{Ps} and $l_{Ps} = 2$ is shown. From top to bottom n_{Ps}=50,35,30,20. The corresponding velocities for $k_v = 1$ are 22 km/s, 31 km/s, 36 km/s, 54 km/s, $k_v = v_r/v_{orb}$ where v_r is the velocity of the Ps and v_{orb} is the orbital velocity of the positron in a circular orbit [30]

	no reflectors	parab. reflector	spher. reflector	par.+spher. reflector	par.+ellips. reflector	same with veloc. limit
Ps which exit from target	1,000,000	1,000,000	1,000,000	1,000,000	1,000,000	1,000,000
Ps which cross antiprotons	11,615	167,200	25,830	219,041	669,285	99,539
- without reflection	11,615	11,615	11,615	11,615	11,615	11,615
- with reflection on upper reflector			14,215	10,723	315,533	42,231
- with reflection on parabolic reflector		155,585		196,703	342,137	45,693
Ps which arrive to antiprotons	4,763	50,800	9,719	65,429	203,606	10,499
- excited by laser beam	938	9,800	1,612	11,999	33,427	5,319
- excited and not reflected	938	700	938	913	412	316
- excited and reflected		9,100	674	11,086	33,015	5,003
Generated antihydrogen atoms	**0.086**	**0.85**	**0.15**	**1.07**	**3.23**	**1.26**
Increase factor		**9.9**	**1.7**	**12.4**	**37.6**	**14.6**

Table 5.1: Simulation results
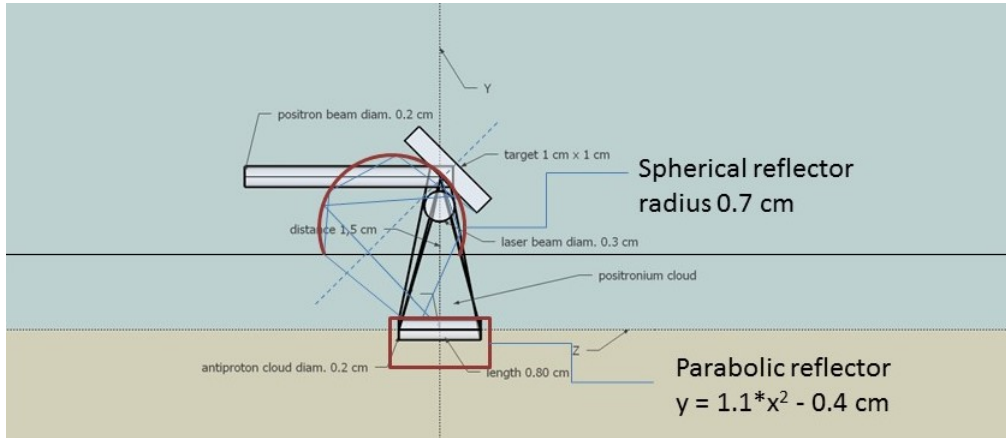
Figure 5.2: Aegis section y-z, spherical reflector at the top, parabolic reflector at the bottom

The idea of reflectors was however abandoned because the possibility to reflect Rydberg positronium was considered doubtful, hardly realizable and with high risk of Rydberg ionization.
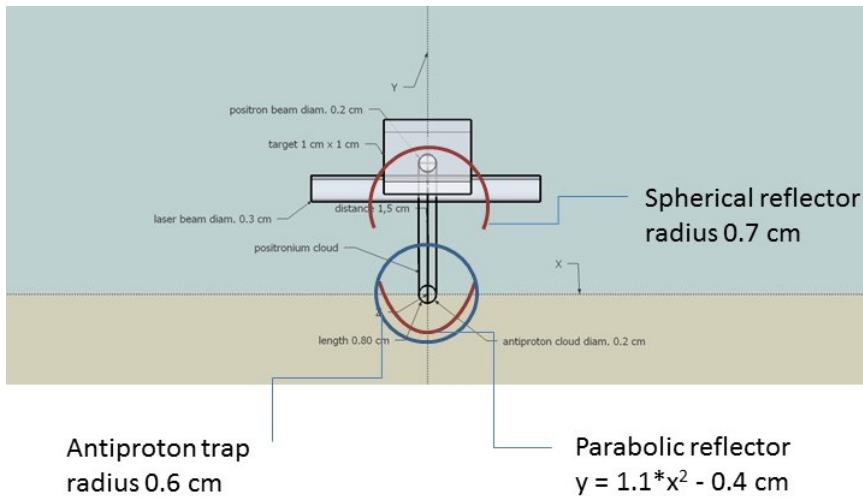
Figure 5.3: Aegis section x-y, spherical reflector at the top, parabolic reflector at the bottom
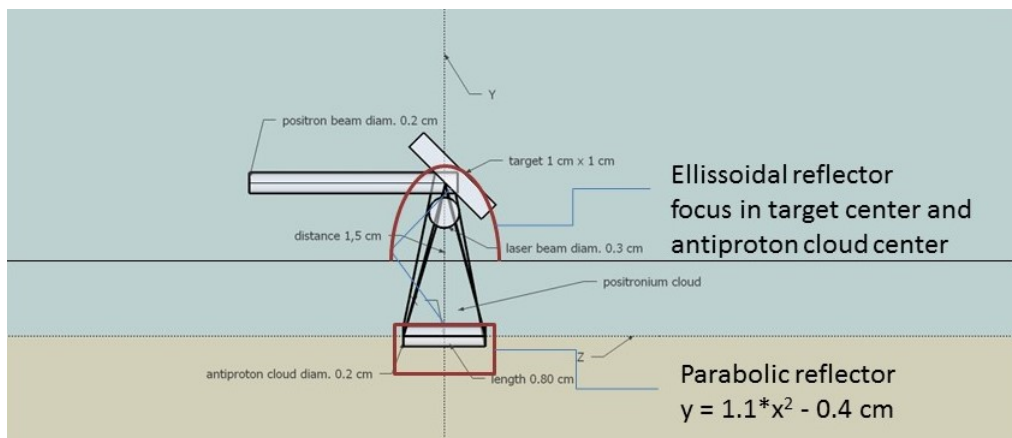
Figure 5.4: Aegis section y-z, ellipsoidal reflector at the top, parabolic reflector at the bottom
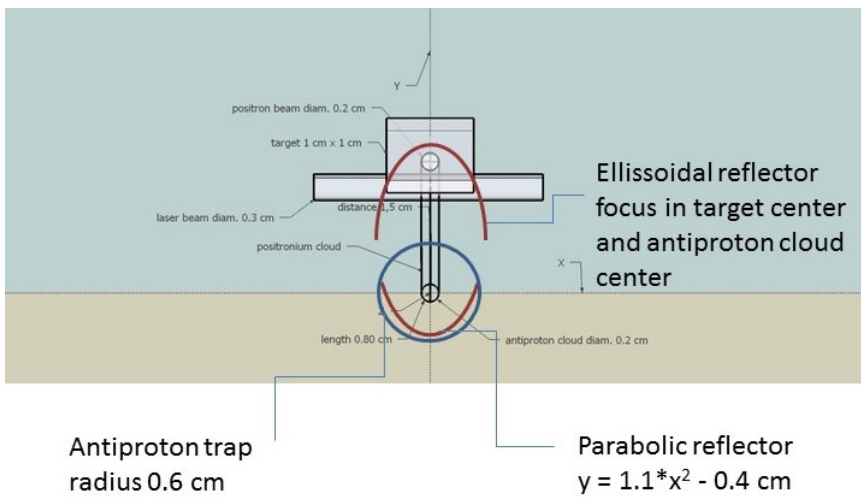
Figure 5.5: Aegis section x-y, ellipsoidal reflector at the top, parabolic reflector at the bottom

Simulation of the production of antihydrogen with the introduction of an ellipsoidal reflector before laser excitation for guiding the cloud of Ps atoms towards the trapped antiprotons

At the beginning of my Phd course in 2015 I have reconsidered the possibility of reflecting Ps on the ground level on an ellipsoidal reflector before the excitation by the laser to a Rydberg level [55]. In this way Ps hits the reflector in ground state, avoiding the ionization losses of Rydberg states. One of the focuses of the reflector was put in the center of the target and the second in the center of the antiproton cloud. A hole of a diameter of 0.2 cm has been simulated to let the positrons reach the target (see Figure 6.1)

To allow reflection of Ps atoms before excitation the laser beam center has been put at a distance of 1 cm from the center of the antiproton cloud, so that the laser beam can't excite the Ps before the reflection.

In this position the width of the laser beam has to be tailored accurately to catch the Ps emitted directly from the target or reflected by the ellipsoid. The radius of the beam has been set to 0.15 cm. To enlarge the laser area the reflection of the laser beam has been simulated, in order to have two laser beams next to each other, with the contact point on the vertical line that connects the center of the target to the center of the antiproton cloud (see Figure 6.2). The radius of the beam is such that it almost touches the electrodes of the antiproton trap, with external radius 0.85 cm.

The program takes account of the magnetic field of 1 tesla in the region of the creation of Ps which causes a magnetic quenching [87]: two thirds of the o-Ps exiting the target have a lifetime of 142 ns ($m_s \pm 1$), one third ($m_s = 0$) mixes with the para state and has a lifetime of 7 ns. The Ps with $ms = 0$ do not contribute to the formation of antihydrogen in all the layouts: the laser delay in the normal layout is 45 ns, to optimize the velocity of the Ps with $m_s \pm 1$ in the generation of antihydrogen, and with the ellipsoid is 180-185 ns.

The result of the simulations shows that the number of the generated antihydrogen atoms is multiplied by a factor of 1.7 with one laser beam and by a factor of 3.1 with a reflected laser beam. These factors are much smaller than the one in the preceding chapter with a parabolic and an ellipsoidal reflector, which was 37.6 and similar to the result with a spherical reflector which was 1.7 (see table 5.1).

The ellipsoidal reflector could be made of quartz on which a metallic net with a 99% transmission rate is deposited. The metallic net can be connected to the ground or to any desired potential not to disturb the electric field of the antiproton trap. Only 1% of the Ps which is reflected will be lost due to the contact with the metal because of pick-off, i.e. the two gamma annihilation of the Ps positron with one electron of the material [88].
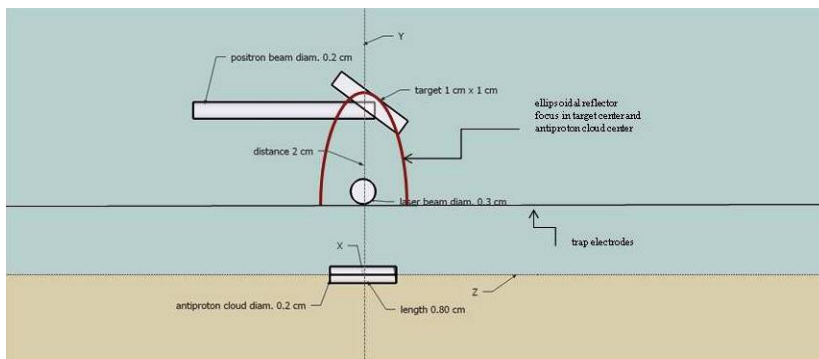
Figure 6.1: Layout of the antihydrogen formation part of AEGIS on the y-z plane, the laser beam is orthogonal to the plane of the figure (parallel to the x axis)
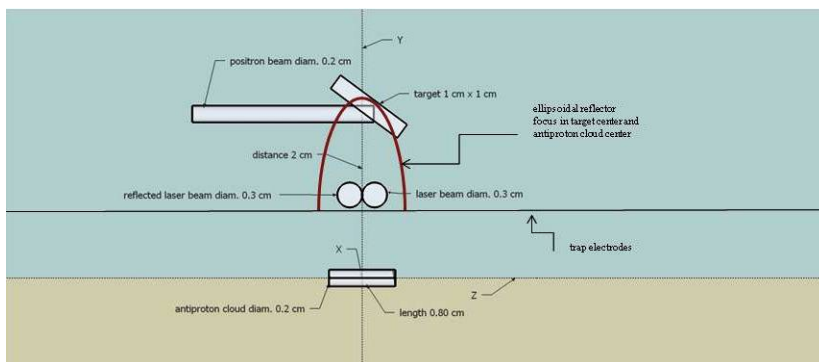
Figure 6.2: Layout of the antihydrogen formation part of AEGIS on the y-z plane, the laser beams are orthogonal to the plane of the figure (parallel to the x axis)

The quartz will need holes for the positrons entrance and the laser beam and a cut to locate the target.

6.1   Simulation description

The program simulates the creation of ortho-positronium atoms from a suitable target and their excitation by a laser beam composed by two laser pulses [43], following them until they reach the antiproton cloud. Each Ps is followed in his trajectory with a time step of 1 ns.

The possible ionization due to mutual Rydberg atoms interactions by induced electric dipole is taken into account [59], as well as laser efficiency and life time of excited states [44].

The simulation has been run with the following geometrical data, which correspond to the layout of the experiment (see Figures 6.1,6.2,6.3):

- the positron beam has a diameter of 0.2 cm,

- the target is a square with a side of 1 cm, slanted at 30 degrees with respect to the positron beam, at a distance of 2 cm from the center of the antiproton cloud
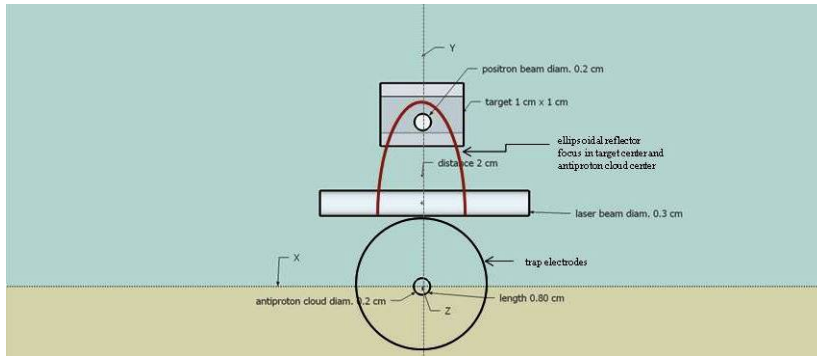
Figure 6.3: Layout of the antihydrogen formation part of AEGIS on the x-y plane, the positron beam, antiproton trap and cloud are orthogonal to the plane of the figure (parallel to the z axis)

- the antiproton cloud is 0.8 cm long with a diameter of 0.2 cm and is centered under the target at a distance of 2 cm,

- in the first layout the laser beam has a diameter of 0.3 cm, its center is located on the vertical axis between the center of the target and the center of the antiproton cloud, with a distance of 1 cm from the center of the antiproton cloud and from the center of the target,

- in the second layout laser beam has been doubled through reflection: for simplicity two parallel laser beams have been simulated with a diameter of 0.3 cm, the contact point is on the vertical axis connecting the center of the target to the center of the antiproton cloud, this being the layout that produces the maximum number of antihydrogen atoms,

- a semi-ellipsoidal reflector has been inserted between the target and the antiproton trap, with the focus in the center of the target and the center of the antiproton cloud, in order to maximize the number of the Ps that hit the antiproton cloud after reflection. A hole of a diameter of 0.2 cm has been simulated for the entrance of the positrons.

The physical data used in the program are the following:

- 1 million Ps atoms generated from the target,

- 1/3 of the Ps with a lifetime of 7 ns (ms=0), 2/3 with a lifetime of 142 ns (($m_s \pm 1$)) due to magnetic quenching [60],

- flat distribution of the emission time of Ps from the target in an interval of 20 ns (duration of the positron bunch),

- uniform distribution of the emission direction of Ps over half of the solid angle,

- Gaussian distribution of the emission point of Ps from the target in the area covered by the incoming positrons, with the maximum in the center of the target and $\sigma = 0.05cm$,

- velocity distribution of the Ps taken from the data from [40] for a cloud temperature of 145K for 10% of the Ps and 1250K for 90% of the Ps,

- two simultaneous laser pulses 5 ns long, with a starting time optimized for maximum production of antihydrogen given the velocity distribution (170 ns after the beginning of the positron bunch), the laser beam has been doubled through reflection,

- laser efficiency 20%,

- final excitation level of Ps n=25, l=2 with a natural decay time of 16.5 μs [44],

- ionization probability computed for every nanosecond according to the formula 4.1 taken from [59],

- cross-section to produce antihydrogen computed in the Aegis proposal for n=30 (see Figure 5.1),

- a semi-ellipsoid with focus in the center of the target and the center of the antiproton cloud.

6.2   Simulation results

In the following table 6.1 the first column shows the simulation result without reflector and the laser beam at a distance of 0.05 cm from the target on the axis between the center of the target and the center of the antiproton cloud. The distance from the center of the antiproton cloud is 1.77 cm. In this layout (see Figure 6.4) there is no significant

	no reflector laser near target	reflector with one laser beam	reflector with two laser beams
Laser delay ns	45	180	185
Ps which exit from the target	1,000,000	1,000,000	1,000,000
Ps which cross antiprotons without reflection	6,443	6,443	6,443
Ps which cross antiprotons with reflection	0	336,701	336,701
Ps which arrive to antiprotons excited by laser without reflection	279	10	16
Ps which arrive to antiprotons excited by laser with reflection	0	481	829
Generated antihydrogen atoms	0.123	0.239	0.433
Increase factor		76%	210%

Table 6.1: Schema of the results of the simulation

increase of the number of generated antihydrogen atoms if the laser beam is doubled through reflection either under the laser beam or on the side. The second column shows the simulation result with the layout of Figure 6.1, the third column with the layout of Figure 6.2

A large amount of Ps that geometrically can arrive to the antiprotons due to reflection are lost because of decay before being excited by the laser or because they don't cross the
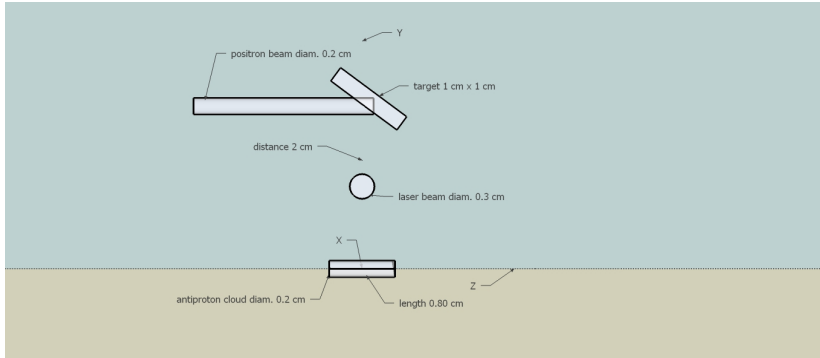
Figure 6.4: Current layout with no reflector of the antihydrogen formation part of AEGIS on the y-z plane, the laser beam is orthogonal to the plane of the figure (parallel to the x axis).

laser spot. Their mean life is very short before being excited to a Rydberg level (142 ns vs. 16500 ns).

The large focusing of the Ps on the antiprotons due to the semi-ellipsoid counterbalances in part the diminished efficiency of the laser excitation due to the distance between the target and the laser.

The laser delay has been optimized to generate the maximum number of antihydrogen atoms (180 ns with one laser beam and 185 ns with two laser beams).

In the experiment the data should be multiplied by 10 because the Ps which exit the target should be 10 million per positron bunch.

Simulation of the creation, propagation and detection of Ps in the positronium chamber of AEGIS

In 2013 a positronium chamber was designed to make experiments on positronium before the AEGIS main apparatus was ready. Figure 2.3 shows the position of the chamber, called positronium test chamber, in light blue near the positron accumulator [53].

One of the goals of the positronium chamber was to to test various targets for the conversion of positrons into Ps and their excitation by a laser beam to the Rydberg level n=25.

The Monte Carlo program was a modification of the one used to simulate the AEGIS experiment because many parts of the process were the same.

The program simulates the creation of ortho-positronium atoms from a suitable target and their excitation by a laser beam, following them until they reach the walls of the chamber. Each Ps is followed in his trajectory with the step of 1 ns. The possible ionization between Rydberg atoms is taken into account as well as laser efficiency and life time of excited states.

If the positronium decays in flight the emission of three gamma rays is simulated, with a flat distribution of directions and a flat distribution of energy between 0 and 511 keV.

If the positronium hits the walls of the chamber, the emission of two gamma rays is simulated in opposite directions with a flat distribution on the solid angle and a fixed energy of 511 keV. The minimum detection energy of the gamma rays is assumed 100 keV.

The simulation has been run with the following geometrical data (see Figure 7.1):

- the positron beam has a radius of 0.1 cm, the entrance hole in the chamber has a radius of 0.2 cm;

- the target is a square with a side of 1 cm perpendicular to the positron beam;

- the chamber is a cylinder with radius 10 cm and length 5 cm in front of the target, with the axis perpendicular to the center of the target;

- the laser beam has a radius of 0.2 cm, its center is located on the axis of the chamber, with a distance of 0.05 cm from the surface of the target, in order not to damage it;

- two gamma ray detectors (PbWO4 scintillators) are placed on opposite sides of the walls of the chamber (top and bottom), their shape is a cylinder with a radius of 1 cm and a length of 6 cm towards the center, the gamma rays can annihilate on their surface.

Schema of the chamber

Detector

chamber radius 10 cm
chamber length 5 cm

positrons entrance hole
hole radius   0.2 cm
beam radius   0.1 cm

Target

Laser
Radius 0.2 cm
distance from target 0.05 cm
efficiency 20%

detector
radius 1 cm
length 6 cm
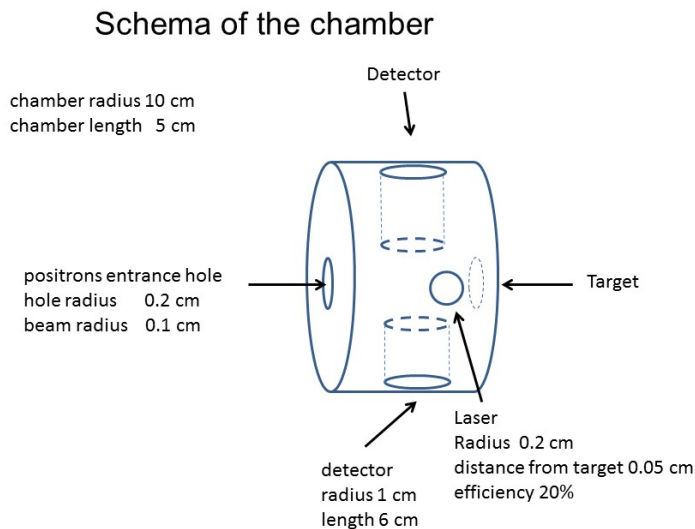
Figure 7.1: Schema of the positronium chamber

The schema of the experimental apparatus is represented in Figure 7.1, in which the laser beam is orthogonal to the plane of the figure (parallel to the x axis).

The physical data are the following:

- 1 million Ps atoms generated from the converter

- flat distribution of the emission time of Ps from the target in an interval of 20 ns (duration of the positron bunch),

- uniform distribution of the emission direction of Ps over half of the solid angle,

- Gaussian distribution of the emission point of Ps from the target in the area covered by the incoming positrons, with the maximum in the center of the target and $\sigma = 0.05cm$,

- velocity distribution of the Ps taken from the data of [40] for a target temperature of 150K,

- laser impulse 5 ns long, with a starting time optimized for maximum production of excited positronium given the velocity distribution (57 ns after the beginning of the positron bunch),

- laser efficiency 20%,

- excitation level of Ps n=25, l=2 with a natural decay time of 16.5 μs,

- ionization probability computed with the formula 4.1.

7.1 The results of the simulation

The laser beam has been turned on 57 nanoseconds after the beginning of the positron bunch for 5 ns. The results in table have been obtained:

Ps from the target	1,000,000
Ps hit by the laser beam	185,674
Ps decayed for mean life	943,266
Ps decayed for ionisation	40
Excited Ps decayed for mean life	2,828
Ps arrived at the chamber walls	56,599
- of which excited by laser beam	34,233
Gamma rays from detector 1	35,887
Gamma rays from detector 2	35,612
Gamma rays of 511 keV	4,260

Table 7.1: Results of the simulation of the positronium chamber

Figures 7.2,7.3,7.4 represent the distribution of the gamma rays arrival time in nanoseconds at the two detectors with the laser beam, without the laser beam and with a laser beam with 100% efficiency which hits all the positronium atoms that exit the target.
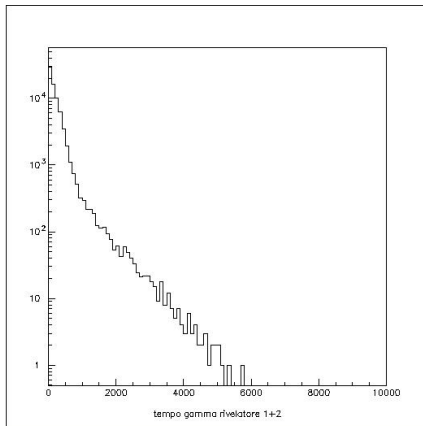
Figure 7.2: Arrival time distribution of gamma rays with laser beam in ns
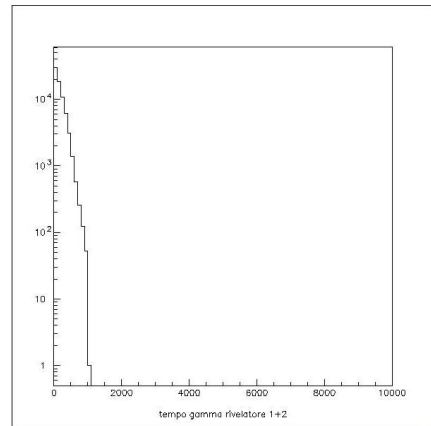
Figure 7.3: Arrival time distribution of gamma rays without laser beam in ns

The effect of the laser excitation is to increase the mean life of Ps and consequently the arrival time distribution is moved to the right of the plot.

For the moment only the excitation of Ps to level n=3 and n=15 has been tested in the positronium chamber [61]. Only one detector was used and it's shape was not cylindrical but almost cubic with dimensions 20x25x25 mm.
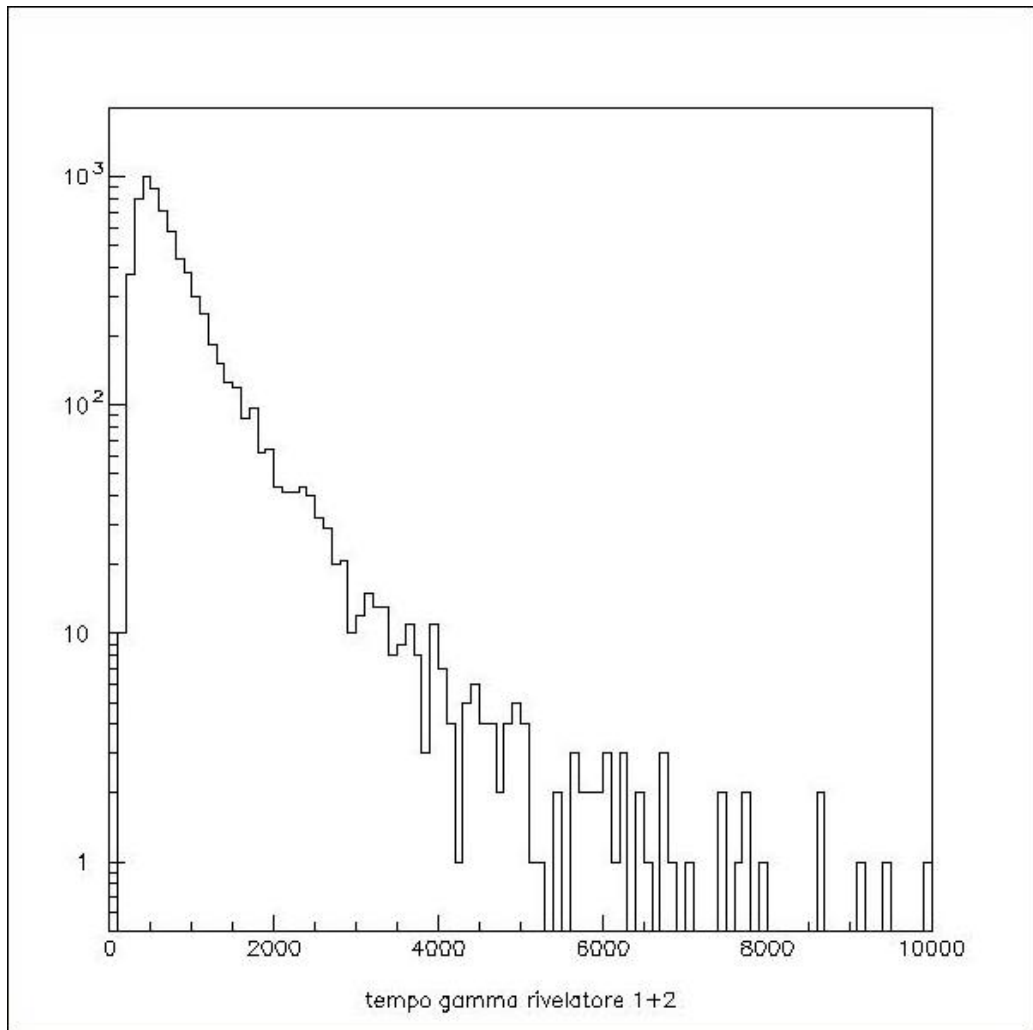
Figure 7.4: Arrival time distribution of gamma rays with infinite laser beam in ns

Simulation of the production of antihydrogen with the introduction of a focusing electric field on the cloud of Rydberg Ps, thanks to their high polarizability and the Stark acceleration

The idea to increase the number of antihydrogen atoms by focusing Ps on the ground level with an ellipsoidal reflector was abandoned because the increase factor was low. A new proposal was put forward, the focusing of moving Ps atoms on the antiproton cloud using an inhomogeneous electric field by the so-called Stark acceleration. The simulation has been done in a B=0 assumption.

The report was sent to the AEGIS collaboration on September 18, 2014 [54]: *"Focusing of positronium atoms to increase Antihydrogen production in the Aegis experiment"*.

It was inspired by the works of Vliegen, Limacher and Merkt [46] [47] [48] who have demonstrated experimentally the possibility of focusing a Rydberg atom beam with argon and hydrogen using the Stark acceleration.

An atom in a Rydberg state has a large electric dipole moment induced by an external electric field which is proportional to n^2 and so its trajectory can be influenced by an electric field. In an inhomogeneous electric field, according to [46], the force f which acts on the Rydberg particles can be expressed in atomic units to a good approximation as:

$$f = -\frac{3}{2} nk\nabla F \tag{8.1}$$

where n is the principal quantum number, k a quantum number which labels the Stark states and runs from $-(n-1-|m|)$ to $(n-1-|m|)$ in steps of 2 and F is the electric field strength in atomic units.

The design of electrodes and charges to produce an inhomogeneous electric field has been studied with Simion 8.1 (a software program which simulates electric fields), the flying of Rydberg Ps has been optimized to focus, through Stark acceleration, both high-field seeking states ($k < 0$) and low-field seeking states ($k > 0$) of Ps on the antiprotons confined in the Penning trap of Aegis.

The maximum electric field acting on Ps has been controlled in order not to reach the Rydberg Ps ionization limit of about 300 V/cm, taking care of an eventual presence of a transverse motional Stark field (in the realistic case of a magnetic field of 1 T). As a consequence the electric field generated by electrodes has been limited to a safety value of $50V/cm$, and correspondingly the electric field gradient, linked to the electrode design, limited to $270V/cm^2$.

The result of the simulation shows that the electric field generated in the small available space between the laser spot and the electrodes of the Penning trap (around 1 cm)

within the ionization limit is insufficient to focus the Ps on the antiprotons with the velocity distribution of the target of reference [40].

Focusing can however be obtained if the velocity distribution is reduced to one tenth, with an average velocity of approximately 10 $mm/\mu s$ instead of 100 $mm/\mu s$. With this distribution the number of generated antihydrogen increases by about 31%. This result comes from the focusing of the slowest Ps on the antiprotons with a focal length which corresponds to the distance between the electrodes and the centre of the Penning trap.

The electrodes design has been chosen as similar to two electrostatic lenses (see Figure 8.3), the first one focuses the low-field seeking states ($k > 0$) and defocuses the high-field seeking states ($k < 0$), the second one defocuses the low-field seeking states ($k > 0$) and focuses the high-field seeking states ($k < 0$). The net effect is a focusing effect. Using only one lens would give no advantage if the quantum number k has a flat distribution between the Rydberg level n-1 and –(n-1), in our case 24 and -24.

The effect of the magnetic field of 1T in the area of the experiment has been ignored in calculating the trajectory of the positronium atoms.

8.1   Simulation description

The program simulates the creation of ortho-positronium atoms from a suitable target and their excitation by a laser beam composed by two laser pulses [43], following them until they reach the antiproton cloud. Each Ps is followed in his trajectory with a time step of 1 ns. The possible ionization due to Rydberg atoms interactions of electric dipole is taken into account as well as laser efficiency and life time of excited states.

The simulation has been run with the following geometrical data, which correspond to the layout of the experiment:

- the positron beam has a diameter of 0.2 cm,

- the target is a square with a side of 1 cm, slanted at 30 degrees with respect to the positron beam,

- the antiproton cloud is 0.8 cm long with a diameter of 0.2 cm and is centered under the target at a distance of 2 cm,

- the laser beam has a diameter of 0.3 cm, its center is located on the vertical axis between the center of the target and the center of the antiproton cloud, with a distance of 0.05 cm between the border of the beam and the surface of the target, in order not to damage it.

The layout of the experimental apparatus is represented in Figure 4.1, in which the laser beam is orthogonal to the plane of the figure (parallel to the x axis).

The physical data used in the program are the following:

- 1 million Ps atoms generated from the target

- flat distribution of the emission time of Ps from the target in an interval of 20 ns (duration of the positron bunch),

- uniform distribution of the emission direction of Ps over half of the solid angle,

- Gaussian distribution of the emission point of Ps from the target in the area covered by the incoming positrons, with the maximum in the center of the target and $\sigma = 0.05 cm$,

- velocity distribution of the Ps taken from the data [40] for a cloud temperature of 145K (see Figure 2.8), called "Trento" velocity,

- two simultaneous laser pulses 5 ns long, with a starting time optimized for maximum production of antihydrogen given the velocity distribution (76 ns after the beginning of the positron bunch),

- laser efficiency 20%,

- final excitation level of Ps n=25, l=2 with a natural decay time of 16.5 μs,

- ionization probability computed for every nanosecond the time to come together according to the formula 4.1,

- cross-section to produce antihydrogen computed in the Aegis proposal for n=30

The layout of the electrodes on the x-y plane of AEGIS and their voltages in shown in the Figure 8.1. Figure 8.2 shows the layout in space.
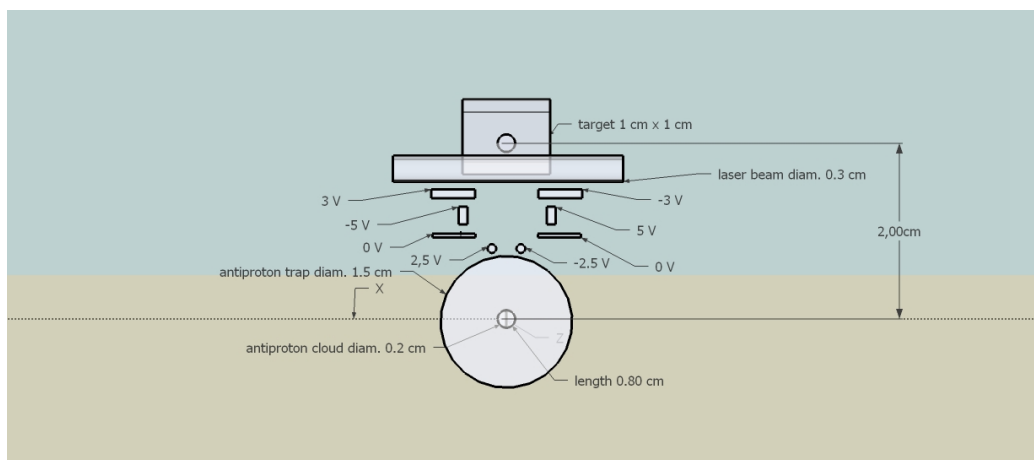
Figure 8.1: Layout of the electrodes on the x-y plane

The four electrodes at the top create the "valley" of the electric field to focus the $k > 0$ Ps, the two wires at the bottom create the "hill" to focus the $k < 0$ Ps, the two electrodes in the middle with 0 voltage isolate the two parts. The voltages do not change in time (see Figure 8.3).

The curves of constant electric field ranging from 0.25 V/mm to 3 V/mm in steps of 0.25 V/mm are shown in the Figure 8.3 obtained with Simion.

The electric field strength along the z-axis and along the x-axis in the lowest and highest point on the z-axis are shown in Figures 8.4,8.5.

The distribution of the field in the two points is such as to obtain a focusing and defocusing of $k > 0$ and $k < 0$ Ps.

The force acting on the Ps has been calculated with the Stark effect formula 8.1. Simion simulation has been obtained with a program written in LUA which takes account of this formula.

Figure 8.6 represents Simion output for a group of 9 Ps emitted from the target and directed vertically (angle $90°$ to the z-axis) on the antiprotons with a slight fan angle with the y-axis, with a velocity of 12 mm/μs and k =24 and -24 respectively. The focusing and defocusing of the electric field can be seen.
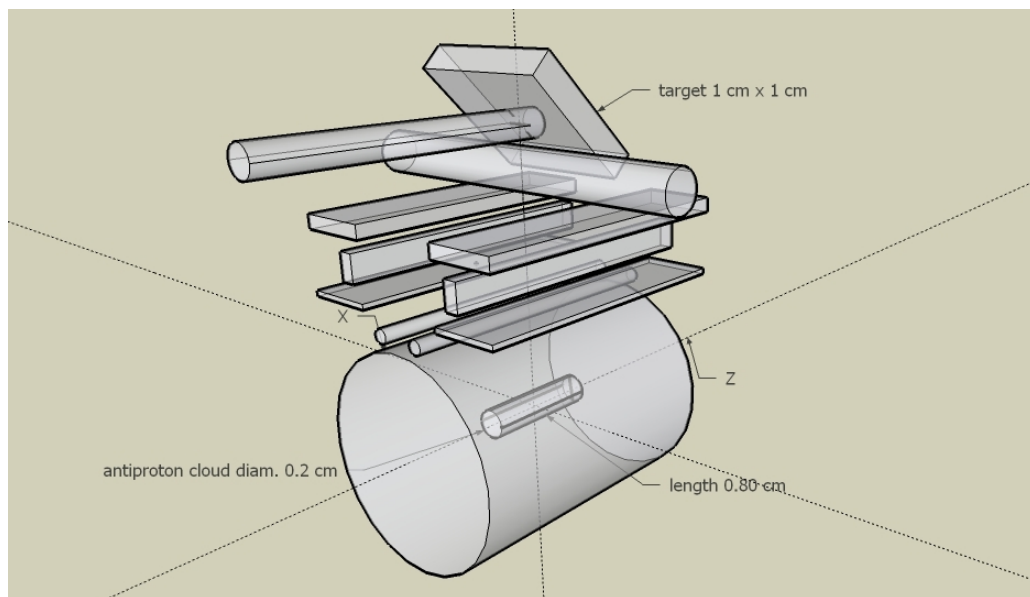
Figure 8.2: Layout of the electrodes in space

8.2   The results of the simulation

The laser beam has been turned on 48 nanoseconds after the beginning of the positron bunch for 5 ns for the "Trento" velocity, 76 nanoseconds for the reduced velocity.

A certain number of Ps, which would have arrived to the antiprotons without the electric field, are defocused. The numbers are given for 10^6 Ps atoms.
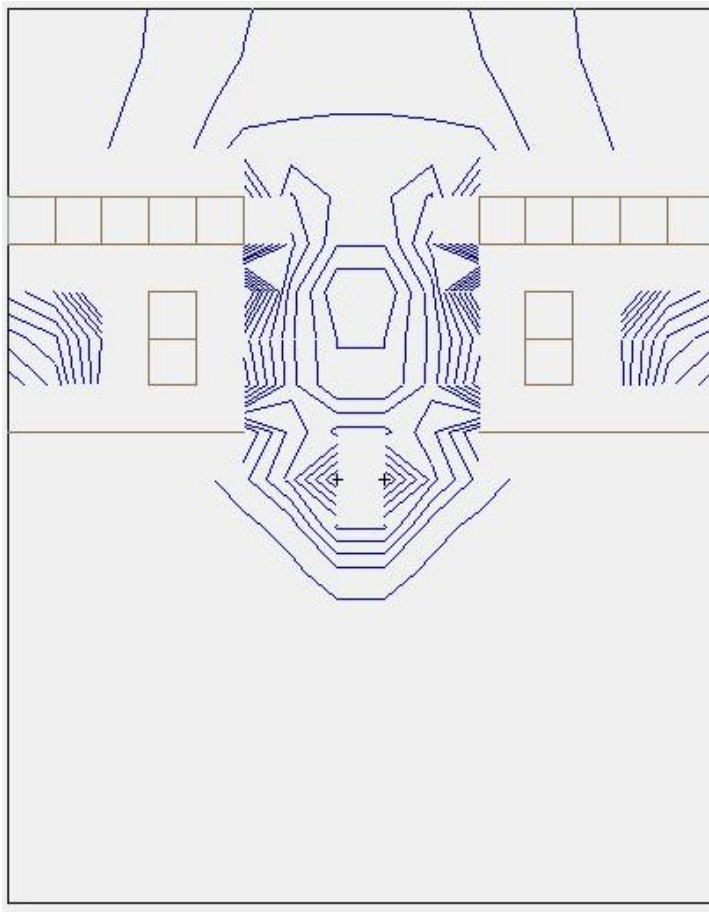
Figure 8.3: Electrodes in grey and electric field strength curves in black (see dimensions in Figure 8.2). The horizontal axis is the x axis, the vertical axis is the y axis.
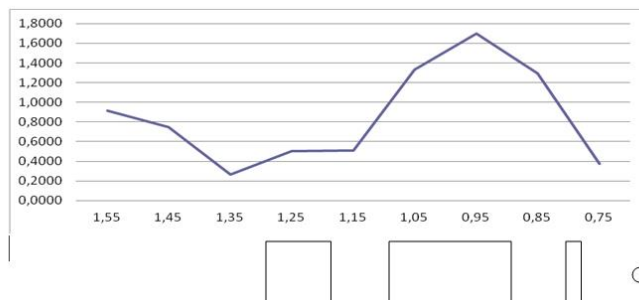
Figure 8.4: Electric field strength in V/mm along y-axis at z=0 cm and x=0 cm, underneath the position of the electrodes
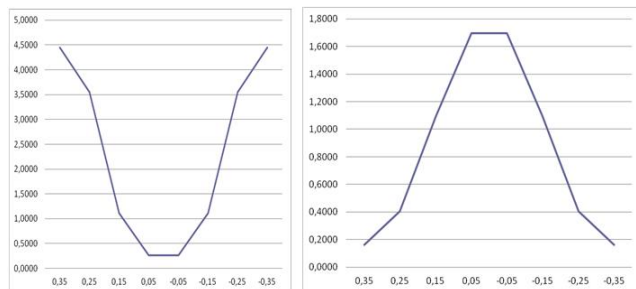
Figure 8.5: Electric field strength in V/mm along x-axis at y=1.35 cm and y=0.95 cm
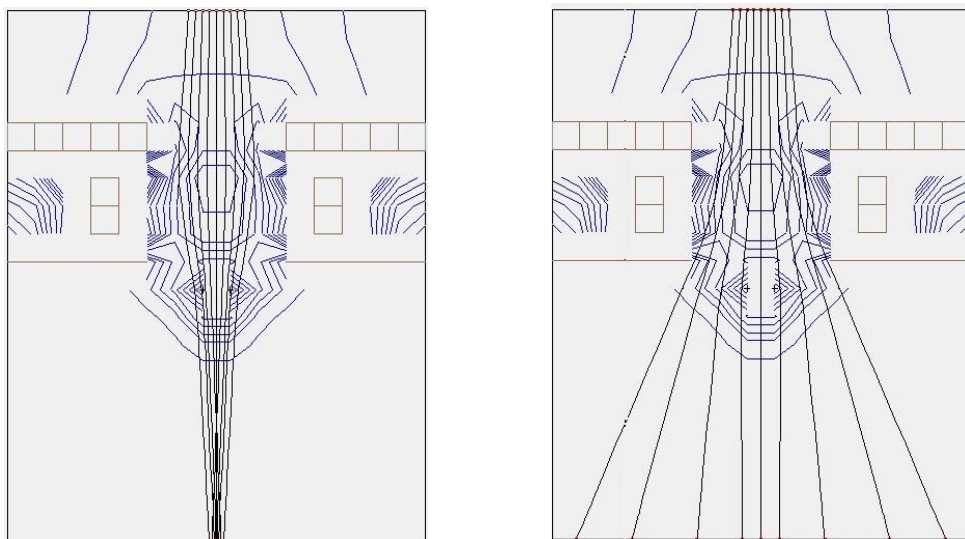
Figure 8.6: Trajectories of Ps with k = 24 (left) and k = -24 (right). The antiproton cloud is at the bottom, the target at the top (see Figure 8.2).

	no electric field Trento velocity	no electric field 1/10 Trento velocity	electric field 1/10 Trento velocity
Laser delay ns	48	76	76
Ps which exit from the target	1,000,000	1,000,000	1,000,000
Ps which cross antiprotons geometrically	6,471	6,471	6,471
Ps which arrive to antiprotons excited by laser	380	338	392
- thanks to the electric field	0	0	68
Increase factor	0	0	21%
Ps which have been defocused	0	0	14
Generated antihydrogen atoms	**0.03**	**0.13**	**0.17**
Increase factor			**31**%

Table 8.1: Schema of the results of the simulation. Trento velocity is the velocity distribution of Figure 4.2 taken from [40]

Simulation of the production of antihydrogen with a Ps transmission target in different positions

At the beginning of 2015 Politecnico di Milano in Como, which is a member of the AEGIS collaboration, started studying a transmission target that could substitute the reflector manifactured by Trento University and used until then.

Compact SiO$_2$/Mesoporous SiO$_2$/Compact SiO$_2$ (parabolic shape)
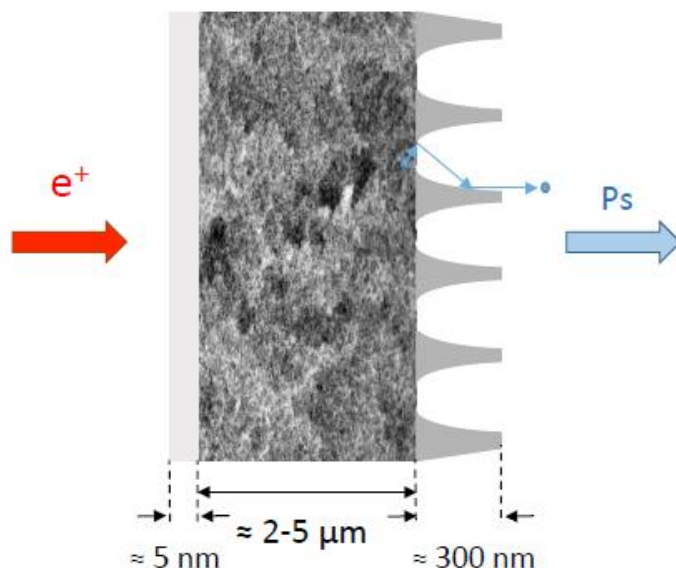
Figure 9.1: Sketch of the design of the positron/positronium transmission target [63]

A transmission target is different from the reflection target planned in the Aegis experiment. Ps exit from the opposite side of the target in relation to impinging positrons (see Figure 9.1).

A transmission target could be located in the antiprotons trap and so would be much nearer to the cloud than the reflector target, with the consequence of increasing for geometrical reasons the number of Ps interacting with antiprotons and consequently the quantity of antihydrogen. Another advantage of the transmission target would be the possibility to direct the emitted Ps normally to its surface depositing on the surface

where the positrons arrive a nanometric thin compact layer of SiO$_2$ and on the other a nanometric mask with parabolic shape channels.

The SiO$_2$ compact layer will be likely deposited with molecular beam epitaxy technique. The function of this layer is to reduce Ps reflection emission so as to enhance Ps emission in vacuum in transmission geometry. A SiO$_2$ parabolic mask will be deposited using 3-D printer technology and will steer Ps atoms [76].

To support his proposal at a collaboration meeting at the beginning of 2015, I modified my simulation program to evaluate the number of antihydrogen atoms that the new layout could produce.

The proposed geometry was to direct the positron beam in the antiproton trap at 3 mm from the axis and to place the target at a low angle with the axis. The surface of the target could be manufactured in such a way to direct most emitted Ps perpendicularly to the surface (see Fig. 9.2, 9.3).

In this case the laser beam would be located between the target and the antiproton cloud on the median of the target with a reduced diameter of the spot of 0.08 cm to fit between the target and the antiproton cloud. The target would be set at a chosen potential not to disturb the electric field in the trap. The way to let the laser beam enter the trap had not yet been studied.

The simulation program was modified to generate 1 million Ps in a random direction or perpendicularly to the target taking into account the new position of the target and the laser beam.

The possibility to double the laser beam through reflection, simulating two parallel laser beams at the same distance from the target was considered (see Figure 9.4.
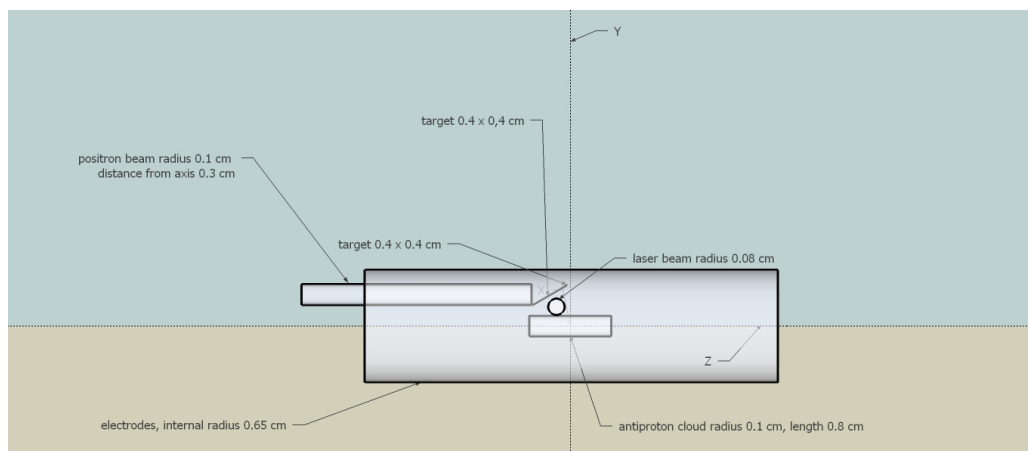
Figure 9.2: Transmission target with one laser beam (y z plane)

The results are represented in Figure 9.5. They were compared with the actual layout and the reflector target with one or two laser beams already shown in Table 6.1.

The quantity of antihydrogen atoms generated with the transmission target was considered satisfactory for 10 million Ps (188) in comparison with the very low number of the actual layout (1).
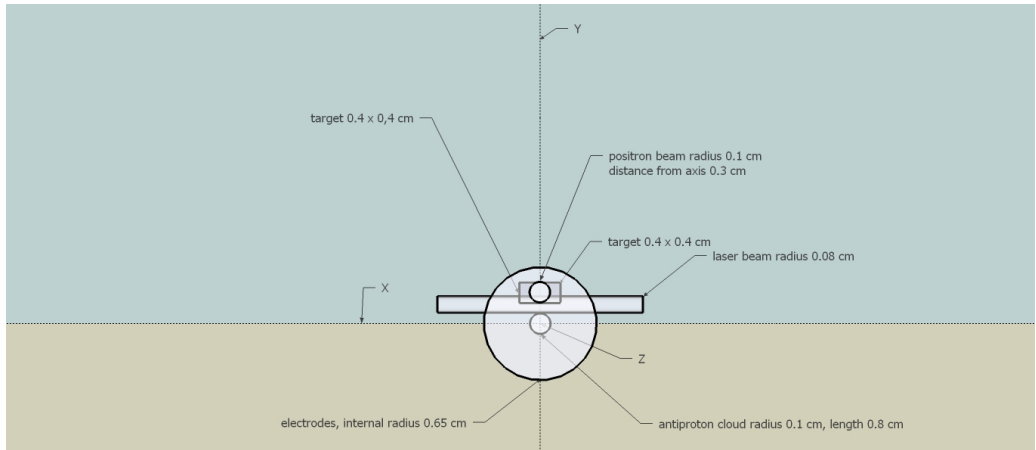
Figure 9.3: Transmission target with one laser beam (x y plane)
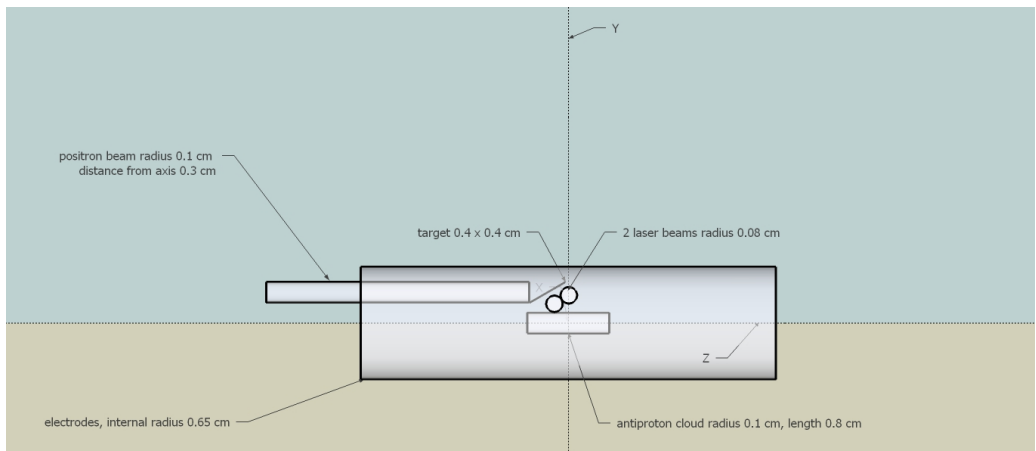
Figure 9.4: Transmission target with two laser beams (y z plane)

	actual layout	reflector with one laser beam	reflector with two laser beams	transmission target with Ps random emission	transmission target with Ps normal emission	transmission target with Ps random emission and two laser beams	transmission target with Ps normal emission and two laser beams
Ps which exit from the target	1,000,000	1,000,000	1,000,000	1,000,000	1,000,000	1,000,000	1,000,000
Laser delay ns	45	180	185	30	30	30	30
Laser spot radius cm	0.15	0.15	0.15	0.08	0.08	0.08	0.08
Distance between target center and antiprotons cloud center cm	2	2	2	0.36	0.36	0.36	0.36
Ps which cross antiprotons without reflection	6,443	6,443	6,443	171,296	1,000,000	171,296	1,000,000
Ps which cross antiprotons with reflection		336,701	336,701				
Ps which arrive to antiprotons excited by laser without reflection	279	10	16	3,943	26,105	4,996	37.914
Ps which arrive to antiprotons excited by laser with reflection		481	829				
Generated antihydrogen atoms	0.1	0.2	0.4	1.5	12.6	2.0	18.8
Increase factor		94%	252%	1,168%	10,160%	1,535%	15,221%
Multiplication factor		1.9	3.5	12.7	102.6	16.3	153.2

Figure 9.5: Results of the simulation with a transmission target

Verification of the calculations of the Genova group on antihydrogen production

In the following weeks the Genova group verified my Monte Carlo simulation with semi-analytical calculations and analysis. The results were sent to the collaboration on March 10, 2015 [62].

They used the following parameters. The distance between the center of the trap and the center of the antiproton cloud was assumed to be 1.53 cm. The shape of the cloud was an ellipsoid with semiaxis 1.5 mm and 10 mm.

The number of positrons available in the accumulator every 360 s (corresponding to 3 AD cycles) was 1.3×10^8.

The efficiency of recatching the positrons in the off axis trap after the excitation of the diocotron mode $\epsilon_{e+}^{recatch}$ was assumed equal to 0.66.

The time length of the pulse of positrons hitting the target was 70ns with flat distribution.

The fraction of positronium passing through the grid on top of the production trap f_{grid} was assumed equal to 0.79 (calculated with a tracking code).

The fraction of atoms that are excited by the lasers f_{laser} was assumed equal to 0.4.

The fraction of Rydberg positronium atoms with velocity below about 10^4m/s was assumed equal to 0.1, reducing this number by 2/3 because of the magnetic field quenching.

The velocity distribution of Ps exiting from the target was assumed a Maxwell distribution with T = 75 K.

The medium cross section was assumed as 4×10^{-10}cm^2, according with Figure 5.1 taken from the Aegis proposal for n=20.

The conclusion of the verification was that the number of antihydrogen atoms generated was 3 for 360s (3 AD cycles).

In the following weeks I modified my program to run the Monte Carlo simulation on the same assumptions of the Genova group.

On June 12, 2015 I sent a note to the collaboration [56] *"Antihydrogen formation: the Monte Carlo simulation (comparisons with the Genova estimate and a new velocity distribution)"*.

In several places, I updated some of the parameters (like the number of available antiprotons) to match the values suggested by the Genova report.

In other places, however, I kept the physical processes in my Monte Carlo realizing that the Genova group had made different choices. I believed my choices were motivated and commented on the effect of different choices made by Genova and by myself on the final result.

In the last version of the Monte Carlo code, I made an important change regarding the velocity distribution of the emitted Ps. I retained the "Trento" distribution for the longitudinal (Ps emission) component, while I used the "Cassidy et al." thermalization assumption for the transverse component [64].

This amounted to assuming thermalization in the transverse direction, which introduced important changes in the final antihydrogen production numbers due to the focusing of Ps emission in the normal direction to the target.

In this simulation I therefore assumed a full transverse thermalization of Ps at the 4 K liquid-He temperature. In addition, I also assumed that for the longitudinal distribution, the same thermalization fraction holds from the 145 K measured down to 4 K.

Note that the thermalization temperature of 4 K is of the same order of the lowest temperature (approximately 1K) allowed by the uncertainty principle applied on the lowest transverse energy level (free kinetical motion) of Ps in the 6 -10 nm nanopores of the Ps converter.

To take full advantage of this focalization I moved the target 0.72 cm to the right in z axis direction to have the maximum amount of Ps in the center of the antiproton cloud and placed the axis of the laser beam on the median to the target, which points to the center of the antiproton cloud. This was a change with respect to the AEgIS nominal geometry.

10.1 The geometry

The layout used is shown in Figure 10.1. There were a few modifications that I made to match the values of the parameters suggested by the Genova report.
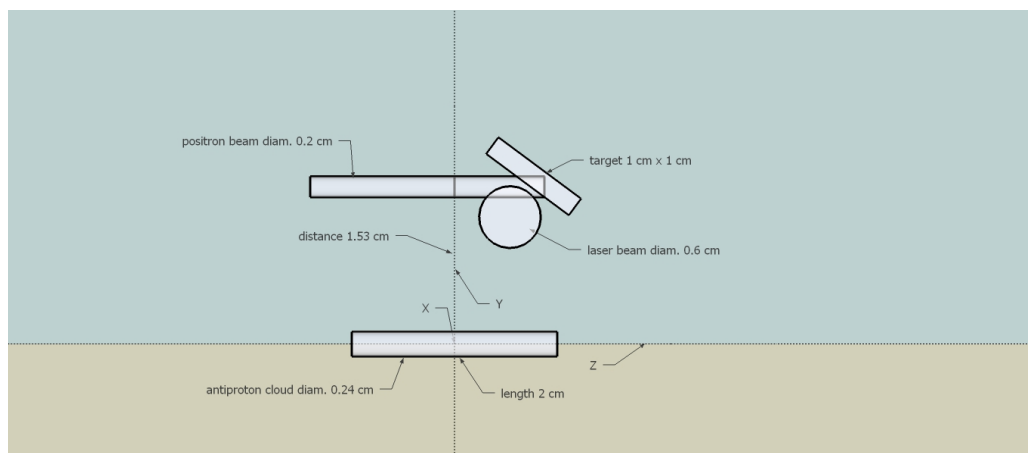
Figure 10.1: Layout of the experiment for transverse thermalization

First of all, the distance between the center of the target and the antiproton cloud on the y axis was 1.53 cm (while I used 2 cm in previous versions of my simulation). As the target was moved 0.72 cm to the right the distance between the center of the target and the center of the antiproton cloud was now 1.69 cm.

In addition, my antiproton cloud cylinder was changed (from the original 0.8 cm length, 0.10 cm radius) to the value of 0.12 cm radius and 2 cm length. This geometry had the same volume and length as the ellipsoid in the Genova report.

As far as the Ps formation is concerned, I made the following assumption about the efficiency: I assumed that – given a certain number of e^+ impinging on the converter, 27% of the impinging e^+ gets out as positronium. This is the efficiency measured in the Trento converters.

For what concerns the velocity of the Ps, I made the following assumptions about the longitudinal and transverse components:

Longitudinal: I assumed that 2.5% (of the total e^+ number) has a Boltzmann mono-dimensional distribution at 4 K. The remaining 24.5% has a 1250 K Boltzmann distribution. I stressed that these two numbers sum up to 27% of the total positron bunch number (see Figure 10.2 left).

Transverse: I assumed a radial velocity Boltzmann distribution with temperature 4 K (see Figure 10.2 right). The combination of the two distributions gave a focalization of the emitted Ps in the normal direction to the target surface (see Figure 10.3).
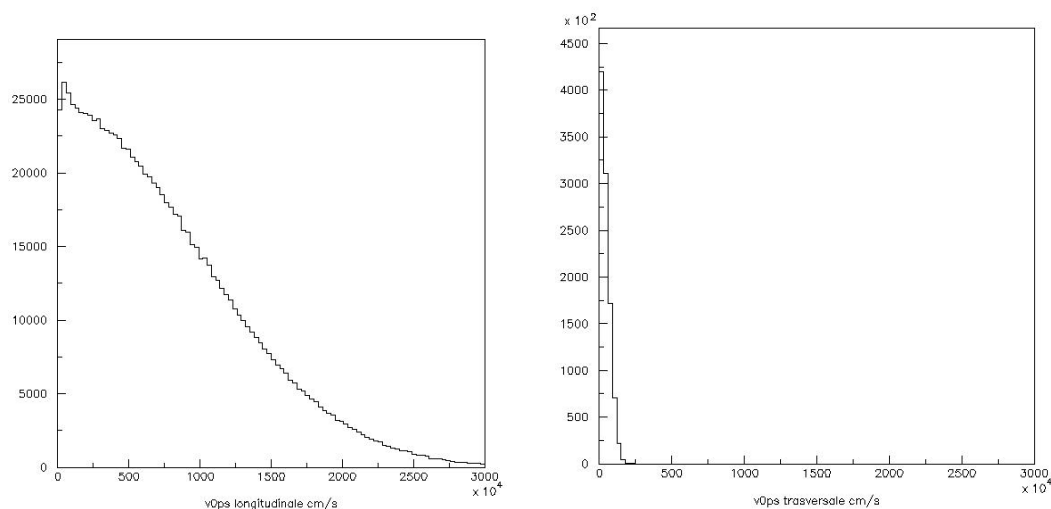
Figure 10.2: (Left) Longitudinal velocity distribution at 4K. (Right) Transverse velocity distribution at 4K

The direction of the Ps was chosen according to the combination of longitudinal and transverse velocities.

The effect of choosing the 3D Boltzmann distribution (Genova report) as opposed to the cylindrical symmetric one (my choice) actually decreased the number of formed antihydrogen, by diminishing the fraction of slow Ps atoms that have a high charge-exchange reaction cross section. So, this seems a pessimistic choice by the Genova group.

The Monte Carlo distribution of the emission time of Ps from the target was assumed to be flat in an interval of 70 ns, in agreement with the Genova assumption and in an interval of 20 ns. A million Ps were simulated as exiting the target. The results were finally scaled up to match the number of Ps assumed by the Genova group (more on this below).

The laser beam, assuming saturation of the transitions, was simulated with a Gaussian shape of the laser excitation efficiency from 0 to 40% with a width (HWHM) of 0.3 cm at 20% (see Figure 10.4).

The axis of the laser beam was at a distance of 0.35 cm from the center of the target
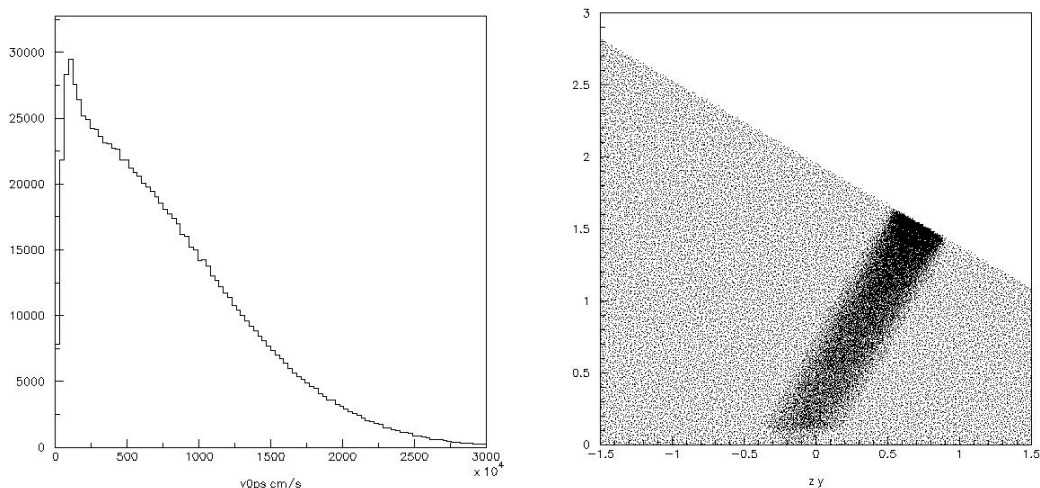
Figure 10.3: (Left) Resulting velocity distribution at 4K. (Right) Trajectories of Ps on the z y plane at 4K

to allow a distance of 0.05 cm between the laser beam with radius 0.3 cm and the target. It was on the normal to the surface of the target. The laser was on for a time interval of 1.5 ns.

The number of antihydrogen atoms generated from 1 million Ps was multiplied by 85.8 to match the number used in the Genova report. See the table at the end of the report.

The number of generated atoms was then reduced to account for the grid of a factor 0.79 as indicated in the Genova report. This factor was never included before in my Monte Carlo.

Here are the numbers of antihydrogen atoms produced in the various simulations.

1. Genova calculation with a positron pulse length of 70 ns : 3 atoms

2. Monte Carlo simulation with the same layout as Genova: 4 atoms

3. Monte Carlo simulation with transverse thermalisation at 145K: 28 atoms

4. Monte Carlo simulation with transverse thermalisation at 4K: 104 atoms

5. Same with a positron pulse length of 20 ns: 110 atoms

6. Transmission target with Ps normal emission and 2 lasers: 112 atoms

10.2   Monte Carlo description

The program is a full one-by-one atom Monte Carlo that simulates the creation of ortho-positronium atoms from a suitable target and their excitation by a laser beam composed by two laser pulses, following them (by tracing) until they reach the antiproton cloud. Each Ps is followed in his trajectory with a time step of 1 ns. The possible ionization
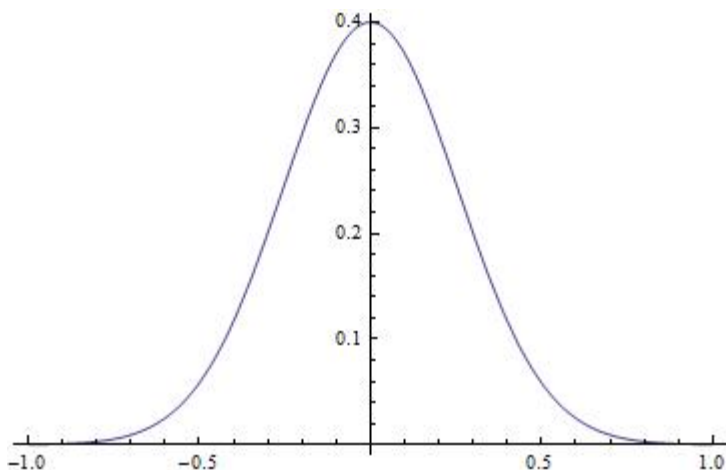
Figure 10.4: Laser efficiency vs distance from the axis in cm

due to Rydberg atoms interactions of electric dipole is taken into account as well as laser efficiency and life time of excited states.

To summarize, the physical inputs to this configuration of the Monte Carlo are:

- 1 million Ps atoms generated from the target (then scaled to the Genova numbers)

- 1/3 of the Ps with a lifetime of 7 ns (ms=0), due to magnetic quenching, 2/3 with a lifetime of 142 ns ($m_s \pm 1$)

- flat distribution of the emission time of Ps from the target in an interval of 70 ns or 20 ns (duration of the positron bunch),

- Gaussian distribution of the emission point of Ps from the target in the area covered by the incoming positrons, with the maximum in the center of the target and $\sigma = 0.05cm$,

- module of velocity distribution of the Ps taken with a longitudinal distribution of 9% at 145 or 4K and 91% of 1260K and a transverse distribution of 145 or 4 K,

- distribution of the emission direction of Ps over half of the solid angle according to the combination of the longitudinal and transverse velocity distribution,

- laser efficiency 40% with the rectangular shape, from 0 to 40% with the Gaussian shape with a width of 0.3 cm at 20%, laser pulse length 1.5 ns,

- final excitation level of Ps n=25, l=2 with a natural decay time of $16.5\mu s$,

- ionization probability computed for every nanosecond the time to come together according to the formula 4.1 taken from [59],

- cross-section to produce antihydrogen computed in the Aegis proposal for n=20 for every simulated Ps according to its velocity,

- 10^5 antiprotons in a cylinder of length 2 cm and radius 0.12 cm,

- number of generated antihydrogen atoms derived from the cross section, the antiprotons density and the length of the path of each Ps in the antiproton cloud (medium length 0.2 cm).

For the transmission geometry only the longitudinal distribution has been considered as the transverse velocity is unknown. The emission direction has been considered in its best hypothesis, that is normal to the target with two parallel laser beams. The radius of the laser beam has been reduced to 0.08 cm, the parallel laser beams have a distance of 0.16 cm.

10.3   The results of the simulation

The table 10.6 shows the results of the simulation for the various cases:

1. Genova calculation with a positron pulse length of 70 ns

2. Monte Carlo simulation with the same layout as Genova (see Figure 10.5)

3. Monte Carlo simulation with transverse thermalisation at 145K

4. Monte Carlo simulation with transverse thermalisation at 4K

5. Same with a positron pulse length of 20 ns

6. Transmission target with Ps normal emission and 2 lasers
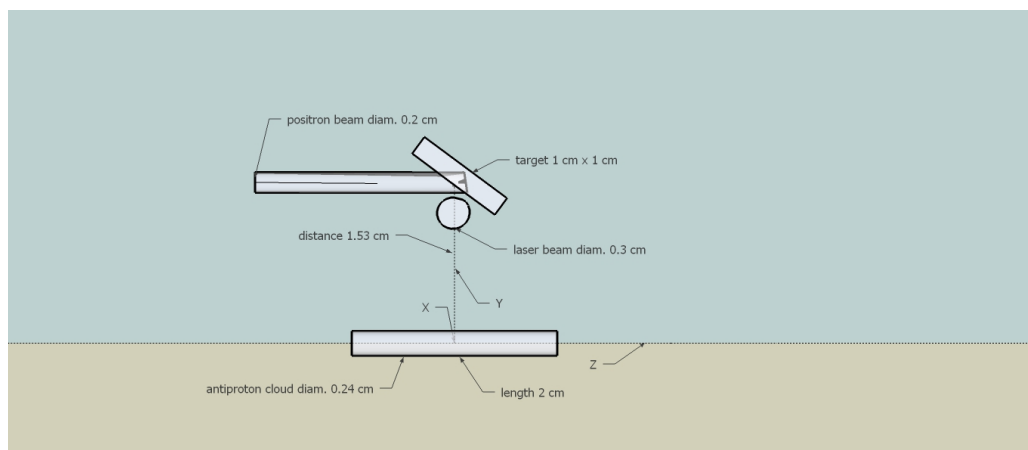
Figure 10.5: Genova layout

The results of my Monte Carlo study matched the results of the Genova report when the Genova parameter numbers were used. This was however a coincidence that came from mutual cancellation effects deriving from two different choices on simulation of the following physics processes:

1. Genova used a 3-D Boltzmann distribution, while I used the basic 1-D as the integration over the space dimensions is automatically produced by the Monte Carlo procedure of extracting the directions. This has the effecting of increasing my antihydrogen results with respect to the Genova evaluation.

2. Genova assumed that all the e^+ gets converted to Ps (efficiency 1), while I used 0.1. This has the effect of increasing the Genova evaluation by an order of magnitude.

3. Both in my Monte Carlo and in the report by Genova we had (incorrectly) assumed that all the Ps is thermalized at the "cold" 75 K component.

Aegis antihydrogen production	1.Genova	2. MC	3. MC	4. MC	5. MC	6. MC (Ferragut)
Ps temperature distribution	75K	9% 145K– 91% 1260K				9% 145K– 91% 1260K
Ps longitudinal temperature dist.			9% 145K - 91% 1260K	9% 4K - 91% 1260K	9% 4K - 91% 1260K	
Ps transverse temperature dist.			145K	4K	4K	
Number positrons on converter	1.3E+08	1.3E+08	1.3E+08	1.3E+08	1.3E+08	1.3E+08
e+ pulse length ns	70	70	70	70	20	70
laser beam delay ns	100	105	75	100	40	70
$\epsilon_{e+}^{recatch}$	0.66	0.66	0.66	0.66	0.66	0.66
useful positrons	8.58E+07	8.58E+07	8.58E+07	8.58E+07	8.58E+07	8.58E+07
Ps exiting from the target	8.58E+07	8.58E+07	8.58E+07	8.58E+07	8.58E+07	8.58E+07
f_{grid}	0.79	0.79	0.79	0.79	0.79	0.79
generated antihydrogen atoms	3	14.9	102.4	384.3	408.7	1119.3
efficiency of Ps production in the target	1	0.27	0.27	0.27	0.27	0.10
generated antihydrogen atoms considering target efficiency	**3**	**4**	**28**	**104**	**110**	**112**
medium cross section n=20	4.00E-10	1.13E-09	2.03E-10	2.63E-10	2.26E-10	5.58E-10

Figure 10.6: Simulation results: 1. Genova calculation with a positron pulse length of 70 ns, 2. Monte Carlo simulation with the same layout as Genova, 3. Monte Carlo simulation with transverse thermalisation at 145K, 4. Monte Carlo simulation with transverse thermalisation at 4K, 5. Same with a positron pulse length of 20 ns, 6. transmission target with Ps normal emission and 2 lasers

In the new simulation with the correct velocity distribution of the Ps, 9% at 145K and 91% at 1260K, I applied the production efficiency of Ps in the target of 27%.

The result was the production of still 4 atoms of anti-hydrogen because the number of atoms have decreased due to the increased velocity and the following decreased cross section but the production efficiency has increased because I also consider the production of fast Ps from the target.

In presence of transverse thermalization effects, the number of generated atoms depends strongly on the temperature. Unfortunately we have some experimental data only for room temperature (at CERN). We also don't know whether the percentage of 9% of

longitudinal thermalisation measured at 145K is valid at 4K. So the results at 4K were not confirmed by any measure.

If they are confirmed the actual AEGIS layout would almost produce the needed beam to measure gravity, 110 antihydrogen atoms in 200 seconds. It is approximately the same amount of the transmission target in the best hypothesis of 2 laser beams and Ps normal emission.

Finally, it has however to be recalled that my Monte Carlo code did not take into account at the time the presence of the 1 tesla magnetic field.

Simulation of the production of antihydrogen with a Ps transmission target in vertical position on axis

In the Lyon collaboration meeting of July 18-19, 2015 it was proposed to generate Antihydrogen on axis with a vertical transmission target that can move sidewards to let antiprotons pass.

I modified my program to simulate this layout and compare the number of generated Hbar with the transmission layout [63], later published in [76], and with the standard reflection layout analyzed by the Genova group [62] and confirmed by the Monte Carlo simulation with my report of June 12, 2015 [56].

The program starts by considering a stationary antiproton cloud and modeling the emission of Ps from the experimental target. Since the program follows the Ps atoms one-by-one with a tracing procedure in time-steps of 1 ns, it is easily suitable to generalizations and inclusions of other physical processes. The main simplification used in the program was the approximation that the 1 tesla magnetic field would not influence the formation of Hbar (i.e. the dynamics of the charge-exchange reaction) other than quenching part of the ortho-Ps. The magnetic field effect was added afterwards.

11.1 The geometry

The layout used is shown in Figure 11.1.
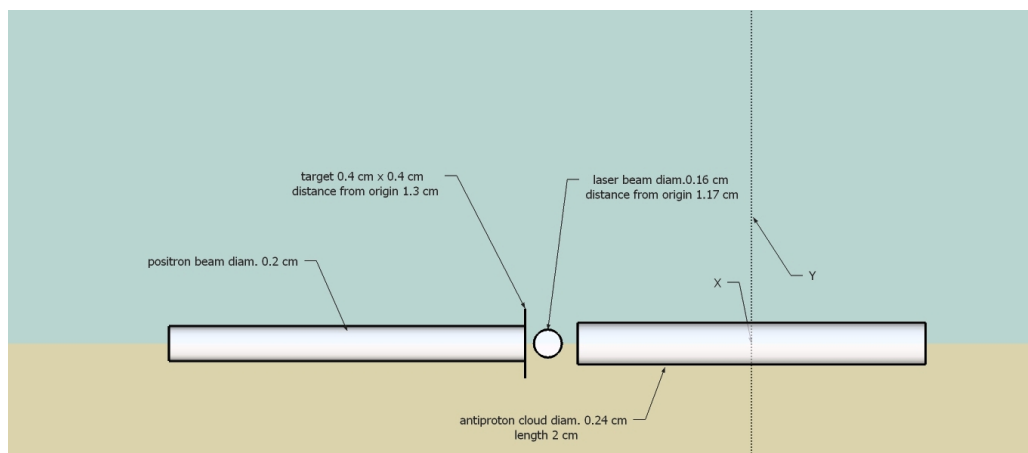
Figure 11.1: Simulated layout of the experiment with a vertical transmission target

The antiproton cloud cylinder has a 0.12 cm radius and 2 cm length. This geometry has the same volume and length as the ellipsoid in the Genova report.

The vertical target is at a distance of 1.3 cm from the origin, that is 0.3 cm from the beginning of the antiproton cloud. The laser beam diameter is 0.16 cm with a Gaussian distribution and the axis is at a distance of 1.17 cm from the origin to maintain a minimal distance of 0.05 cm from the target and allow to insert before the antiprotons cloud two grids.

The first should be positively polarized to reflect the re-emitted positrons and the second set at a negative potential to repel the secondary electrons, with the same potential of the first electrode of the antiproton trap to have a region with no electric field after the grid. [79]. This way ground-state o-Ps could cross the two grids without being affected by the electric field. The quantity of positrons and electrons will depend on the type of transmission target that is being studied by AEGIS Collaboration [76] [78].

Two simulations have been done:

1. Isotropic emission of Ps from the target

2. Normal emission of Ps from the target along the z axis

In both cases the assumed velocity distribution of Ps is the one of the Trento group with 9% at 145K and 91% at 1260K for comparison with the results of the other layouts. No transversal thermalisation has been assumed for the moment as the characteristics of the transmission target that will be used are still unknown.

As far as the Ps formation is concerned, I have made the following assumption about the efficiency: I have assumed that 10% of the e^+ impinging the converter gets out as Ps. This is the efficiency indicated by Ferragut in his presentation in February and estimated for similar targets in other works [65, 66].

The Monte Carlo distribution of the emission time of Ps from the target was assumed to be flat in an interval of 20 ns. A million Ps have been simulated as exiting the target. The results were finally scaled up to match the number of Ps assumed by the Genova group.

The laser beam, assuming saturation of the transitions, has been simulated with a Gaussian shape of the laser excitation efficiency from 0 to 40% with a width (HWHM) of 0.8 cm at 20%. The laser is on for a time interval of 1.5 ns.

The assumed number of positrons is 1.3×10^8.

Here are the numbers of antihydrogen atoms produced in the two simulations:

1. Vertical transmission target with Ps random emission: 11 atoms

2. Vertical transmission target with Ps normal emission: 1105 atoms

   Here are the numbers of antihydrogen atoms produced in the previous simulations (see report of June 12, 2015 [56]):

3. Genova calculation with a positron pulse length of 70 ns : 3 atoms

4. Monte Carlo simulation with the same layout as Genova (Figure 10.5): 4 atoms

5. Monte Carlo simulation with transverse thermalisation at 145K: 28 atoms

6. Monte Carlo simulation with transverse thermalisation at 4K (Figure 10.1): 104 atoms

7. Same with a positron pulse length of 20 ns: 110 atoms

8. Transmission target with Ps normal emission and 2 lasers (Figure 9.4): 112 atoms

With random emission the vertical target is not much better than the reflection target because of the limited solid angle of the antiproton cloud cross section.

There is a factor 100 between random emission and normal emission, due to the fact that in the second case all the Ps can geometrically hit the antiprotons and that the distance travelled inside the cloud is the whole length of 2 cm.

The real effect can be smaller because I have simulated a cloud with a cylindrical shape while the actual shape is an ellipsoid.

The possibility of normal emission of Ps from the target depends on the transverse thermalisation and on the possibility to superimpose a special profile on the target to direct the emission of Ps in the forward direction.

An article on the characterization of a transmission target has been published by the AEGIS collaboration in May 2017 after my simulations [76]. The article concludes that this type of target is promising for antihydrogen production with around 10% of o-Ps formed but that is has to be improved to reach the same number of Ps (20%) and temperature produced by reflection targets. A set of polarized grids with high transmission coefficients has to be placed between the target and the antiproton cloud to deviate positrons (around 10% of implanted positrons) and secondary electrons (16%) emitted by the target.

11.2   Monte Carlo description

The program is a full one-by-one atom Monte Carlo that simulates the creation of ortho-positronium atoms from a suitable target and their excitation by a laser beam composed by two laser pulses, following them (by tracing) until they reach the antiproton cloud. Each Ps is followed in his trajectory with a time step of 1 ns. The possible ionization due to Rydberg atoms interactions of electric dipole is taken into account as well as laser efficiency and life time of excited states.

To summarize, the physical inputs to this configuration of the Monte Carlo are the same as in the previous chapter:

- 1 million Ps atoms generated from the target (then scaled to the Genova numbers)

- 1/3 of the Ps with a lifetime of 7 ns (ms=0), due to magnetic quenching, 2/3 with a lifetime of 142 ns ($m_s \pm 1$)

- flat distribution of the emission time of Ps from the target in an interval of 20 ns (duration of the positron bunch),

- Gaussian distribution of the emission point of Ps from the target in the area covered by the incoming positrons, with the maximum in the center of the target and $\sigma = 0.05 cm$,

- module of velocity distribution of the Ps taken with a distribution of 9% at 145 or 4K and 91% of 1260K,

- distribution of the emission direction of Ps over half of the solid angle,

- laser efficiency 40% with the rectangular shape, from 0 to 40% with the Gaussian shape with a width of 0.08 cm at 20%, laser pulse length 1.5 ns,

- final excitation level of Ps n=25, l=2 with a natural decay time of 16.5 μs,

- ionization probability computed for every nanosecond the time to come together according to 4.1 formula taken from [59],

- cross-section to produce antihydrogen computed in the Aegis proposal for n=20 for every simulated Ps according to its velocity,

- 10^5 antiprotons in a cylinder of length 2 cm and radius 0.12 cm,

- number of generated antihydrogen atoms derived from the cross section, the antiprotons density and the length of the path of each Ps in the antiproton.

11.3   The results of the simulation

The result of the simulation is described in Figure 11.2. The comments of the result are in paragraph 11.1.

Aegis antihydrogen production	1. MC	2. MC	3. Genova	4. MC	5. MC	6. MC	7. MC	8. MC
Ps temperature distribution	9% 145K–91% 1260K	9% 145K–91% 1260K	75K	9% 145K–91% 1260K				9% 145K–91% 1260K
Ps longitudinal temperature dist.					9% 145K - 91% 1260K	9% 4K - 91% 1260K	9% 4K - 91% 1260K	
Ps transverse temperature dist.					145K	4K	4K	
Number positrons on converter	1.3E+08	1.3E+08	1.3E+08	1.3E+08	1.3E+08	1.3E+08	1.3E+08	1.3E+08
e+ pulse length ns	20	20	70	70	70	70	20	70
laser beam delay ns	60	30	100	105	75	100	40	70
$\epsilon_{e+}^{recatch}$			0.66	0.66	0.66	0.66	0.66	
useful positrons	8.58E+07	8.58E+07	8.58E+07	8.58E+07	8.58E+07	8.58E+07	8.58E+07	8.58E+07
Ps exiting from the target	8.58E+07	8.58E+07	8.58E+07	8.58E+07	8.58E+07	8.58E+07	8.58E+07	8.58E+07
f_{grid}			0.79	0.79	0.79	0.79	0.79	
generated antihydrogen atoms	107.9	11050	3	14.9	102.4	384.3	408.7	1119.3
efficiency of Ps production in the target	0.1	0.1	1	0.27	0.27	0.27	0.27	0.10
generated antihydrogen atoms considering target efficiency	**11**	**1105**	**3**	**4**	**28**	**104**	**110**	**112**
medium cross section n=20	5.36E-10	4,07E-10	4.00E-10	1.13E-09	2.03E-10	2.63E-10	2.26E-10	5.58E-10

Figure 11.2: Schema of the results of the simulation: 1. vertical transmission target with Ps random emission, 2.vertical transmission target with Ps normal emission, 3. Genova calculation with a positron pulse length of 70 ns, 4. Monte Carlo simulation with the same layout as Genova, 5. Monte Carlo simulation with transverse thermalisation at 145K, 6. Monte Carlo simulation with transverse thermalisation at 4K, 7. same with a positron pulse length of 20 ns, 8. transmission target with Ps normal emission and 2 lasers

Simulation of the production of antihydrogen taking into account the 1T magnetic field

My first simulations had not taken into account the 1T magnetic field in the production area, apart from the reduction of lifetime of Ps due to the magnetic quenching (1/3 of the Ps with a lifetime of 7 ns for ms=0 and the remaining 2/3 with a lifetime of 142 ns when $m_s \pm 1$).

In the second half of 2015, I have concentrated my efforts in taking into account the magnetic field in the various experimental layouts that have been proposed and which were included in my report of July 14, 2015. Preliminary results have been presented at the Aegis Collaboration Meeting at CERN on November 23, 2015 and the final report was sent to the collaboration on December 10, 2015 [58].

Among the various layouts, the last one considered is the vertical transmission target, the one which produces more antihydrogen atoms and likely the one that the collaboration will follow in the future.

Contrary to the conclusions of my report of July 14 on the vertical target, the effect of the magnetic field is important if the Ps exits in the normal direction to the target because, even if the Ps direction is parallel to the magnetic field, the plane of the internal rotation of the e^- and the e^+ has a random orientation relative to the magnetic field, as pictured in a classical approach of the dynamics, and as used in my modeling and simulations.

In this chapter the influence of the magnetic field on the motion of a Ps atom is considered, while the charge exchange cross-section has been derived from the AEGIS proposal ignoring the magnetic contribute. In the following chapter I completed the simulations by modifying the cross section to take into account the magnetic field.

12.1   The model

The classical model of Ps motion in a magnetic field has been derived from the article of Peter Schmelcher [67]. The paper deals with the effect of internal motion on center of mass propagation of Ps in various regimes and determines a transition from linearity to a Brownian-like behavior (deconfinement) if internal motion changes from regularity to chaos.

Calculations in the article have been done with a 2.7 T magnetic field. In the 1T field there is no chaotic internal motion.

The Hamiltonian of a neutral particle system in a homogeneous magnetic field possesses a constant of motion, the so-called pseudomomentum K [68]. This pseudomomentum is closely related to the collective motion of the system in the magnetic field and can be used to perform a pseudoseparation of the centre of mass motion.

Starting from the Hamiltonian in Cartesian coordinates the pseudoseparation consists of a canonical transformation which introduces the pseudomomentum and the centre of mass coordinate R_s as a canonically conjugated pair of variables (the other conjugate pair, describing internal motion, being the relative position r and the relative momentum p). The conserved pseudomomentum is defined as:

$$\boldsymbol{K} = \boldsymbol{P} + \frac{e}{2}\,\mathbf{B} \times \boldsymbol{r} \tag{12.1}$$

where P is the center of mass momentum of the Ps.

After the pseudoseparation the Hamiltonian is the following:

$$H = \frac{\boldsymbol{K}^2}{2M} - \frac{e}{M}(\boldsymbol{K} \times \mathbf{B}) \cdot \boldsymbol{r} + \frac{1}{2\mu}\,\boldsymbol{p}^2 + \frac{e^2}{8\mu}(\mathbf{B} \times \boldsymbol{r})^2 + V \tag{12.2}$$

where $M = 2m$ and $\mu = m/2$, m being the electron mass. V is the Coulomb potential.

The second term of the Hamiltonian is the motional Stark term: the atom experiences an induced constant electric field oriented perpendicular to the magnetic field. The fourth term is the quadratic Zeeman effect. The linear Zeeman effect term is missing because the electron and the positron have equal mass and opposite charge. The equations of motion are the following:

$$\dot{\boldsymbol{R}}_s = \frac{1}{M}\,\boldsymbol{K} - \frac{e}{M}(\mathbf{B} \times \boldsymbol{r}) \tag{12.3}$$

$$\dot{\boldsymbol{K}} = 0 \tag{12.4}$$

$$\dot{\boldsymbol{r}} = \frac{1}{\mu}\,\boldsymbol{p} \tag{12.5}$$

$$\dot{\boldsymbol{p}} = -\frac{e}{M}\,(\mathbf{B} \times \boldsymbol{K}) + \frac{e^2}{4\mu}\,\mathbf{B} \times (\mathbf{B} \times \boldsymbol{r}) - e^2\,\frac{\boldsymbol{r}}{|\boldsymbol{r}|^3} \tag{12.6}$$

12.2   The integration method

These equations are integrated with a Runge Kutta method at 5th order with adaptive step (Dormand and Prince). The integration routine is called for a tenth of a nanosecond by the Monte Carlo simulation program when the Ps is excited to n=25.

Initial conditions of the relative e^-/e^+ motion are p = 0.02 a.u. and r = 1250 a.u., corresponding to n=25 and a circular movement of r tangential to the sphere formed by r (1 a.u. = 0.528×10^{-8} cm). The initial point (ϑ, φ) of r, and the orientation (α) of p on the tangential plane are randomized (see Figure 12.1).

The integration routine calculates the position of the center of mass of the Ps a tenth of nanosecond after the start at the initial position. Now, the velocity direction is derived and the new data assumed for the rest of the motion. This is correct because the integration gives a linear trajectory with oscillations for long integration periods and no change in the module of velocity.

The action of the motional Stark term (an induced electric field) can determine ionization on Ps. In this case the distance between the electron and the positron increases already after a tenth of nanosecond. The selected distance to consider the Ps ionized has been set to 3000 a.u., more than twice the initial distance of 1250 a.u.. The velocity of the
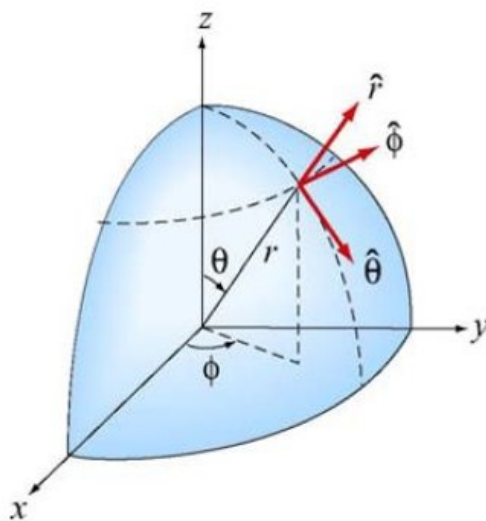
Figure 12.1: Random initial conditions of the internal motion of e^+ and e^-

center of mass decreases strongly when the Ps ionizes for energy conservation because the Coulomb potential energy increases.

The minimum Ps velocity for ionization depends on the layout but is usually around 30 km/s. Not all the Ps with higher velocity will ionize. It depends on the initial random conditions (see Figure 12.1). In the vertical target with normal emission there is no ionization as the Ps trajectory is parallel to the magnetic field.

12.3   Simulated trajectories

The effect of the magnetic field on the Ps trajectory is a defocusing both on the x-y plane normal to the magnetic field and on the y-z plane parallel to the magnetic field (see Figure 12.3).

The defocusing on the x-y plane is maximally important in all the layouts (see Figure 12.4). In the case of the vertical target both defocusing are equally important for geometric reasons.

As the antiproton cloud dimension on the x-y plane is smaller than on the y-z plane (diameter 0.24 cm vs length 2 cm) a small deviation angle on the x-y plane can make the Ps miss the antiproton cloud.

One can see the decrease of the number of antihydrogen atoms when the emission of Ps from the target is predominantly normal to the surface. When the emission is random, the deviation is in part compensated by the Ps which are not emitted from the center of the target.

The deviation is larger for slow Ps, as expected. Noting that the slower Ps population is the one having a higher probability to create antihydrogen, the effect on the number of generated atoms is relevant (see Figure 12.4 right).
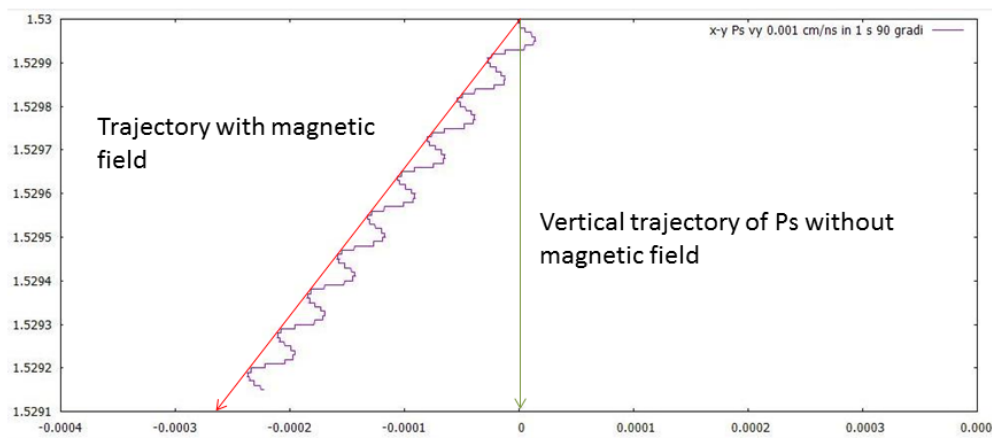
Figure 12.2: Center of mass movement of Ps on the x-y plane (B on the z axis) in 1 ns for a Ps velocity of 0.001 cm/ns for a given choice of initial internal conditions (vertical axis y, orizontal axis x in cm)

12.4 Simulated layouts with magnetic field

The following layouts have been simulated as they were described in the previous chapters:

1. Genova layout (Figure 10.5)

2. Layout to optimize transverse thermalisation at 145K and 4K (Figure 10.1)

3. Transmission target with random and normal emission (Figure 9.2)

4. Vertical transmission target with normal emission (Figure 11.1)

12.5 Monte Carlo description

The program is a full one-by-one atom Monte Carlo that simulates the creation of ortho-positronium atoms from a suitable target and their excitation by a laser beam composed by two laser pulses, following them (by tracing) until they reach the antiproton cloud. Each Ps is followed in his trajectory with a time step of 1 ns. The possible ionization due to Rydberg atoms interactions of electric dipole is taken into account as well as laser efficiency and life time of excited states.

To summarize, the physical inputs to this configuration of the Monte Carlo are the same as in the previous chapter:

- 1 million Ps atoms generated from the target (then scaled to the Genova numbers),

- 1/3 of the Ps with a lifetime of 7 ns (ms = 0), due to magnetic quenching, 2/3 with a lifetime of 142 ns ($m_s \pm 1$),

- flat distribution of the emission time of Ps from the target in an interval of 20 ns (duration of the positron bunch),

Figure 12.3: Example of internal trajectory of r on the x-z plane in 1 ns in atomic units

- Gaussian distribution (sigma of 0.05 cm) of the emission point of Ps from the target in the area covered by the incoming positrons, with the maximum in the center of the target,

- module of velocity distribution of the Ps taken with a distribution of 9% at 145 or 4K and 91% of 1260K,

- distribution of the emission direction of Ps over half of the solid angle,

- laser efficiency 40% with the rectangular shape, from 0 to 40% with the Gaussian shape with a width of 0.08 cm at 20%, laser pulse length 1.5 ns,

- final excitation level of Ps n=25, l=2 with a natural decay time of 16.5 μs,

- ionization probability computed for every nanosecond the time to come together according to formula 4.1 taken from [59],

- cross-section to produce antihydrogen taken from the the Aegis proposal for n=20 for every simulated Ps according to its velocity,

- 10^5 antiprotons in a cylinder of length 2 cm and radius 0.12 cm,

- number of generated antihydrogen atoms derived from the cross section, the antiprotons density and the length of the path of each Ps in the antiproton.
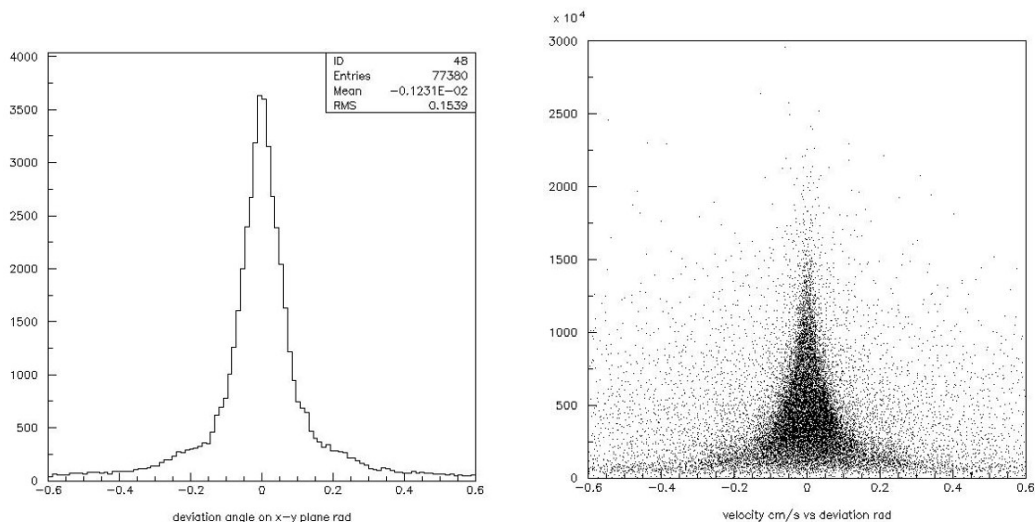
Figure 12.4: On the left deviation angle on the x-y plane for Genova layout for 44220 Ps excited by the laser to n=25, on the right Ps velocity in cm/s vs deviation angle

12.6   The results of the simulation with magnetic field

The results of the simulations with a uniform magnetic field of 1T along the z axis are represented in the Figure 12.5.

The percentage of ionized Ps on excited Ps is relevant when the Ps trajectory is normal to the magnetic field but has not much effect on the number of antihydrogen atoms because the Ps velocity to produce ionization is higher than 50 km/s, while at this velocity the cross section of the charge exchange process is low (see Figure 12.6).

Layout	AntiH without magnetic field	AntiH with magnetic field	Percentage
Genova layout	4	4	100%
Transverse thermalisation at 145K	28	12	43%
Transverse thermalisation at 4K	110	38	35%
Transmission target with random emission	17	17	100%
Transmission target with normal emission	83	70	84%
Vertical transmission target with normal emission	1105	480	43%

Figure 12.5: The results of the simulation with magnetic field. The percentage is the ratio between the number of antihydrogen atoms with magnetic field and without magnetic field
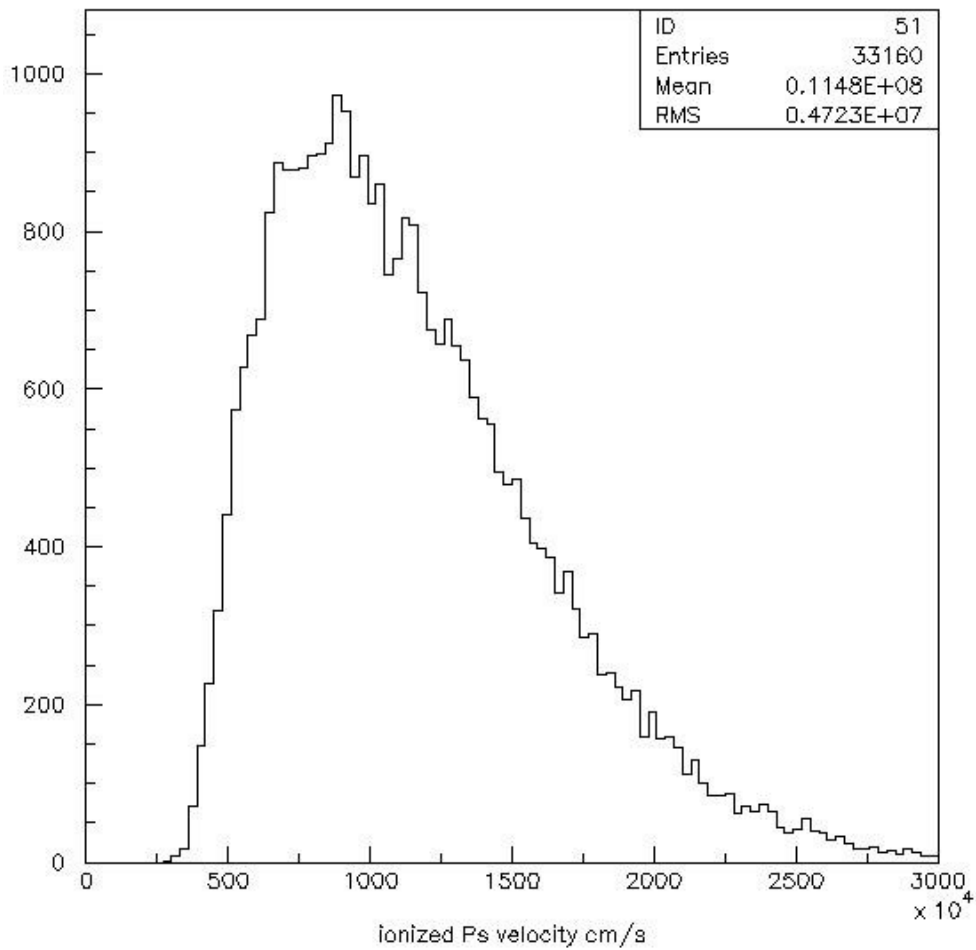
Figure 12.6: Ionized Ps velocity distribution in cm/s for the Genova layout

Calculation of the cross section of the charge exchange reaction without and with the 1T magnetic field

The previous simulations were based on the cross section of the charge exchange reaction 2.1 to produce antihydrogen computed for the AEGIS proposal in 2007 [30] and plotted in Figure 5.1 for different n_{Ps} as a function of k_v. The magnetic field was not considered.

I have written a program to compute the cross section without and with the magnetic field. In the same period the Genova group has made different calculations that were published in August 2016 [69], so I was able to compare the results under the same assumptions.

The calculation is totally classical and is based on the Classical Trajectory Monte Carlo Method (CTMC) [70]. The use of a classical approach is justified by the fact that positronium is in a Rydberg state and the distance between the electron and the positron is large. For n=20 the maximum distance is 800 atomic units.

The CTMC method has been introduced in Ref. [70] to calculate cross sections for charge transfer and ionization of hydrogen atoms by protons and has been applied to model three-body processes [71] and multielectron targets [72].

The procedure solves the classical equation of motion for a three body system made of the positron and the electron bound initially in the moving positronium atom and the antiproton, initially fixed at the origin of the axes, neglecting the spin of the particles. The total Hamiltonian in atomic units in absence of the magnetic field is given by

$$H_{tot} = \frac{p_{\bar{p}}^2}{2m_{\bar{p}}} + \frac{p_{e^+}^2}{2} + \frac{p_{e^-}^2}{2} - \frac{1}{r_{e^+e^-}} - \frac{1}{r_{\bar{p}e^+}} - \frac{1}{r_{\bar{p}e^-}} \qquad (13.1)$$

where $\vec{r}_{\bar{p}}$ and $\vec{p}_{\bar{p}} = m_{\bar{p}}\vec{v}_{\bar{p}}$ are the position and the momentum of the antiproton in the laboratory reference frame, $\vec{r}_{e^+}, \vec{p}_{e^+}, \vec{r}_{e^-}, \vec{p}_{e^-}$ are the corresponding quantities for the positron and the electron, $r_{e^+e^-}, r_{\bar{p}e^+}, r_{\bar{p}e^-}$ are the distances between each couple of particles.

For the magnetic field the Lorentz Force $\mathbf{v} \times \mathbf{B}$ in atomic units has been added to the equations of motion of the particles.

The calculation of the cross section is done simulating between 10,000 and 100,000 trajectories of positronium starting with a fixed velocity from a distant position from the antiproton along the y axis. Each Ps is followed until it approaches the antiproton and afterwards until the electron is far enough. The antihydrogen is formed if at the end of the simulation the positron is bound to the antiproton. The trajectories that don't conserve the energy with a precision of 0.1% are discarded. The following sections describe:

- the choice of the initial conditions

- the integration of the equations of motion

- the final conditions

- the calculation of the cross section

13.1   Choice of the initial conditions

The antiproton is initially at rest in the origin of the axes. The center of mass of the Ps is initially at a certain distance from the antiproton on the y axis with a fixed velocity towards the antiproton (see Figure 13.1) .
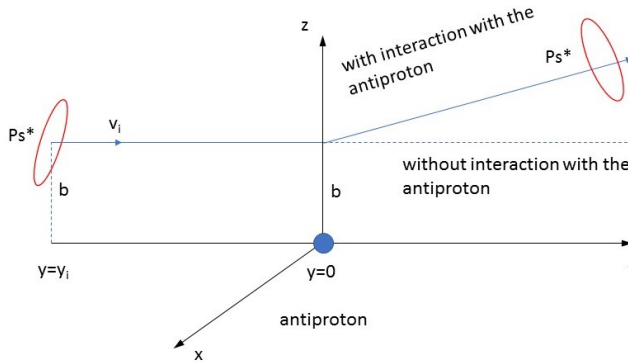
Figure 13.1: Schema of the scattering without magnetic field of a Ps in a Rydberg state with and without the interaction with an $\bar{p}$ at the origin of axes. The Ps^* trajectory starts from a position y_i with a velocity v_i and an impact parameter b.

The cross section is calculated as a function of $k_v = v_r/v_{orb}$, where v_r is the velocity of the Ps and v_{orb} is the velocity of the positron in the center of mass of the Ps averaged over its orbit (see Figure 5.1). The orbital velocity for the n level has been calculated for a circular orbit with the formula in atomic units:

$$v_{orb} = \frac{1}{2n} \tag{13.2}$$

k_v has been chosen between 0.015 and 2.5 because it is the range in which the cross section is significant for the experiment and for comparison with [69].

The impact parameter of the trajectory is determined moving the center of mass of the Ps on the x-z plane perpendicular to the trajectory randomly in a circle with radius b_{max}, which is chosen as the maximum value of the impact parameter for which Ps produces antihydrogen.

The initial position of e^+ an e^- is determined separating the center-of-mass motion from the relative motion of the two particles. The relative motion is that of a particle of reduced mass μ=1/2 in the Coulomb potential and the classical orbits for the bound system are Kepler elliptical orbits.

The semi-major axis is

$$a_e = \frac{n^2}{\mu} = 2n^2 \tag{13.3}$$

and the energy of the level n is

$$E_n = \frac{1}{4n^2} \tag{13.4}$$

The semi-minor axis is related to the classical angular momentum :

$$L_c = \sqrt{l(l+1)} \tag{13.5}$$

by the formula

$$b_e = \frac{nL_c}{\mu} = 2n\sqrt{l(l+1)} \tag{13.6}$$

The position on the ellipse has been determined with two different methods.

With the first method I have chosen a random position on the ellipse based on an algorithm developed in 1990 by Charles P. Reeve [77], which generates uniformly-spaced points on the surface of a M-dimensional ellipsoid.

With the second method I have solved the motion equation of the selected elliptical trajectory for one period and then I have picked up a time value with random uniform distribution between 0 and the ellipse period, as done by [69].

The two methods have produced very similar results.

For the random position on the ellipse the initial positions of e^+ and e^- have been derived as well as the initial velocities which are tangential to their orbits and in opposite directions. The module of the velocity is derived from the conservation of the angular momentum L_c. The two particles follow two elliptical trajectories which cross each other, the minimum distance is b_e and the maximum distance is a_e.

When the cross section has been calculated for a specified l of the Ps, the formula 13.6 has been used. When the cross section has been calculated for a level n, the classical squared angular momentum L_c^2 has been randomized with uniform distribution between 0 and its maximum allowed value, considering that $l = 0, 1, ...n-1$, according to the microcanonical ensemble of reference [70].

The orientation of the ellipse plane is linked to the projection of the angular momentum along the z axis and thus to the m quantum number of the Ps. A random rotation with three Euler angles has been done to take into account this quantum number.

13.2 Integration of the equations of motion

I have used a fifth-order Runge-Kutta method with a variable time interval. The energy at the end of the trajectory was compared with the initial one and the trajectories with a difference of more than 0.1% were discarded. The percentage of the discarded trajectories depends on the velocity of the Ps, with a maximum of 3% for the lowest one without magnetic field. With the magnetic field the percentage was much higher, with a maximum for the lowest velocities of 30%.

The distance between the Ps and the antiproton at the beginning of the trajectory has been chosen as twice the maximum impact parameter.

The time length of the calculation has been chosen as 20% longer than the time needed for the Ps to reach the antiproton, in order to understand whether the positron has been captured by the antiproton and the electron has left the positron.

13.3 Final conditions

After the interaction we have four possible cases:

- antihydrogen formation

- elastic scattering

- inelastic scattering

- ionization

To understand if antihydrogen has been formed it is sufficient to compute the energy of the two couples of particles $E_{e^+e^-}$ and $E_{\bar{p}e^+}$.

$$E_{e^+e^-} = \frac{p_{e^+}^2}{2} + \frac{p_{e^-}^2}{2} - \frac{1}{r_{e^+e^-}} \tag{13.7}$$

$$E_{\bar{p}e^+} = \frac{p_{\bar{p}}^2}{2m_{\bar{p}}} + \frac{p_{e^+}^2}{2} - \frac{1}{r_{\bar{p}e^+}} \tag{13.8}$$

If $E_{e^+e^-} > 0$ and $E_{\bar{p}e^+} < 0$ the positron is bound to the antiproton and antihydrogen is formed.

If $E_{e^+e^-} < 0$ and $E_{\bar{p}e^+} > 0$ the electron and the positron are still bound in the Ps. The principal quantum number n' can be computed from equation 13.4, if n' is equal to n the collision is elastic, otherwise it is inelastic.

If $E_{e^+e^-} > 0$ and $E_{\bar{p}e^+} > 0$ the Ps is ionized.

The principal quantum number n of the antihydrogen is calculated from its energy according to formula 13.4, the l quantum number is calculated from its classical angular momentum according to equation 13.5.

13.4   Calculation of the cross-section

The cross-section is calculated from the number of generated antihydrogen atoms $N_{\bar{H}}$, the number of simulated Ps atoms N_{tot} and the maximum value of the impact parameter b_{max} to produce antihydrogen [70]:

$$\sigma = \pi b_{max}^2 \frac{N_{\bar{H}}}{N_{tot}} \tag{13.9}$$

while the standard (rms) error is

$$\Delta\sigma = \sigma \sqrt{\frac{N_{tot} - N_{\bar{H}}}{N_{tot} N_{\bar{H}}}} \tag{13.10}$$

The number of trajectories is between 10,000 and 100,000 depending on the time taken by the calculation, which is inversely proportional to the Ps initial velocity. The standard error is too small to be represented in the plots.

13.5   Cross-section without and with magnetic field

The cross section has been calculated for Ps with n=20 and l=2, which are in an interesting range for the AEGIS experiment due to the laser energy. To compare the results with the paper of the Genova group [69] a calculation has been done for n=18 and a statistical mixture of l, as described in section 13.1.

In the case without magnetic field, a comparison has also been done with the two center convergent close coupling (CCC) method for $n_{Ps} = 3$ and a statistical mixture of l, [73, 74] which uses quantum mechanics formula and was the first to predict a rise of the cross section at low energies. Figure 13.2 compares the results of the CTMC method and the CCC method, demonstrating that CTMC can also be used for non Rydberg levels with good approximation.
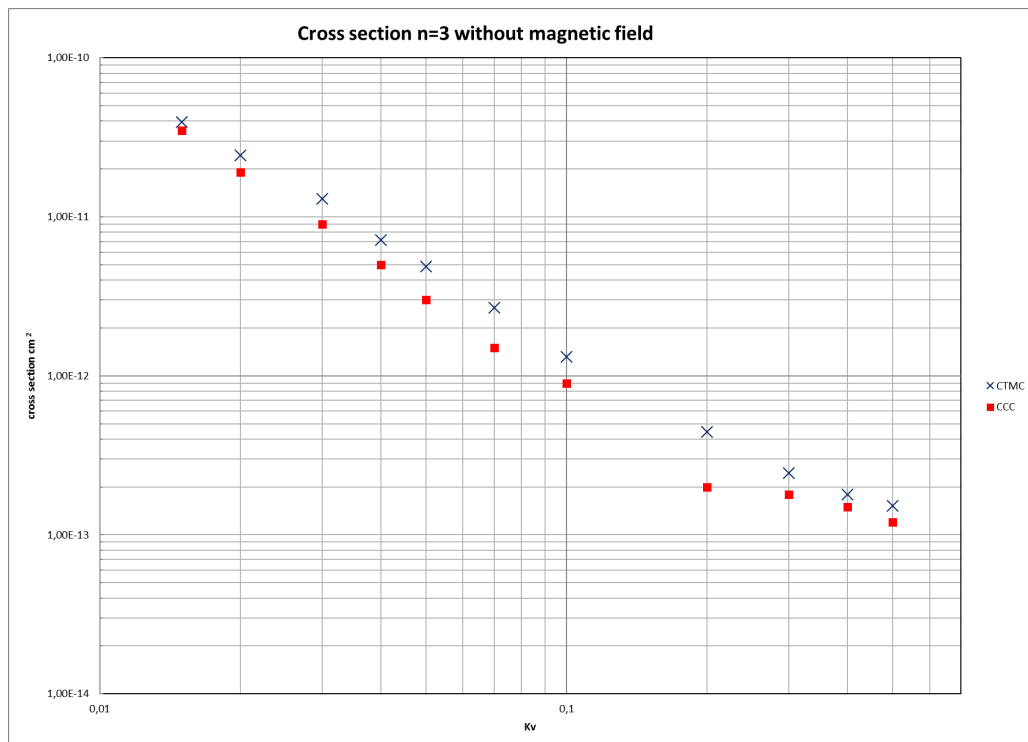
Figure 13.2: Comparison between cross sections in cm^2 calculated with the CTMC (blue X) and CCC (filled red squares) at low energy as a function of k_v.

To verify that the cross section is proportional to n^4 of the Ps the cross section σ/n^4 has been calculated for n=3 and n=18 as a function of k_v between 0.015 and 2.5. The values are almost the same on the whole range (see Figure 13.3).

The magnetic field has been simulated with an intensity of 1T as in the AEGIS experiment in two directions: parallel and perpendicular to the the direction of the Ps. The perpendicular direction is the one of the actual layout, the parallel direction is the one of the transmission target, which is being studied to increase the number of generated antihydrogen.

The trajectories of Ps have been studied in detail to understand whether the conditions of section 13.3 were sufficient to discriminate between the various final states and the length of the simulation was sufficient. The distances of the positron and the electron from the antiproton have been plotted as a function of time.

Figures 13.4,13.5,13.6,13.7, 13.8,13.9,13.10,13.11,13.12,13.13 show some of the cases.

For $k_v > 2$ the cross section drops while for $k_v < 0.3$ the cross section rises (see Figure 13.16); when there is no magnetic field it rises as $1/k_v^2$, or equivalently as $1/E_{Ps}^{cm}$
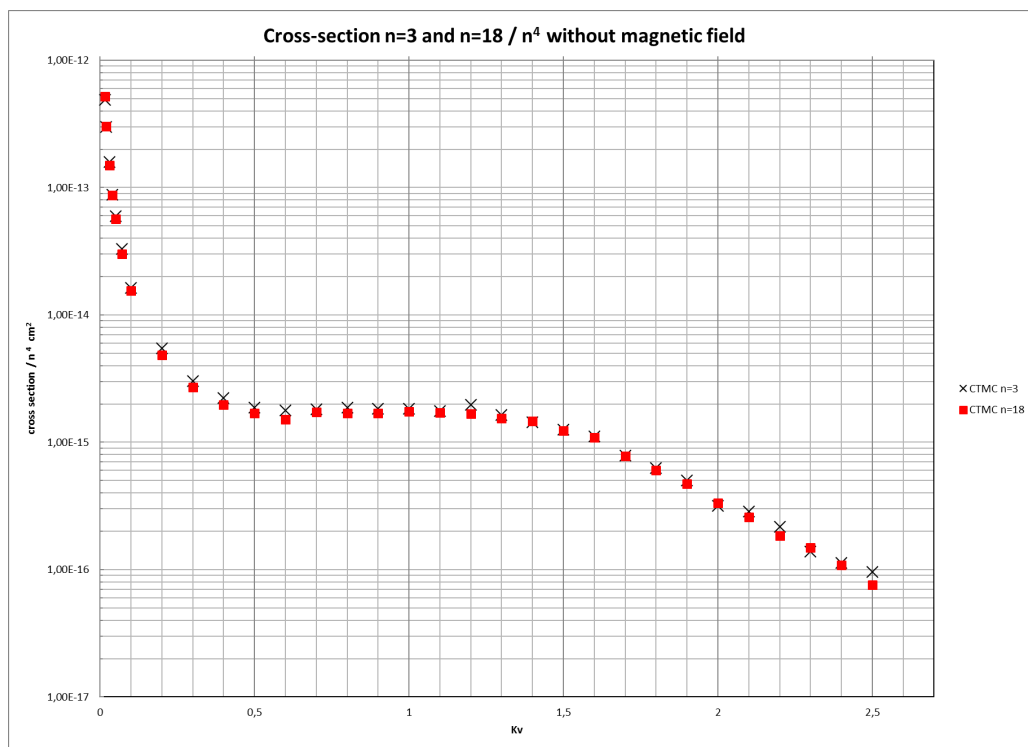
Figure 13.3: Comparison between cross sections/n^4 in cm^2 calculated for n=3 (black X) and n=18 (red square) for a statistical mixture of l as a function of k_v.

(see Figure 13.15).

The increase of the cross section for low Ps velocities would be interesting for AEGIS, but the presence of the magnetic field of 1T lowers the values, especially when the direction of the field is perpendicular to the direction of the Ps.

The Genova group has made a different simulation of the magnetic field which leads to a higher cross section for low Ps velocities.

The basic idea of the method is that the magnetic field has a strong influence on the simulation depending from how far the initial position of the Ps is from the antiproton, due to the effect of the field on the trajectory. The choice of the impact parameter consequently depends from the initial distance and affects the result of the calculation.

The Genova group's method is to randomize a position of the Ps on the x-z plane which contains the antiproton, make the Ps go back to the initial position reversing the direction of the magnetic field and not taking into account the electromagnetic field of the antiproton and then start the simulation. The maximum impact parameter is computed on the x-z plane of the antiproton.

I believe that this method is in contradiction to the standard procedure to calculate a cross section and favors the Ps trajectories that pass near the antiproton. The result is a higher value of the cross section, even higher for some value of k_v than the cross section without magnetic field. Figure 13.14 compares the results with n=18 and a statistical mixture of l.

The results of the simulation for n=18 and a statistical mixture of l without magnetic

Figure 13.4: Ps trajectory with n=20, l=2 without magnetic field with $k_v = 0.1$, impact parameter 9220 au, initial position 25,000 au. Antihydrogen is formed and the electron escapes.

field are shown in Figure 13.15 with the fit $\sigma/n_{Ps}^4 = \frac{s_1}{k_v^2} + s_2$, $s_1 = 1.32 \times 10^{-16} cm^2$, $s_2 = 1.12 \times 10^{-15} cm^2$ for $k_v < 0.6$ taken from [69].

Figure 13.15 shows that the magnetic field lowers the charge-exchange cross section for values of $k_v < 0.2$.

Figure 13.16 shows the cross-section for $n = 20, l = 2$ without (blue line) and with magnetic field perpendicular (red line) and parallel (green line) to the Ps initial direction. The comparison with the cross section calculated for the AEGIS proposal (see Figure 5.1) has been added in yellow. One can see that in the case of parallel direction the cross section is higher than in the case of perpendicular direction.

13.6 Antihydrogen principal quantum number

The principal and the azimuthal quantum numbers of the antihydrogen are obtained inserting in the formula 13.4 and 13.5 the energy and angular momentum of the antihydrogen.

The distribution of the principal quantum number of antihydrogen produced has been analyzed for n_{Ps} = 20 and l_{Ps}=2 for different k_v without magnetic field (see Figure 13.17) and with magnetic field of 1T (see Figure 13.18)

The distribution is peaked around $n_0 = n_{Ps}\sqrt{2}$ because kinematic calculations show that antihydrogen can form when positronium and antiproton are at rest only if the Q value of the reaction is positive, where Q is the difference of the binding energy of the initial positronium and the final antihydrogen:

$$Q = \frac{1}{4n_{Ps}^2} - \frac{1}{2n_{\bar{H}}^2} \tag{13.11}$$

In the distributions with the magnetic field of 1T the peak is slightly higher. and the distribution wider.
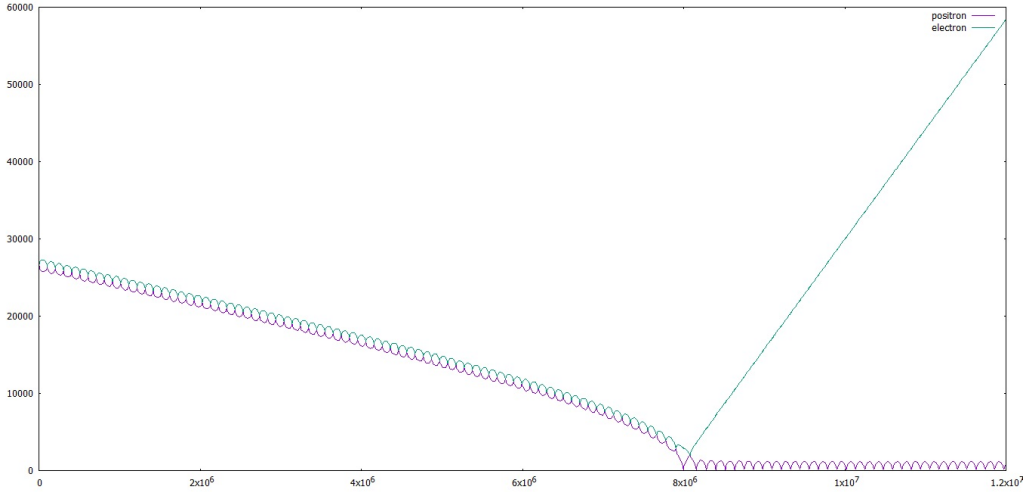
Figure 13.5: For the same Ps of Figure 13.4 plot of the distance of the electron and the positron from the antiproton in function of time in au. Antihydrogen is formed and the electron escapes.

13.7   Antihydrogen azimuthal quantum number

The distribution of the azimuthal quantum number l depends from the Ps velocity represented by k_v. For high values of k_v high values of l are more probable, following higher values of n. The presence of the magnetic field widens the distribution of l. This is illustrated in Figures 13.19 and 13.20.

13.8   Impact parameter

The maximum impact parameter b_{max} is inversely related to the velocity of the Ps and is smaller without magnetic field than with magnetic field. The faster the Ps, the less time the positronium spends near the antiproton, so it is captured only at short distances. The magnetic field provokes a bending of trajectories that permits to Ps that would pass far from the antiproton without magnetic field to pass nearer.

Figure 13.21 on the top shows the distribution of the maximum impact parameter b_{max} for different k_v for n=20 and l=2 with and without magnetic field. As shown in the same figure on the bottom for n=3 and n=20, the distribution depends only on the semi-major axis of the Ps orbit $2n^2$, as confirmed by Figure 11 of [69]. The reason is that the semi-major axis determines how near to the antiproton the positron can get in its rotation around the Ps center of mass.

13.9   Antihydrogen velocity

The velocity of antihydrogen is important to measure its gravity acceleration because very slow atoms are needed given that the dominant factor is the temperature. The Ps atoms produce a recoil of antihydrogen in the flight direction of the Ps, assuming the antihydrogen is initially at rest (see bottom plot in Figure 13.23).

If the Ps are emitted by the target in reflection mode, the flight direction is on the y-axis and normal to the magnetic field which is directed on the z-axis. If the Ps are
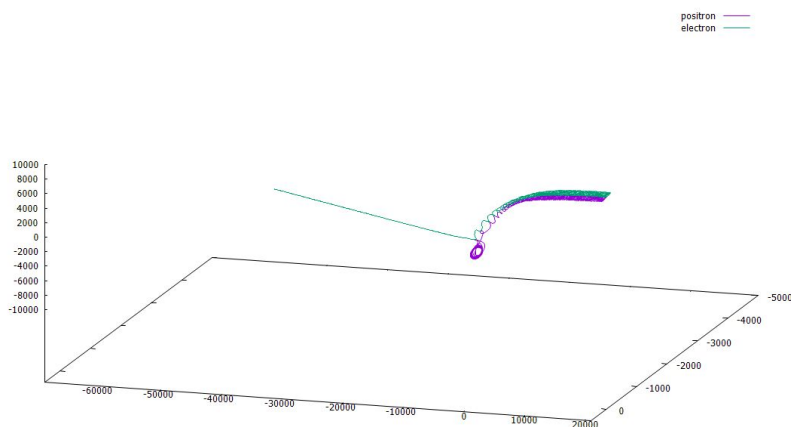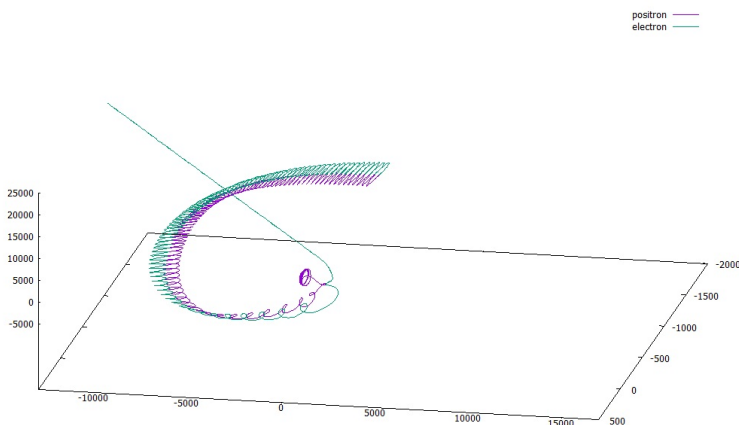
Figure 13.6: Ps trajectory with n=20,l=2 in a 1T magnetic field with $k_v = 0.1$, impact parameter 12582 au, initial position 2,000 au. Antihydrogen is formed and the electron escapes.

emitted by the target in transmission mode the flight direction is on z-axis and parallel to the magnetic field.

This effect could be useful to form a beam of antihydrogen atoms in the z direction but the velocity is significant only for k_v values over 1.5, when the cross section of the charge exchange reaction diminishes.

The antihydrogen velocity in the Ps flight direction has been analyzed without and with magnetic field for $k_v = 0.015$, 0.1, 1 and 1.8 along the y-axis (see Figures 13.22 and 13.24). For a comparison the distribution of the velocity on the transverse direction has been plotted in Figures 13.23 and 13.25. The presence of the magnetic field broadens all the distributions as the flight direction is modified and not all the Ps trajectories are in the y direction when they arrive near the antiproton (see Figure 13.25). The distribution of the angle between the Ps flight direction and the antihydrogen recoil has a maximum near π (see Figure 13.23). The position of the maximum is reduced by the magnetic field (see Figure 13.25.

13.10   Asymmetry of the distribution of the antihydrogen canonical angular momentum with the magnetic field

The presence of the magnetic field creates an asymmetry of the distribution of the component of the antihydrogen canonical angular momentum in the direction of the field towards high values. This asymmetry has been calculated in [75] and [69] for various values of n and B. In absence of magnetic field the distribution is simmetric.

The canonical angular momentum, which is conserved, is different from the angular momentum which is not. The formula for the canonical angular momentum $\mathcal{L}_z$ along z is

$$L_z = m(xv_y - yv_x) \tag{13.12}$$

$$\mathcal{L}_z = L_z + qB(x^2 + y^2)/2 \tag{13.13}$$

Figure 13.7: For the same Ps of Figure 13.6 plot of the distance of the electron and the positron from the antiproton in function of time in au. Antihydrogen is formed and the electron escapes.

where the quantities refer to the positron rotating around the antiproton.

This asymmetry is important for precision spectrometry experiments which need to trap antihydrogen with a magnetic field and build up a substantial quantity of it. Antihydrogen with positive canonical angular momentum will be attracted by the trap if the magnetic field increases in magnitude toward the wall of the trap [75].

AEGIS doesn't need to trap antihydrogen but accelerates it as soon as it is created through the Stark effect to send it to the moiré deflectometer.

I have verified the asymmetry calculating the canonical angular momentum once the antihydrogen is formed for $n_{Ps} = 20$ and l_{Ps}=2 for k_v= 0.05, 0.1, 0.5, 1, 1.8 for B=1T parallel to z and perpendicular or parallel to the Ps initial trajectory.

The asymmmetry toward positive value is reduced if the velocity of the Ps increases.

Fig. 13.26 represents the formation of antihydrogen from Ps and the trend of $\mathcal{L}_z$.

Fig. 13.27 represents the distribution of $\mathcal{L}_z$ when the magnetic field of 1T is parallel to the initial trajectory of Ps for various values of k_v.

Fig. 13.28 represents the distribution of $\mathcal{L}_z$ when the magnetic field of 1T is perpendicular to the initial trajectory of Ps for various values of k_v.

The distribution is more peaked around zero in the first case than in the second and the reduction of the asymmetry for high values of k_v is more visible.
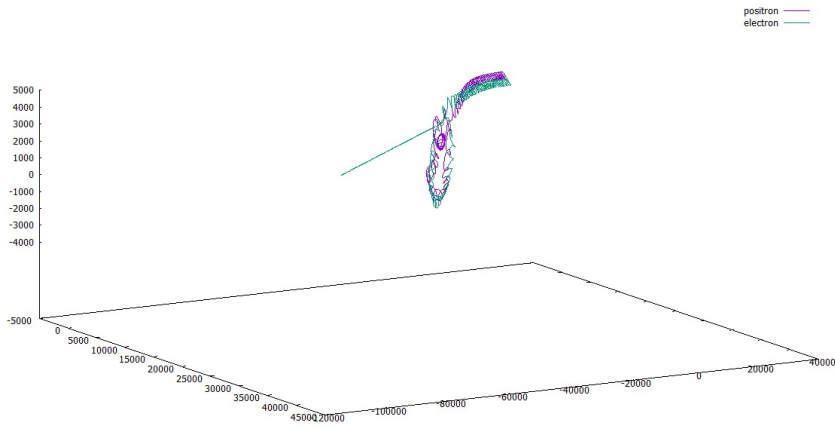
Figure 13.8: Ps trajectory with n=20,l=2 in a 1T magnetic field with $k_v = 0.2$, impact parameter 3694 au, initial position 40,000 au. Antihydrogen is formed and the electron escapes.
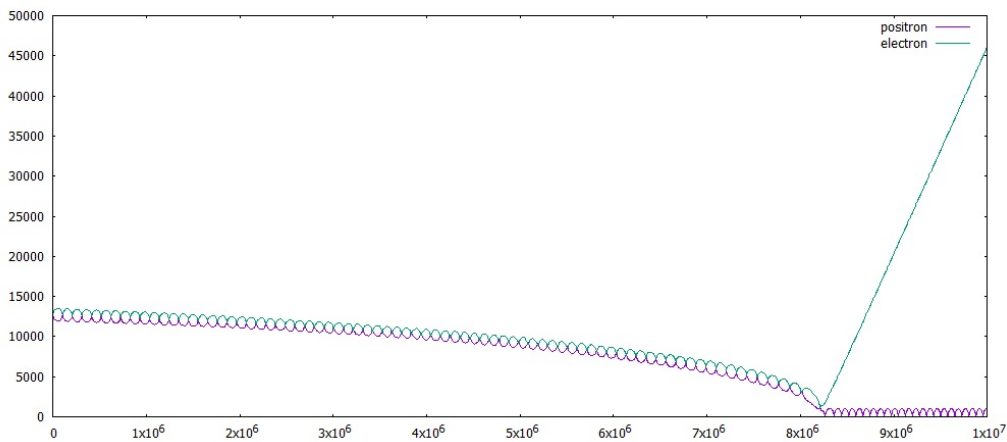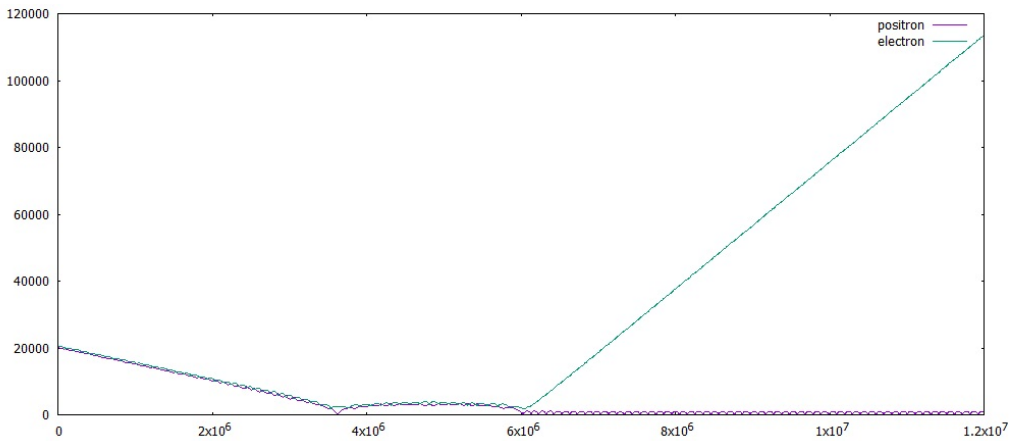

Figure 13.9: For the same Ps of Figure 13.8 plot of the distance of the electron and the positron from the antiproton in function of time in au. Antihydrogen is formed and the electron escapes.
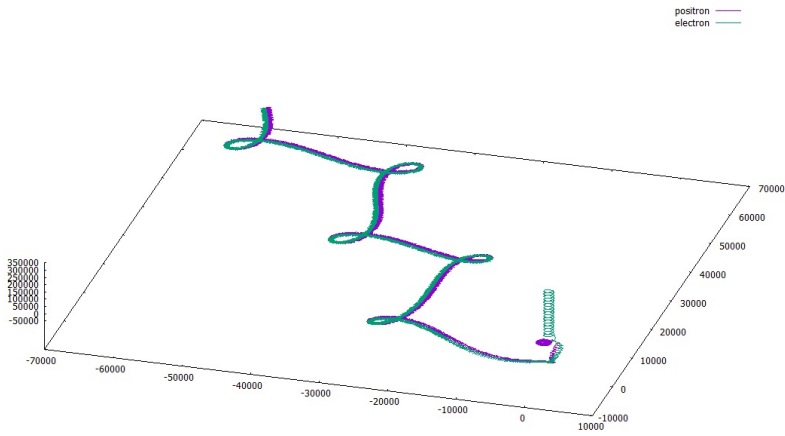
Figure 13.10: Ps trajectory with n=20,l=2 in a 1T magnetic field with $k_v = 0.02$, impact parameter 59218 au, initial position 65,000 au. Antihydrogen is formed and the electron escapes.
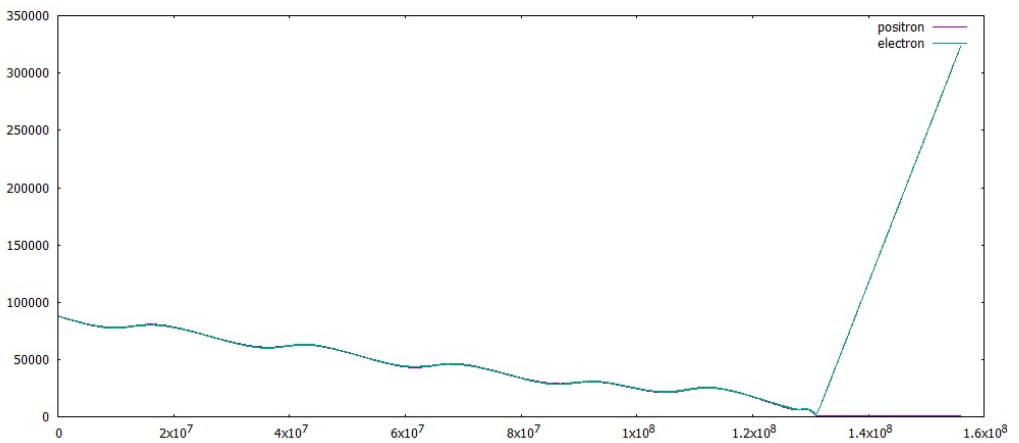
Figure 13.11: For the same Ps of Figure 13.10 plot of the distance of the electron and the positron from the antiproton in function of time in au. Antihydrogen is formed and the electron escapes.
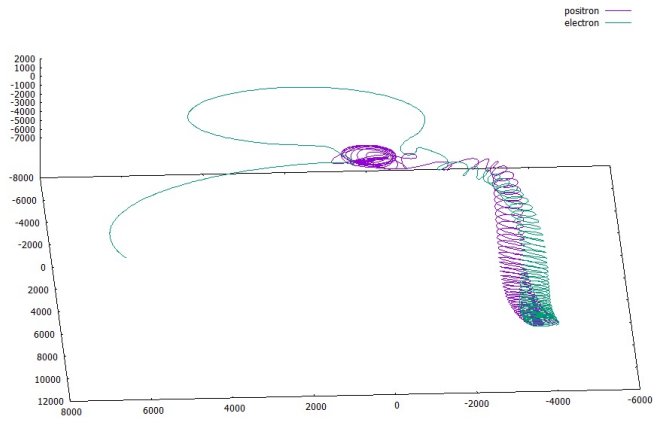
Figure 13.12: Ps trajectory with n=20,l=2 in a 1T magnetic field with $k_v = 0.1$, impact parameter 7257 au, initial position 10,000 au. Antihydrogen is formed and the electron escapes after a bounce.
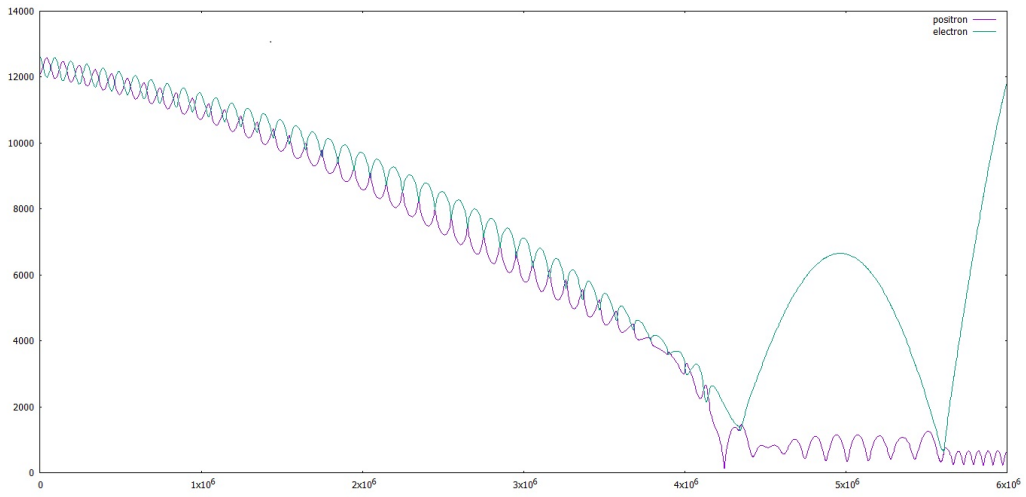
Figure 13.13: For the same Ps of Figure 13.12 plot of the distance of the electron and the positron from the antiproton in function of time in au. Antihydrogen is formed and the electron escapes after a bounce.
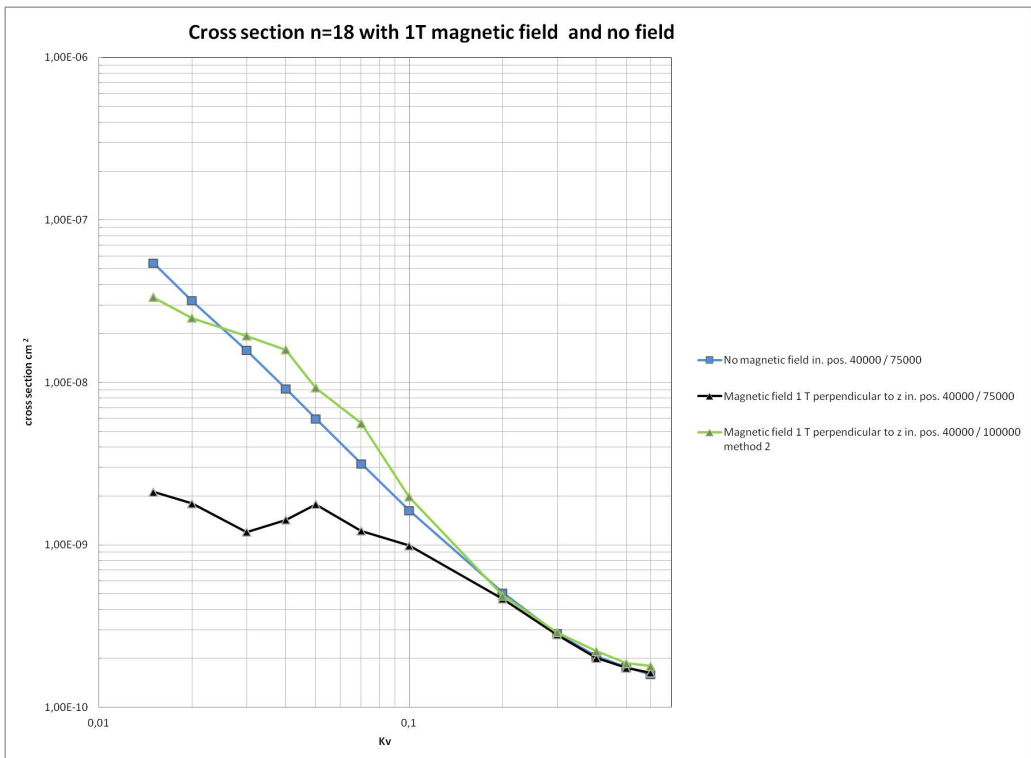
Figure 13.14: Charge-exchange cross section in cm^2 of Ps with n=18 as a function of k_v with B=0 (blue) and B=1T perpendicular to the Ps direction calculated in a standard way (black) and with the Genova group method (green).
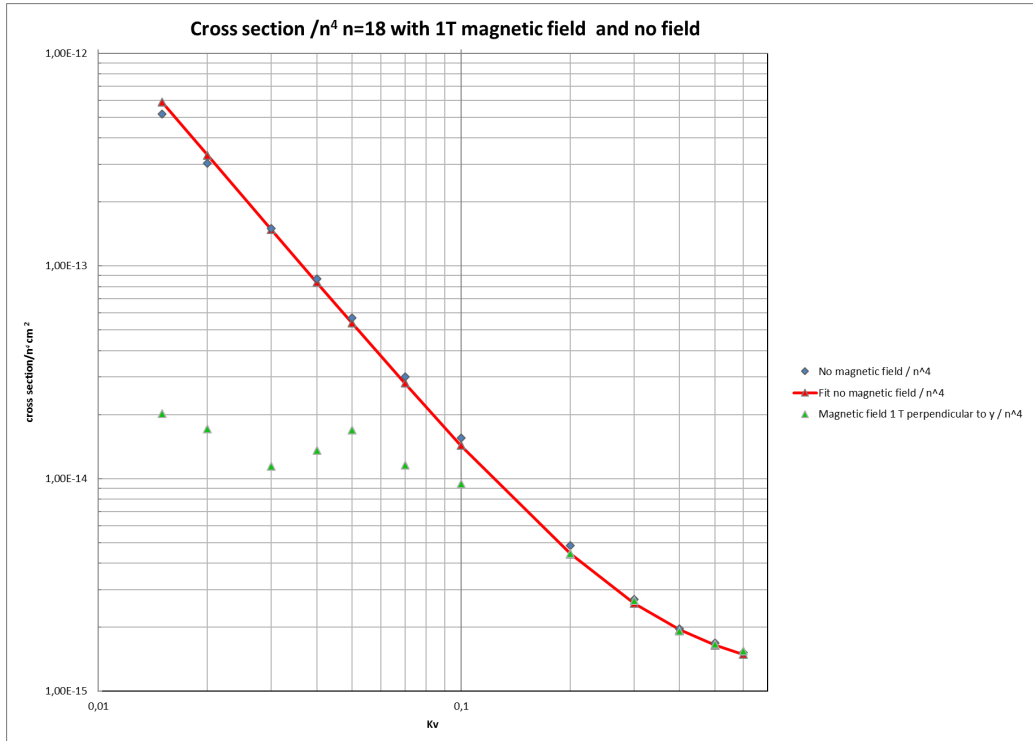
Figure 13.15: Charge-exchange cross section in cm^2 of Ps with n=18 divided by n^4 as a function of k_v with B=0 (blue square) and B=1T perpendicular to the Ps direction (green triangle). The plot refers to the region of low k_v values where without magnetic field the cross section can be fitted with the function (red line) $\sigma/n_{Ps}^4 = \frac{s_1}{k_v^2} + s_2$, $s_1 = 1.32 \times 10^{-16} cm^2$, $s_2 = 1.12 \times 10^{-15} cm^2$ taken from [69]
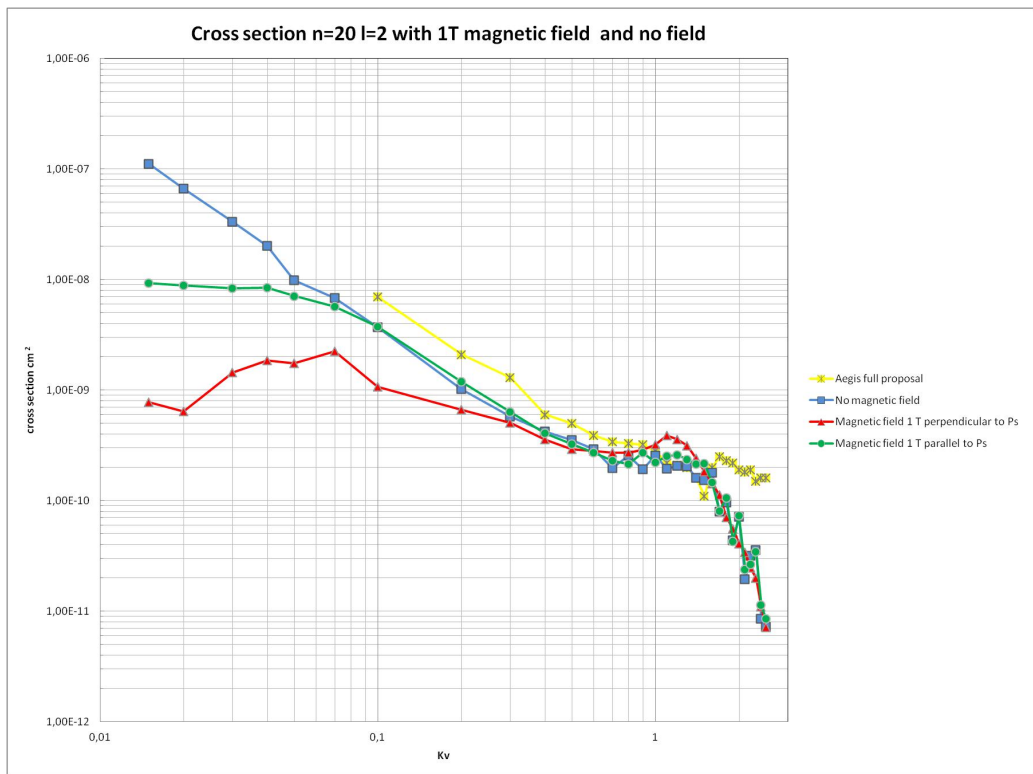
Figure 13.16: Charge-exchange cross section in cm^2 of Ps with n=20, l=2 as a function of k_v with B=0 (blue) and B=1T perpendicular (red) and parallel to the Ps initial direction (green). The AEGIS proposal cross-section used in the previous simulations is plotted in yellow.
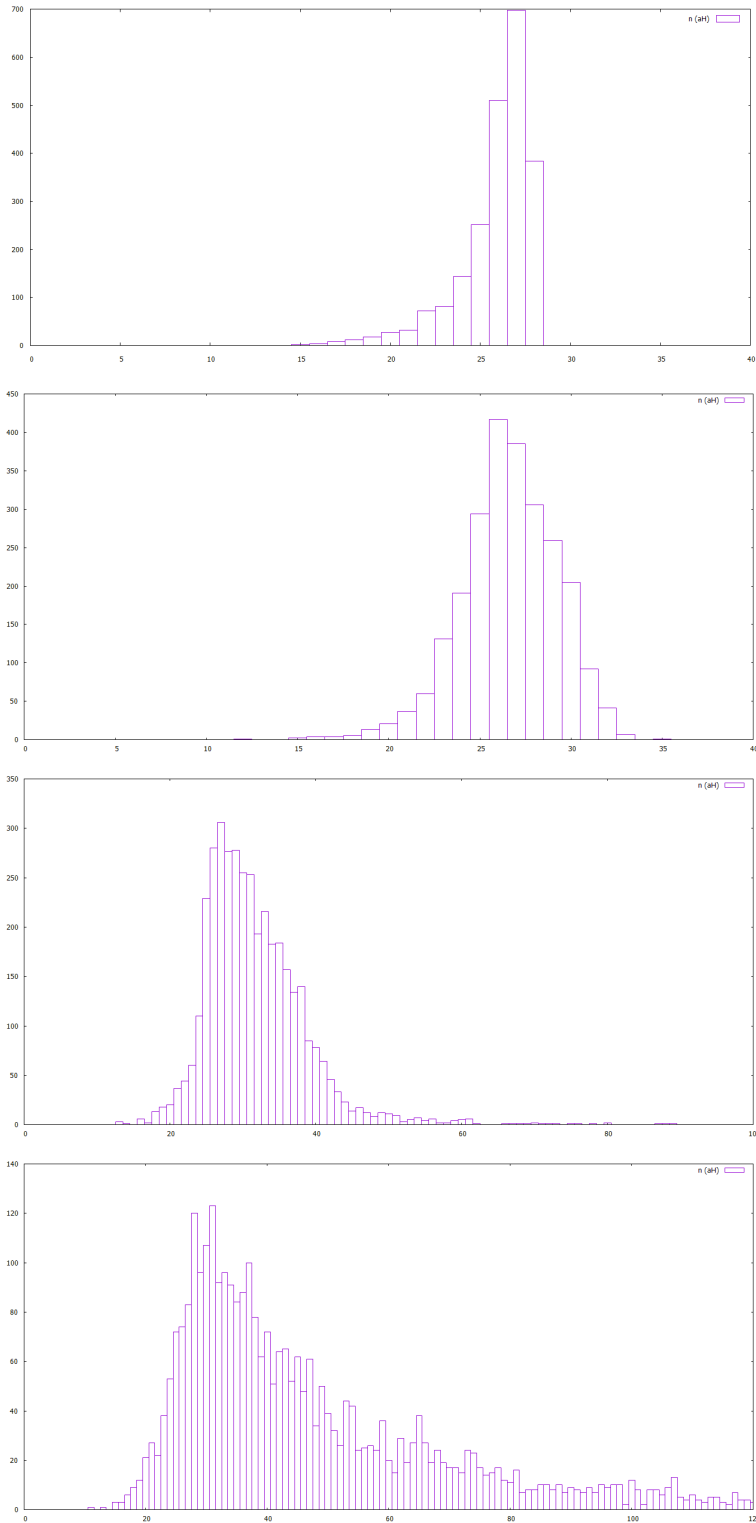
Figure 13.17: Distribution of the principal quantum number n of antihydrogen produced by interaction with Ps with $n_{Ps} = 20$ and $l_{Ps} = 2$ without magnetic field with $k_v = 0.015, 0.5, 1.0, 1.5$ from top to bottom. The peak at $n = 20\sqrt{2} = 28$ is visible, for low velocities $n < 28$.
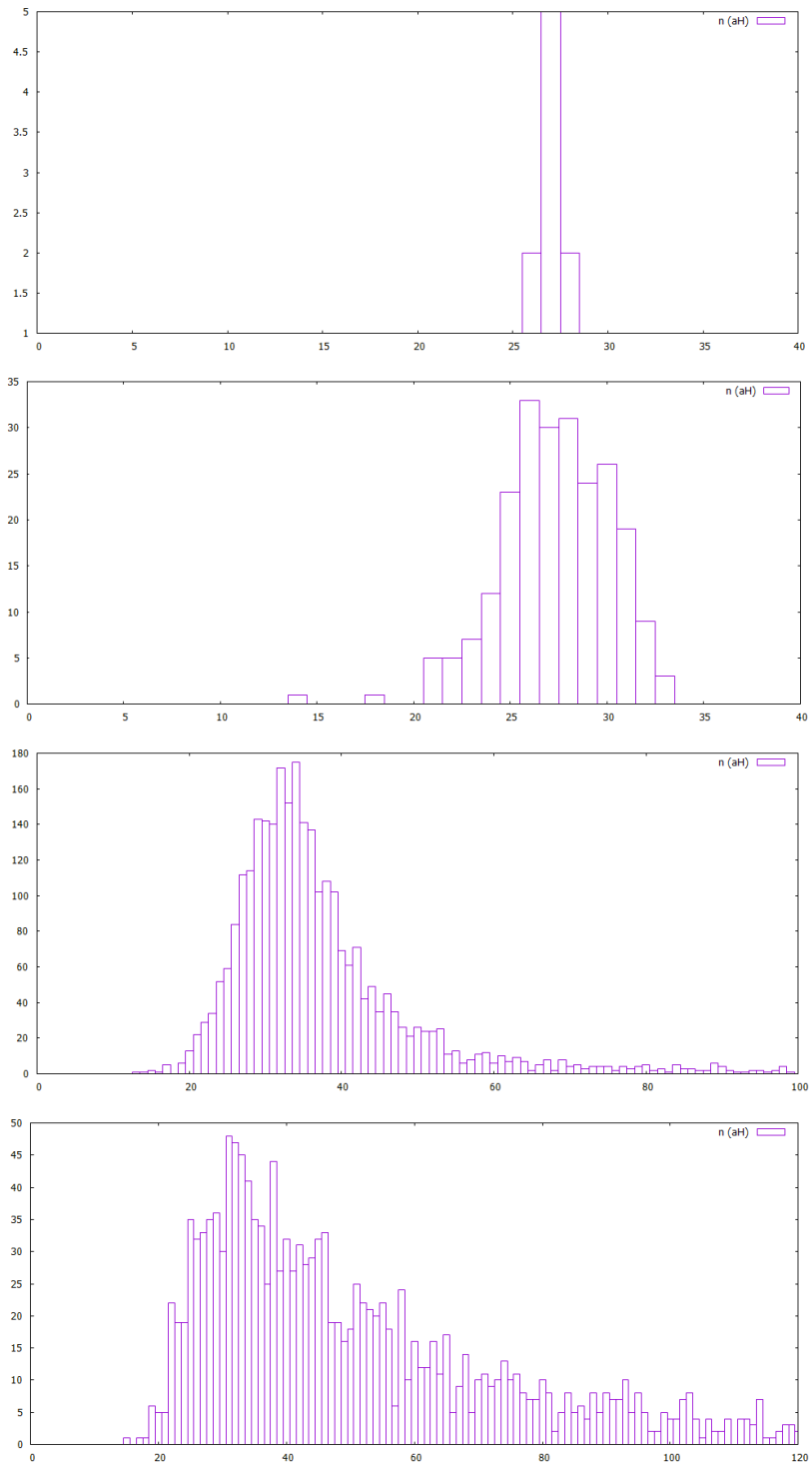
Figure 13.18: Distribution of the principal quantum number n of antihydrogen produced by interaction with Ps with $n_{Ps} = 20$ and $l_{Ps} = 2$ with magnetic field of 1T with $k_v = 0.015, 0.5, 1.0, 1.5$ from top to bottom.
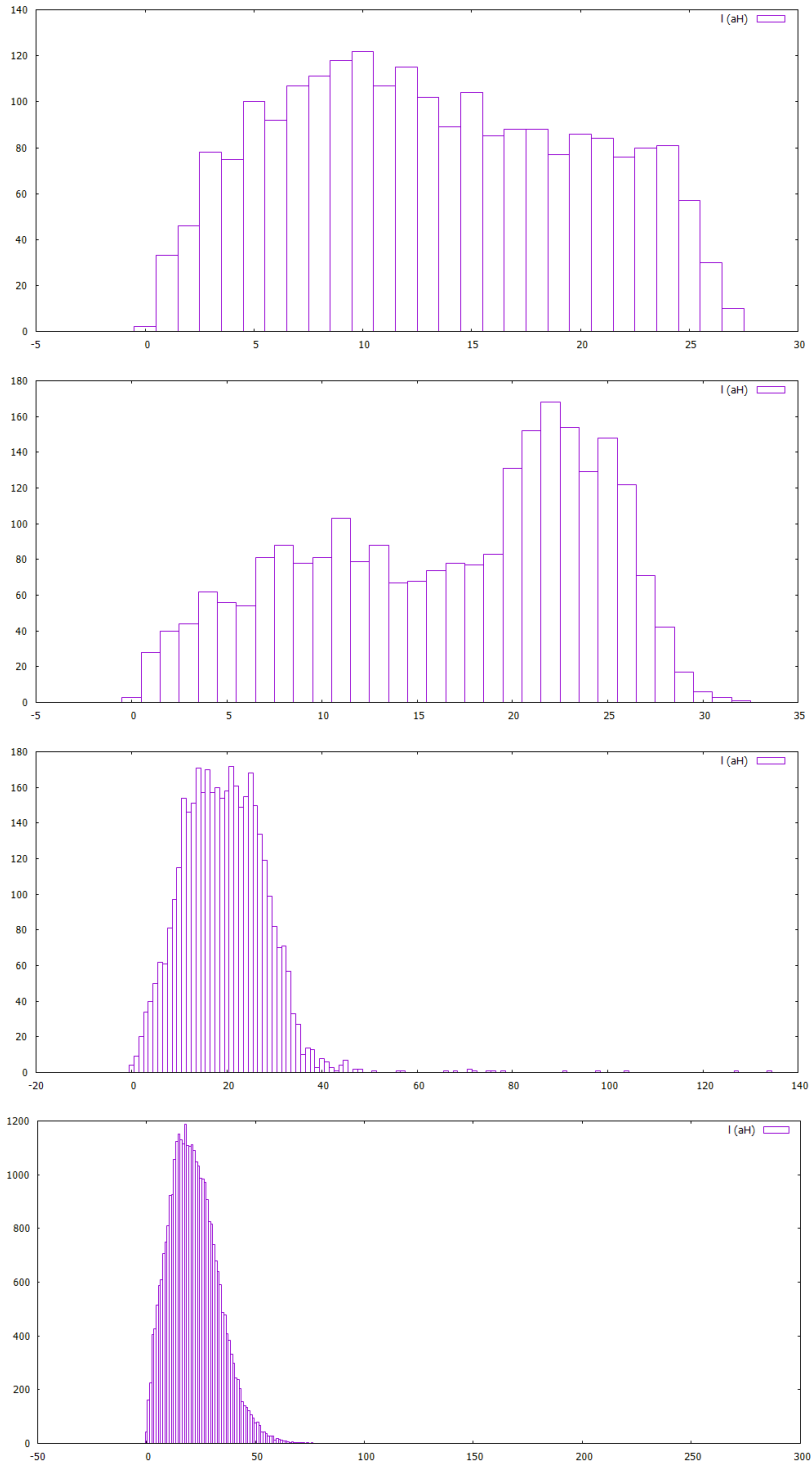
Figure 13.19: Distribution of the azimuthal quantum number l of antihydrogen produced by interaction with Ps with $n_{Ps} = 20$ and $l_{Ps} = 2$ without magnetic field with $k_v = 0.015, 0.5, 1.0, 1.5$ from top to bottom.
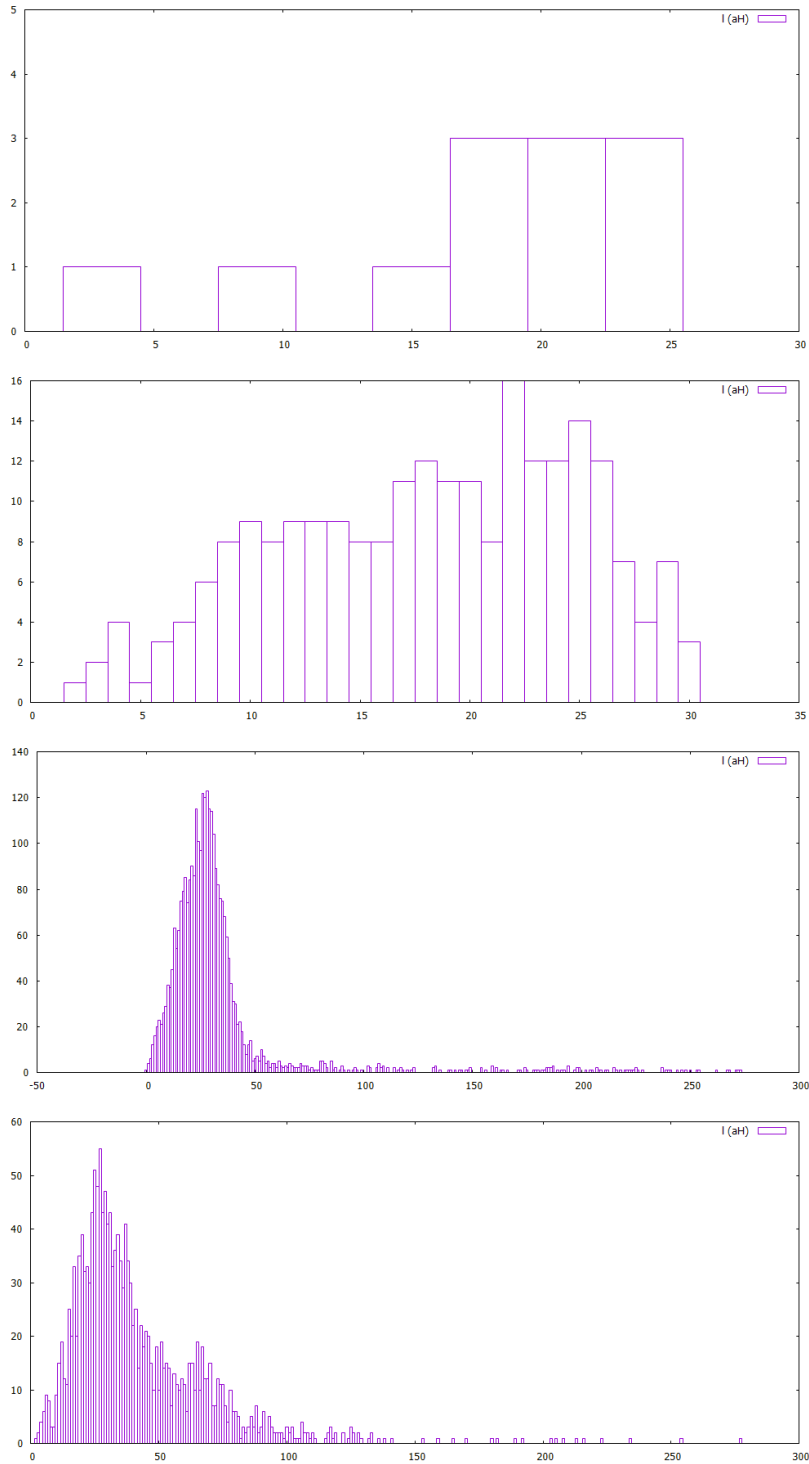
Figure 13.20: Distribution of the azimuthal quantum number l of antihydrogen produced by interaction with Ps with $n_{Ps} = 20$ and $l_{Ps} = 2$ with magnetic field of 1T with $k_v = 0.015, 0.5, 1.0, 1.5$ from top to bottom.
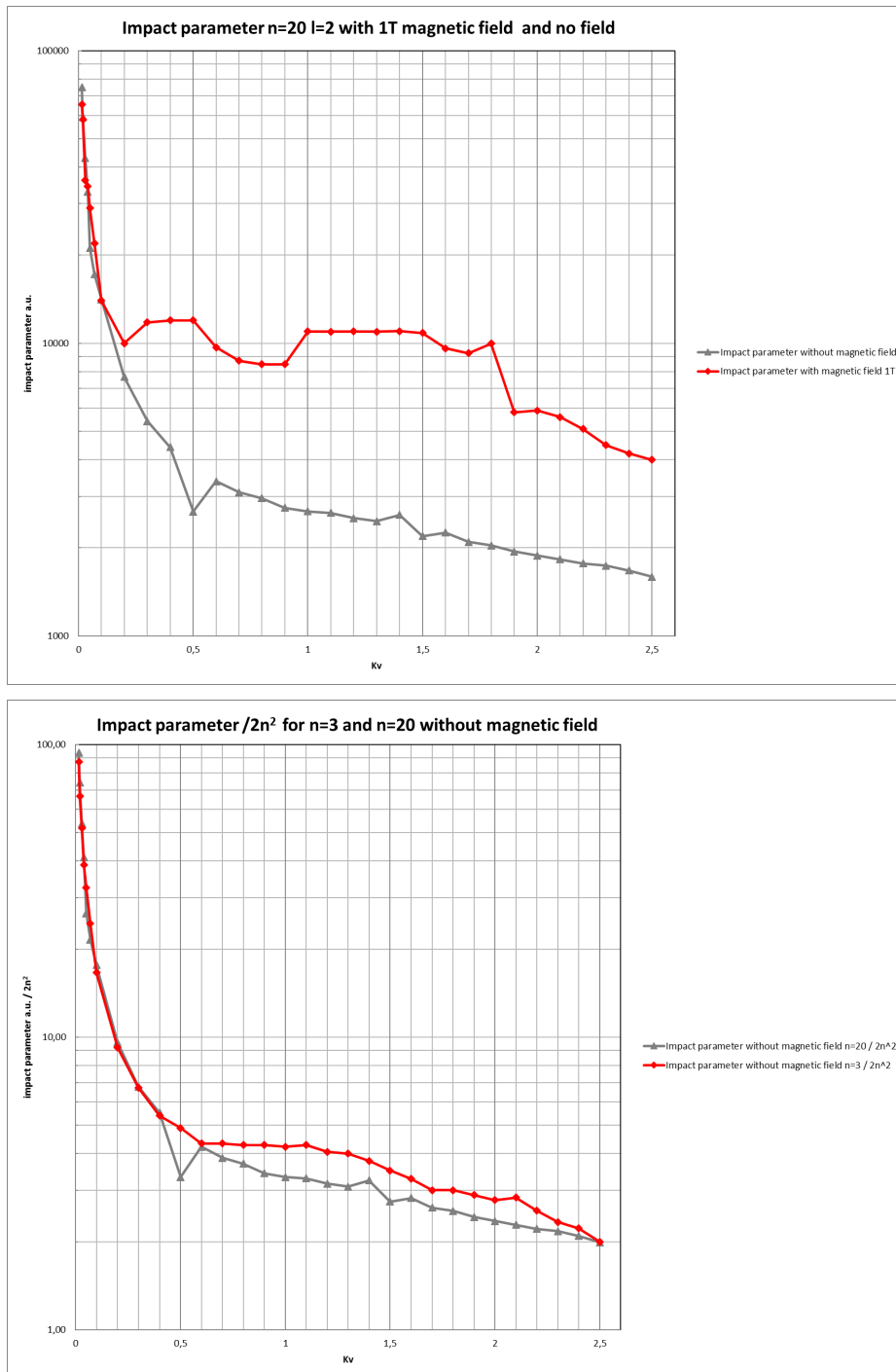
Figure 13.21: Top: maximum impact parameter b_{max} in a.u. vs k_v with (red) and without (grey) a magnetic field of 1T perpendicular to the direction of the Ps. Bottom: impact parameter $b_{max}/2n^2$ in a.u. for *n*=20 (grey) and *n*=3 (red) without magnetic field, the values are almost identical dividing the parameter by the length of the semi-major axis.
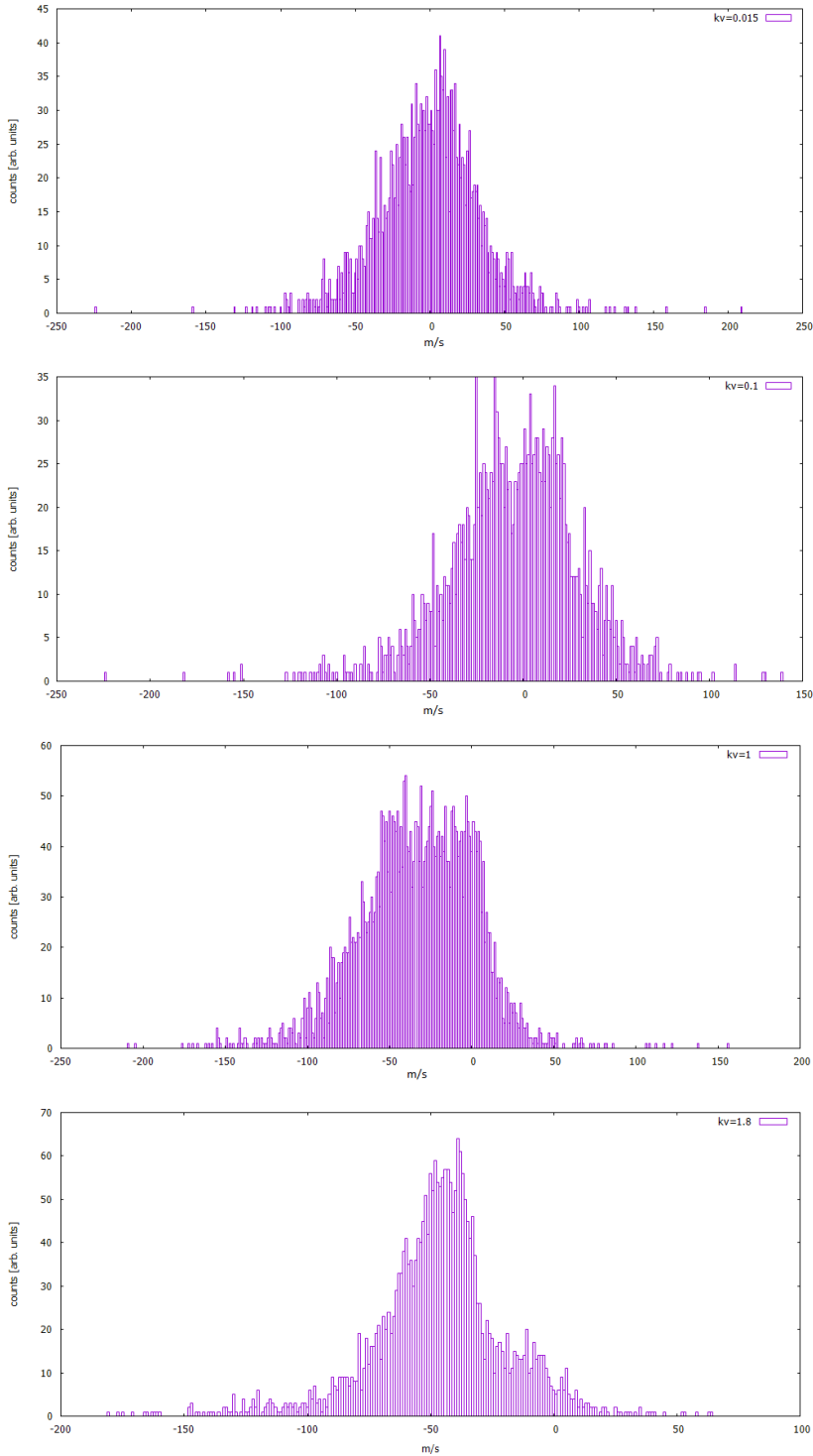
Figure 13.22: Distribution of the antihydrogen velocity in m/s along the y axis with no magnetic field for Ps with $n=20$, $l=2$ and $k_v=$ 0,015, 0.1, 1, 1.8 from top to bottom. One can see the peak moving to the left proportionally to the Ps velocity.
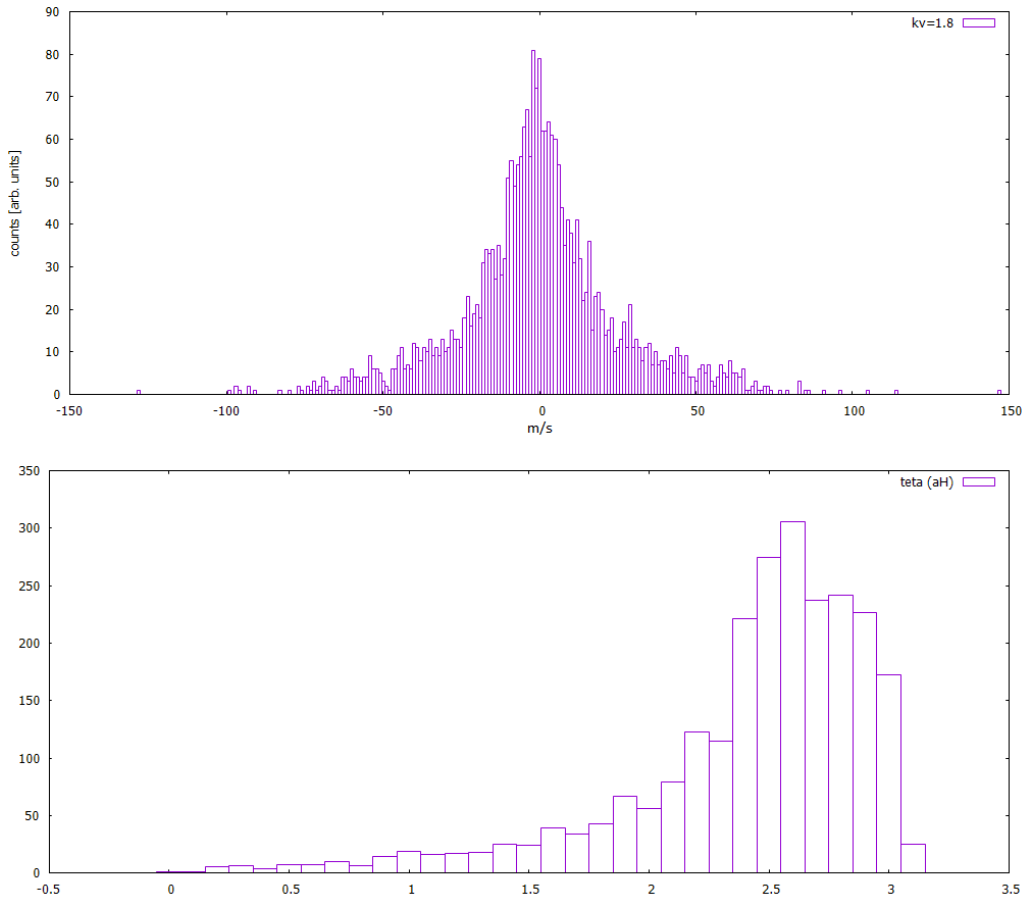
Figure 13.23: Top: distribution of the antihydrogen velocity in m/s along the transverse direction x with no magnetic field for Ps with $n=20, l=2$ and $k_v=1.8$, which is centered on 0. Bottom: distribution of the angle in radians between the Ps flight direction and the antiproton recoil for the same Ps.
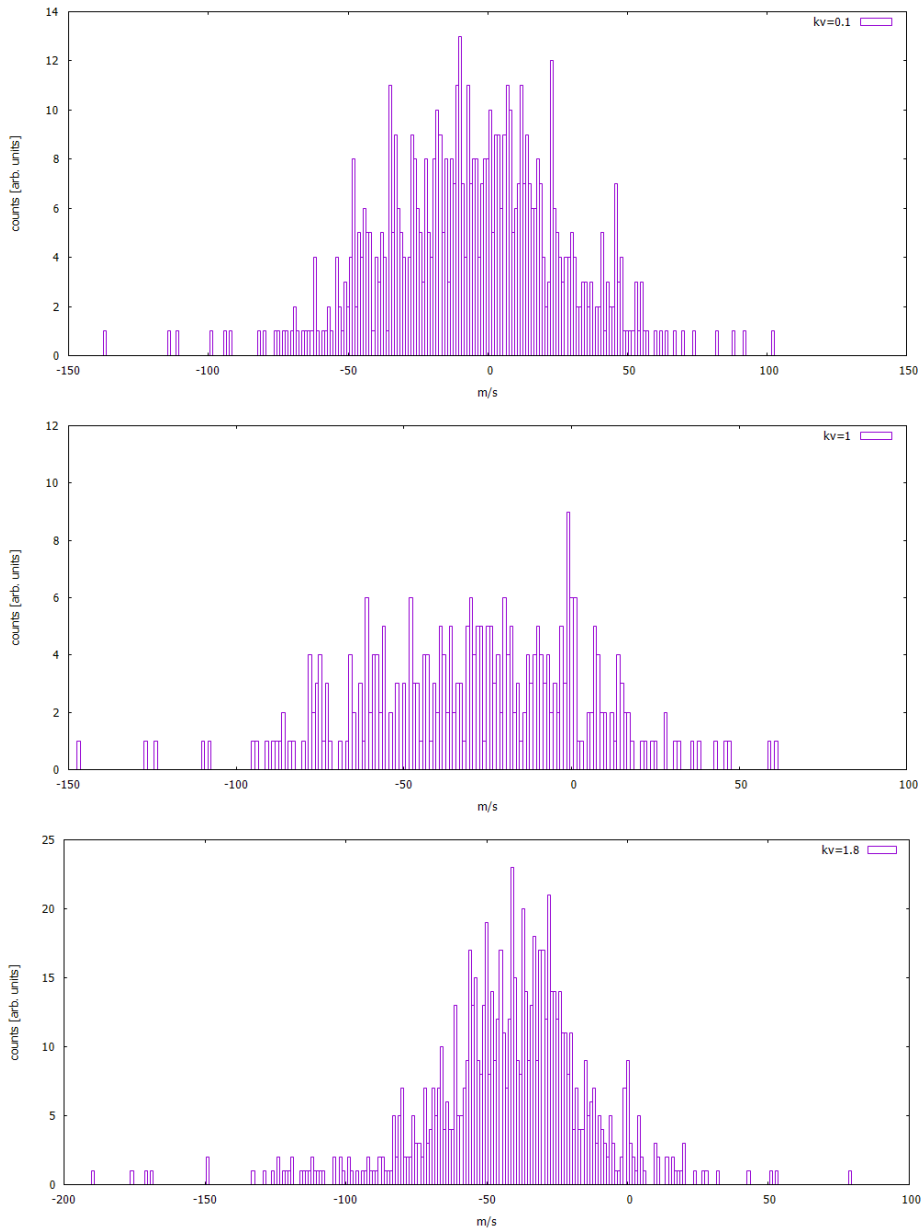
Figure 13.24: Distribution of the antihydrogen velocity in m/s along the y axis with 1T magnetic field for Ps with $n=20, l=2$ and $k_v= 0.1, 1, 1.8$ from top to bottom. One can see the peak moving to the left proportionally to the Ps velocity.
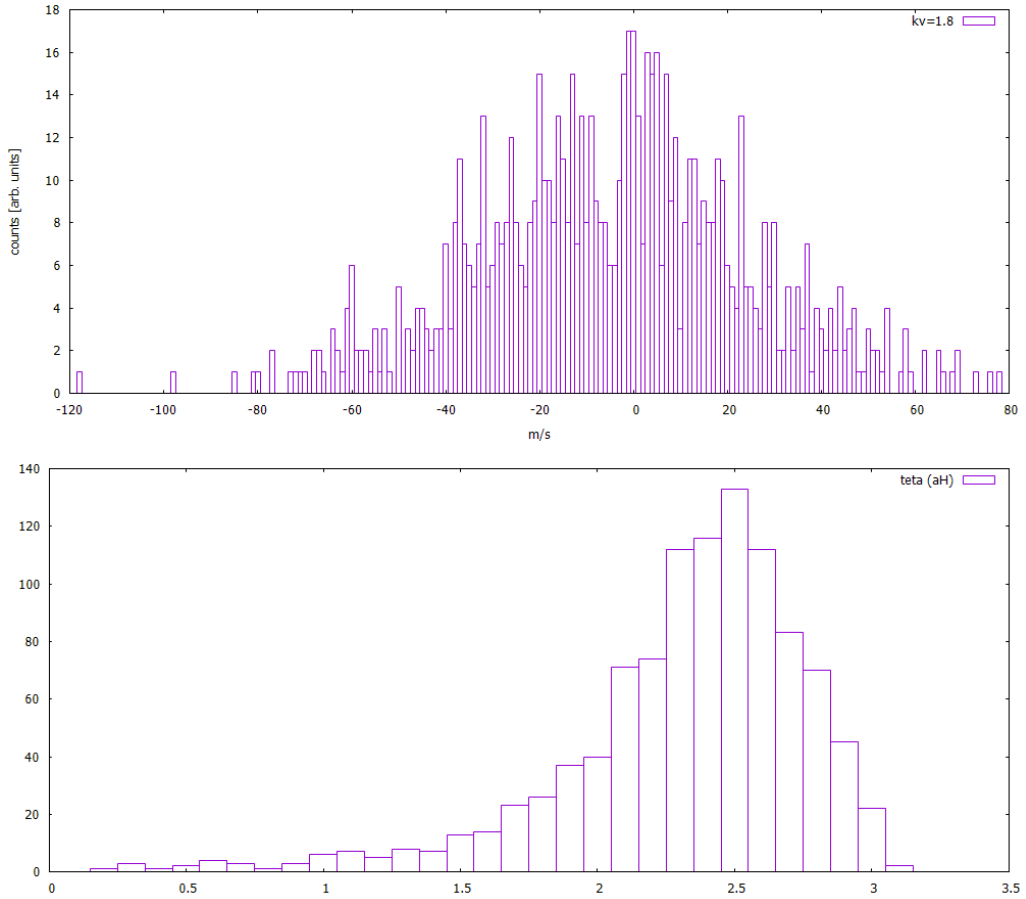
Figure 13.25: Top: distribution of the antihydrogen velocity in m/s along the transverse direction x with 1T magnetic field for Ps with $n=20,l=2$ and $k_v=1.8$, which is centered on 0. The distribution with magnetic field is wider than the one without it in Figure 13.23. Bottom: distribution of the angle in radians between the Ps flight direction and the antiproton recoil for the same Ps, which shows that the angle is smaller than the one without magnetic field Figure 13.23

.
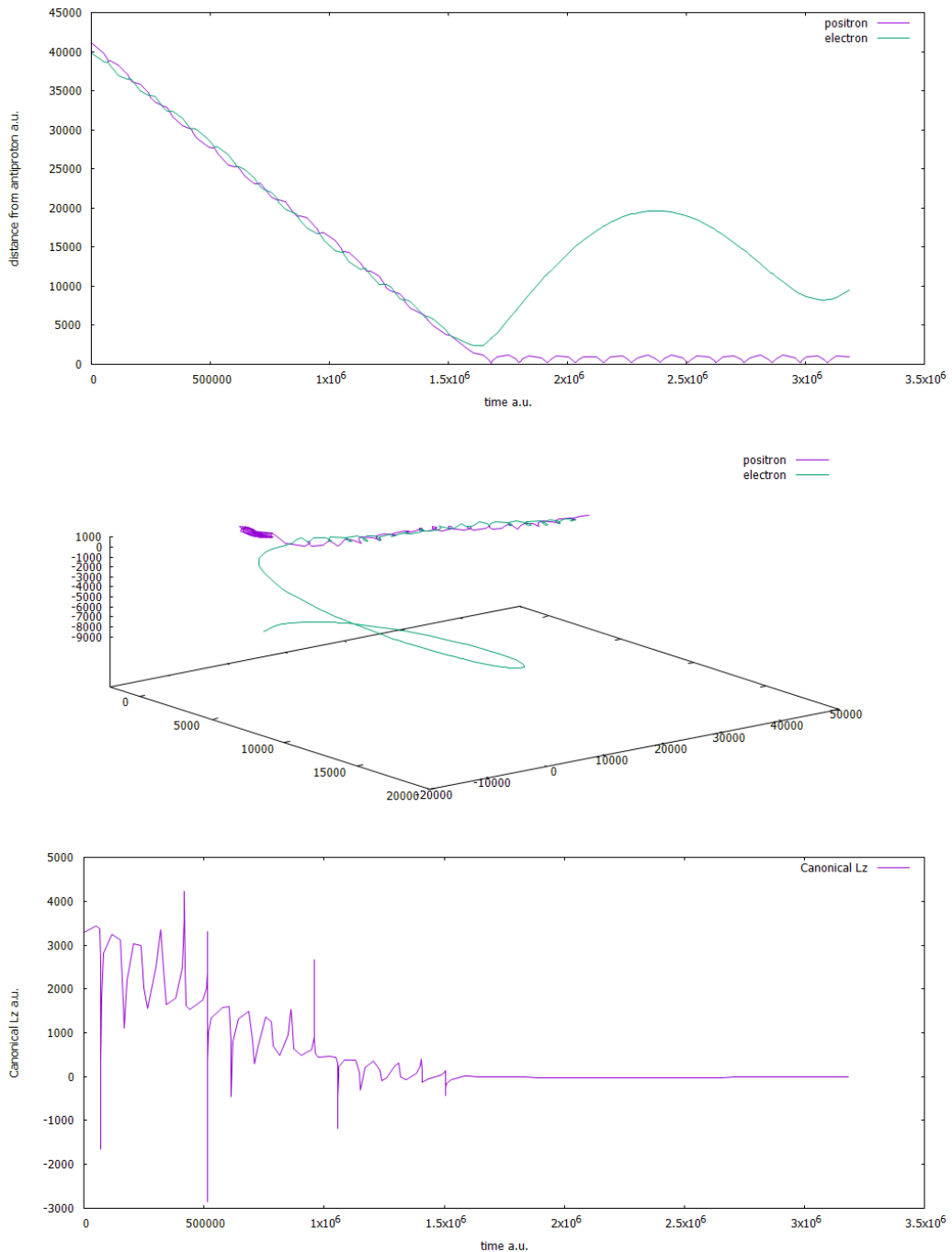
Figure 13.26: Top and middle: Ps trajectory with n=20, l=2 with a magnetic field of 1T parallel to z and perpendicular to the Ps initial direction, with $k_v = 1$, impact parameter 6376 au, initial position 40,000 au.: at the top the distance of the positron and the electron from the antiproton is plotted, in the middle the trajectory of the two particles in space, the direction of the magnetic field is vertical pointing to the top. Bottom: the plot of the canonical angular momentum with time, antihydrogen is formed around 1.6×10^6 a.u. from the beginning of the simulation, as can be seen from the plot at the top.
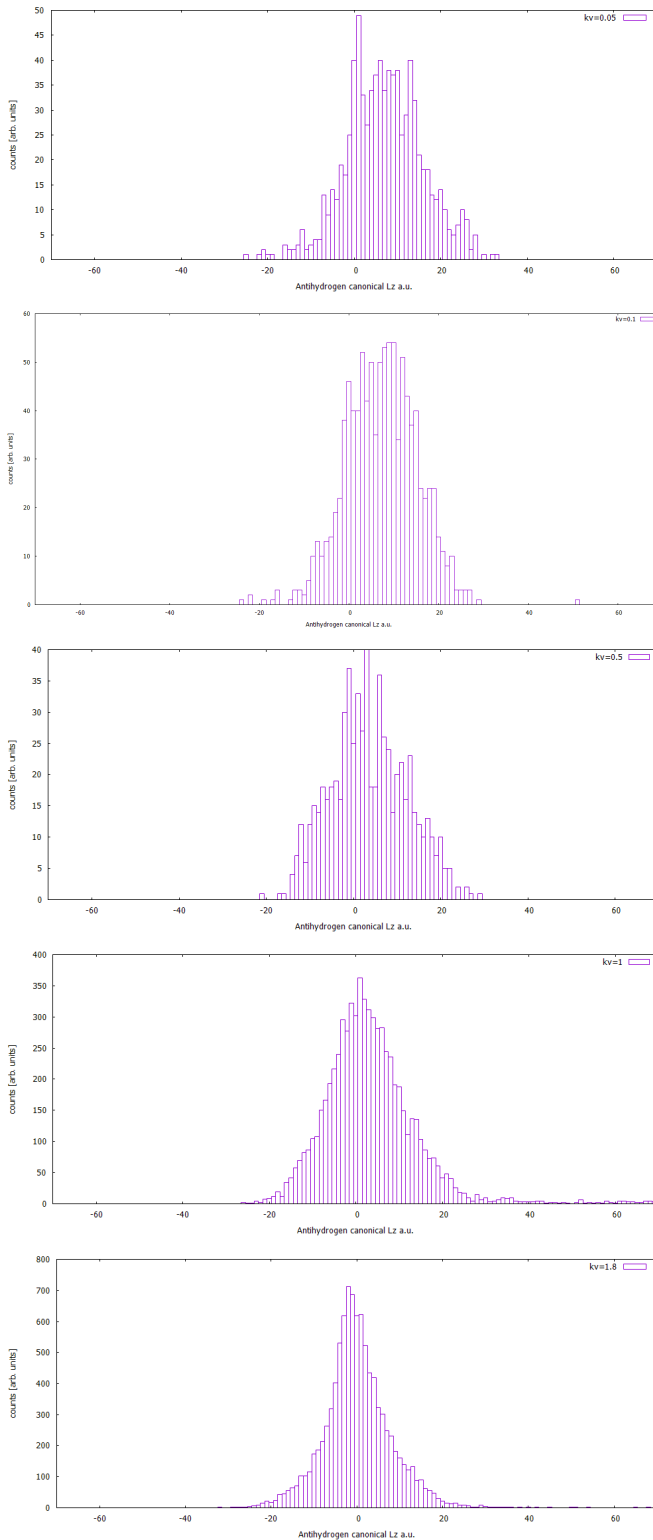
Figure 13.27: Distribution of the canonical angular momentum along the z axis $\mathcal{L}_z$ with 1T magnetic field parallel to the Ps initial trajectory for Ps with $n = 20, l = 2$ and k_v=0.05, 0.1, 0.5, 1, 1.8 from top to bottom. The distribution is asymmetric towards high values of $\mathcal{L}_z$ and the asymmetry is higher for low values of k_v.
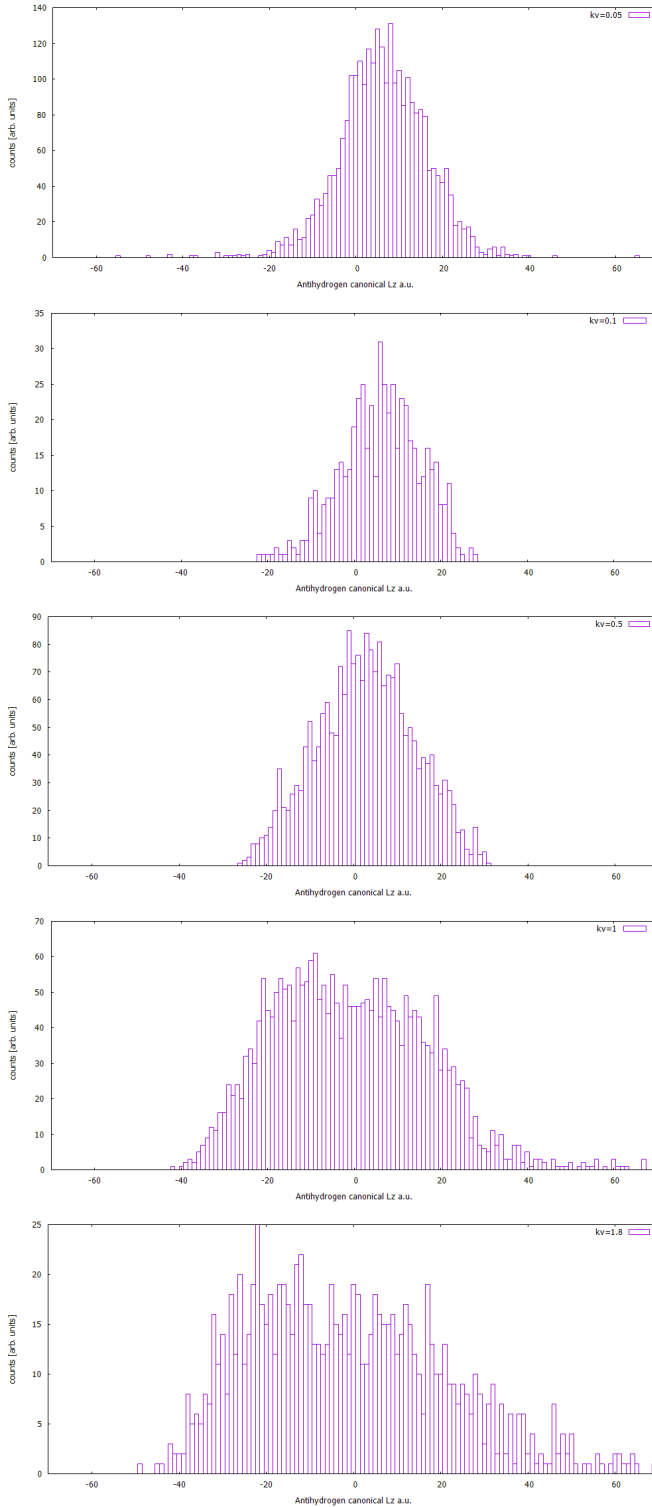
Figure 13.28: Distribution of the canonical angular momentum along the z axis $\mathcal{L}_z$ with 1T magnetic field perpendicular to the Ps initial trajectory for Ps with $n=20$, $l=2$ and $k_v = 0.05, 0.1, 0.5, 1, 1.8$ from top to bottom. The distribution is asymmetric towards high values of $\mathcal{L}_z$ and the asymmetry is higher for low values of k_v

Simulation results with the new cross sections

The cross section calculated in the previous chapter have been inserted in the Monte Carlo simulation program described in chapter 12 where the cross sections of the AEGIS proposal had been used.

The different cases described in Figure 12.5 have been analyzed producing new results which can be seen in Figure 14.1. For reflection target the cross section with the magnetic field perpendicular to Ps has been used, for transmission target the one with the magnetic field parallel to Ps because the Ps trajectories are mostly in these directions.

To make the comparison easier the table in Figure 12.5 (Aegis proposal cross sections) has been reproduced in Figure 14.2.

All the results with magnetic field are lower than with the AEGIS proposal because the cross section values are lower (see Figure 13.16).

The advantage of using the transmission target is still relevant, especially with the vertical target where 365 antihydrogen atoms are produced per burst every 200 seconds, more that one per second. This number could be enough for the gravity measurement with the 1% precision.

Layout	AntiH without magnetic field	AntiH with magnetic field	Percentage
Genova layout	4	2	50%
Transverse thermalisation at 145K	18	12	66%
Transverse thermalisation at 4K	75	37	49%
Transmission target with random emission	31	8	26%
Transmission target with normal emission	150	34	23%
Vertical transmission target with normal emission	1833	364	20%

Figure 14.1: Simulation results with the new cross sections. The percentage is the ratio between the number of antihydrogen atoms with magnetic field and without magnetic field.

Layout	AntiH without magnetic field	AntiH with magnetic field	Percentage
Genova layout	4	4	100%
Transverse thermalisation at 145K	28	12	43%
Transverse thermalisation at 4K	110	38	35%
Transmission target with random emission	17	17	100%
Transmission target with normal emission	83	70	84%
Vertical transmission target with normal emission	1105	480	43%

Figure 14.2: Simulation results with the AEGIS proposal cross sections. The percentage is the ratio between the number of antihydrogen atoms with magnetic field and without magnetic field.

Conclusions

It is expected that in 2018 the AEGIS experiment will produce the first antihydrogen atoms with the reflection target configuration.

It will then be possible to compare the results of my simulations with the experimental data and evaluate whether the number of antihydrogen atoms obtained may be sufficient to test their gravity acceleration with the moiré interferometer, with the 1% precision foreseen by the Aegis proposal.

In 2018 it is expected that a new self-standing transmission target [78] will be tested at CERN and the results compared with the carbon-supported one, studied in reference [76]. This type of target could produce more Ps and less electrons and positrons that would disturb the antiproton cloud.

According to the result of this test the collaboration will have to decide whether to use in 2018 the reflection target or the transmission one to measure gravity.

Another important topic worth studying that can influence the number of antihydrogen atoms produced by the reflection target is the possible transversal thermalisation of Ps exiting the pores. According to R. Caravita the tests in the positronium chamber seem in favor of this possibility. According to my simulations a transversal thermalization at 4K produces 10 times the antihydrogen atoms than with no thermalization, around 37 atoms per shot, which takes place every 360 seconds.

This number could increase if the number of accumulated antiprotons is higher than 10^5 thanks to a better accumulation process. The latest measures is of 3.5×10^5 antiprotons. As the number of antihydrogen atoms is proportional to the antiprotons density, the number of atoms of my simulations should be multiplied by 3.5.

Therefore, it is clear that my simulations constitute a useful benchmark to compare with the experimental results, and to test various aspects of the complex Aegis experiment.

Recently a new Monte Carlo simulation was performed which took into account the actual distance between the center of the target and the center of the antiproton cloud, 1.31 cm instead of 1.53 cm, the increased number of antiprotons, 3.5×10^5 and the measured dimensions of the antiproton cloud, an ellipsoid with radius 2 mm and half-lengths in the range of 0.5-1.1 mm. The number of antihydrogen atoms should be 8 with an optimal delay time of the laser beam of 85 ns from the beginning of the positron beam on the target, which was 38 ns long. The laser beam length was 1 ns. The result heavily depends on the delay time, so that the laser can excite slow Ps which produce more antihydrogen. The result has been confirmed by a calculation by S. Mariazzi of AEGIS Collaboration.

A new Monte Carlo simulation is being written by Nicola Zurlo which takes into account the exact geometry of the central part of the experiment based on the CAD design. It will be interesting to compare the results of my simulation with the new one.

A recent proposal is to laser cool the Ps that exit from the target in order to increase the cross section of the charge exchange reaction that produces antihydrogen thanks to the lower velocity. A test could be made in the positronium chamber and new simulations with the reduced velocity performed.

A recent article by A.S. Kadyrov et al. [89] has applied the quantum CCC method to the charge exchange process 2.1 which creates antihydrogen in the AEGIS experiment for the principal quantum number n of Ps between 4 and 5, but without considering the presence of the magnetic field.

Contrary to expectation from earlier work [73] for n=3 the cross-section increases only slightly for low energies. It seems that the cross-section grows as n^2 instead of n^4 as in CTMC calculations due to quantum-mechanical effects governed by the Wigner threshold law [90]. But it is possible that for higher n and for Ps De Broglie wavelength small compared to its size, the classical n^4 scaling would be restored.

Kadyrov's results could limit the advantage of reducing the Ps velocity with laser cooling for low n values because the Ps wavelength would become larger than the Ps size.

Anyway, the AEGIS experiment deals with charge exchange reactions with Ps excited to Rydberg levels in presence of magnetic field, hence in a regime well described by a classical framework, and we are confident in the results here presented.

Appendices

Description of the Monte Carlo program

The main program is written in Fortran using the technique of structured programming. The routine for the magnetic field simulation is written in C++ to interface with the ODEINT library.

The same program has been used for all the simulations described in the thesis except the one related to the positronium chamber, for which the program has been heavily modified, and the calculation of the cross-section for which a new program has been written in C++.

The program is called psimul.f and has around 3200 lines of code.

The value of a set of parameters allows to choose the simulation to perform, the number of Ps to simulate and the geometrical and physical data of the experimental apparatus.

Initially the position of the center of the laser beam and of a possible second and third laser beam are computed based on the position and orientation of the target.

The cloud of Ps is represented by a set of vectors which have the dimension equal to the number of Ps one wants to simulate. The vectors contain time of creation from the target, initial position, direction and velocity, current position and velocity, state, level of excitation, mean life, reflection points on the reflectors, whether the trajectory of the Ps crosses the antiprotons cloud.

At the beginning of the simulation the vectors are filled with the initial values of the Ps, randomized according to the chosen statistical distributions of time, position, direction, velocity, mean life. The trajectory is calculated with a direct flight or taking into account the reflectors to decide whether the Ps will cross the antiprotons cloud. If there is an electric field which bends the trajectory this calculation is omitted. The cloud is approximated to a cylinder with the same volume.

The Ps cloud is followed with an iteration over steps of 1 ns until all the Ps which cross the cloud have arrived to it or are decayed or ionized. One third of the Ps have a lifetime of 7 ns due to magnetic quenching, two third a lifetime of 142 ns. The excited Ps have a lifetime of 16500 ns for the level with quantum numbers n=25, l=2.

The laser beam is shot after a chosen number of ns after the beginning of the simulation, when Ps start to exit from the target. The excitation of every Ps is determined based on its position and the gaussian shape and efficiency of the laser beam. If the Ps is excited its mean life is increased. The possibility of decay is computed every ns.

The Ps can be ionized by nearby particles according to the Robicheaux formula 4.1.

If there is an electric field the trajectory of excited Ps is computed according to the k quantum number, which is randomized between $n - 1$ and $-n + 1$. The distribution of the electric field in space is contained in a file obtained from a Simion program.

When a Ps arrives to the antiprotons cloud the length of the trajectory in the cloud is obtained and the number of antihydrogen atoms is computed based on the cross-section for its velocity, the density of antiprotons ans the length of the trajectory.

In the presence of a 1T magnetic field two cross-sections are considered for parallel and perpendicular direction of the Ps in relation to the magnetic field.

If there is a magnetic field the programs calls a routine written in C++ at the moment of laser excitation. The routine computes with Runge Kutta method 5 with adaptive step the deviation in direction of the Ps due to the magnetic field and the final distance between the electron and the positron after a tenth of ns according to Schmelcher [67]. Initial positions and velocities of the electron and the positron are randomized.

It has been seen that this time is sufficient to have precise data. If the distance is larger than 3000 a.u. the Ps is considered ionized and is abandoned.

Description of the CTMC program

The program is called ctmcnew.cpp, is written in C++ and has around 1200 lines of code.

It simulates the charge exchange process 2.1 for a parametrical number of Ps. Each Ps is directed along the Y axis towards an antiproton which is initially at rest at the origin of axes. The distance from the antiproton, the velocity, the maximum impact parameters, the principal quantum number are parametric, the impact parameter is randomized between 0 and its maximum. The azimutal quantum number can be parametric or randomized to compute the cross-section for all initial l.

The initial elliptical orbit of e+ and e- is determined by the quantum numbers n and l. The initial position on the orbit is randomized with a uniform distribution on the ellipse or with a rotation of the particles on the orbit for a random time from a fixed initial position. The two choices give the same result. The direction of motion is also randomized.

The equations of motions of e+ and e- are integrated with the Runge Kutta 5 adaptive step. The antiproton can be fixed or can move. They consider the Coulomb forces between the three particles and the magnetic field, which can be parallel or perpendicular to the Ps direction and has a parametric strength.

In case of magnetic field the program can simulate the method used by the Genova group and randomize an impact parameter with the Ps near the antiproton. The Ps then goes back to a desired distance from the antiproton not considering the electric interaction with it and with inverted velocity and magnetic field and then it's motion towards the antiproton is simulated completely.

Antihydrogen is formed if the sum of the energies of the antiproton and the positron is negative and the sum of the energies of the electron and the positron is positive.

The conservation of energy is tested. The integration time is parametric in relation to the time taken by the Ps to arrive near the antiproton.

The final n and l of the antihydrogen atom are computed as well as its velocity and a file prepared for statistical reasons. The total cross-section and the statistical error are computed based on the generated ps, the antihydrogen atoms and the maximum impact parameter.

The program can be run also on one Ps with specific initial conditions for test reasons. In this case a file is produced with the trajectories of e+ and e-.

Bibliography

[1] P. Perez et al., *Hyperfine Interactions* **233**, 21-27 (2015).

[2] M.M. Nieto and T. Goldman, *Phys. Rep.* **205**, 5 221-281 (1982).

[3] C. Will, *Theory and experiment in gravitational physics*, (Cambridge University Press, Cambridge, 1993).

[4] J.C. Maxwell, *Phil. Trans. R. Soc. London* **155**, 492-493 (1865).

[5] M.M. Nieto, T. Goldman and R.J. Hughes, *Aust. Phys.* **25**, 259-262 (1988).

[6] J. Scherk, *La Recherche* **8**, 878-880 (1977).

[7] J. Scherk, *Phys. Lett. B* **88**, 265-267 (1979).

[8] J. Scherk, *Supergravity*, 43-51 (North Holland, Amsterdam, 1979).

[9] J. Scherk, *Unification of the Fundamental Particle Interactions*, 381-409 (Plenum, New York, 1980).

[10] K.I. Macrae and R.J. Riegert, *Nucl. Phys. B* **244**, 513-522 (1984).

[11] T. Goldman, R.J. Hughes and M.M. Nieto, *Proc. First Workshop on Antimatter Physics at Low Energy*, 185-197 (Fermilab, Batavia, Il. 1986).

[12] R.J. Hughes, T. Goldman and M.M. Nieto, *Fundamental Symmetries*, 185-197 (Plenum, New York, 1987).

[13] S. Bellucci and V. Faraoni, *Phys. Rev. D* **49**, 2922 (1994).

[14] J.D. Bekenstein, *Phys. Rev. D* **70**, 083509 (2004); erratum *Phys. Rev. D* **71**, 069901 (2005)

[15] J. W. Moffat, JCAP 0603 (2006) 004, gr-qc/0506021.

[16] D. Mota and D. Shaw, *Phys. Rev. D* **75**, 063501 (2007).

[17] J. Barrow and R. Scherrer, *Phys. Rev. D* **70**, 103515 (2004).

[18] C. Alvarez and R. Mann, *Phys. Rev. D* **55**, 1732 (1997).

[19] M.M. Nieto, T. Goldman and R.J. Hughes, *Phys. Rev. D* **36**, 3684-3687 (1987).

[20] F.S. Witteborn and W.M.Fairbank, *Phys. Rev. Letters* **19**, 1049-1052 (1967).

[21] A.J. Dessler, F.C. Michel, H.E. Rorschach and G.T. Trammel, *Phys. Rev.* **168**, 737-743 (1968).

[22] W.M. Fairbanks, *Proc. XXIIIrd Rencontre de Moriond*, 629-644 (Editions Frontières, Gif-Sur-Yvette, 1988).

[23] T. Goldman and M.M. Nieto, *Phys. Lett. B* **112**, 437-440 (1982).

[24] N. Beverini et al, *Los Alamos Report LA-UR-86-260*, CERN experiment PS-200, (1986).

[25] The ALPHA Collaboration and A.E. Charman, *Nature Communications* **2787**, (2013).

[26] P. Morrison, *Am. J. Phys.* **26**, 358-368 (1958).

[27] L.I. Schiff, *Phys. Rev. Lett.* **1**, 254-255 (1958).

[28] L.I. Schiff, *Proc. Natl. Acad. Sci.* **45**, 69-80 (1959).

[29] M. L. Good, *Phys. Rev.* **121**, 311-313 (1961).

[30] G. Drobychev, et al, *CERN-SPSC-2007017*, (2007).

[31] M. Doser et al, *Class. Quantum Grav.* **29**, (2012) 184009.

[32] M. Hori and J. Walz, *Progress in Particle and Nuclear Physics* **72**, 206-253 (2013).

[33] S. Gerber et al, *High Sensitivity Experiments Beyond the Standard Model-HISEBSM*, (2016).

[34] P. Yzombard, et al, *Phys. Rev. Lett.* **114**, 213001 (2015).

[35] R.G. Greaves and C.M. Surko, *Phys. Plasmas* **4**, 1528 (1997).

[36] C. Canali et al, *Europ. Phys. Journal D* **65**, 499 (2011).

[37] D.W. Gidley et al, *Annu. Rev. Mater. Res.* **36**, 49 (2006).

[38] S. Mariazzi,A. Salemi and R. Brusa *Phys. Rev. B* **78**, 085428 (2008).

[39] P. Crivelli et al *Phys. Rev. A* **81**, 052703 (2010).

[40] S. Mariazzi, P. Bettiotti and R. Brusa *Phys. Rev. Lett.* **104**, 243401 (2010).

[41] R. Ferragut et al, *J. Phys.: Conf. Ser.* **225**, 012007 (2010).

[42] S. Mariazzi, P. Bettotti, S. Larcheri, L. Toniutti and R.S. Brusa *Phys. Rev. B* **81**, 235418 (2010).

[43] S. Cialdi et al, *Nucl. Instrum. Methods Phys. Res. B* **269**, 1527 (2011).

[44] F. Castelli, I. Boscolo, S. Cialdi, M.G. Giammarchi and D. Comparat, *Phys. Rev. A* **78**, 052512 (2008).

[45] S. Mariazzi, L. Toniutti, N. Patel and R. Brusa, *Appl. Surf. Sci.* **255**, 191–3 (2008).

[46] E. Vliegen and F. Merkt, *Phys. Rev. Lett.* **97**, 033002 (2006).

[47] E. Vliegen, P.A. Limacher and F. Merkt, *Eur. Phys. J. D* **38**, 1623-1636 (2005).

[48] E. Vliegen and F. Merkt, *Journal of Physics B* **39**, L241-L247 (2006).

[49] M.K. Oberthaler et al, *Phys. Rev. A* **54**, 3165 (1996).

[50] S. Aghion et al. (AEGIS Collaboration), *JINST* **8**, P08013 (2013).

[51] S. Aghion et al. (AEGIS Collaboration), *JINST* **9**, P06020 (2014).

[52] M. Sacerdoti, *AEgIS-INT report*, **2010-01**, (March 2, 2010).

[53] M. Giammarchi, M. Sacerdoti, Z. Mazzotta, *AEgIS-INT report*, **2013-02**, (July 1, 2013).

[54] M. Sacerdoti, *AEgIS-INT report*, **2014-01**, (September 18, 2014).

[55] M. Sacerdoti, *AEgIS-INT report*, **2015-01**, (January 29, 2015).

[56] M. Sacerdoti, *AEgIS-INT report*, **2015-03**, (June 12, 2015).

[57] M. Sacerdoti, *AEgIS-INT report*, **2015-04**, (July 14, 2015).

[58] M. Sacerdoti, *AEgIS-INT report*, **2015-05**, (December 10, 2015).

[59] F. Robicheaux, *J. Phys. B: At. Mol. Opt. Phys.* **38**, S333-S342 (2005).

[60] F. Villa, "Laser system for Positronium excitation to Rydberg levels for Aegis experiment", *Phd Thesis at the University of Milan*, p. 76, fig. 3.2 (2010/11).

[61] S. Aghion et al. (AEGIS Collaboration), *Phys. Rev. A* **94**, 012507 (2016).

[62] Genova group, *Aegis-INT report*, **2015-02**, (March 10, 2015)

[63] S. Aghion, "Study of thin films and mesoporous materials by means of Positron Annihilation Spectroscopy for applied and fundamental Physics", *Phd Thesis at Politecnico di Milano*, fig. 4.27 (2016/2017).

[64] D. Cassidy et al., *Phys. Rev. A* **81**, 012715 (2010).

[65] S. L. Andersen, R. R. Johansen, J. B. Overgaard, J. K. Mortensen, K. K. Andersen, H. D. Thomsen, M. D. Lund, J. Chevallier, H. Knudsen, U. I. Uggerhoj, *Eur. Phys. J. D* **68** (5), 124 (2014).

[66] S. L. Andersen, D. B. Cassidy, J. Chevallier, B. S. Cooper, A. Deller, T. E. Wall, U. I. Uggerhoj, *Journal of Physics B: Atomic, Molecular and Optical Physics* **48** (20) 204003 (2015).

[67] P. Schmelcher, *J. Phys B* **25**, 2697-2708 (1992).

[68] J.E. Avron, I. W. Erbst and B. Simon, *Annals of Physics* **114**, 431-451 (1978).

[69] D. Krasnický, R. Caravita, C. Canali, and G. Testera, *Physical Review A* **94**, 022714 (2016).

[70] R. Abrines and I.C. Percival, *Proc. Phys. Soc.* **88**, 861 (1966).

[71] R. E. Olson, *Phys. Rev. A* **24**, 1726 (1981).

[72] R. E. Olson, in *Springer Handbook of Atomic, Molecular and Optical Physics*, edited by G.W. F. Drake (Springer Science and Business Media, New York, 2006), p. 869.

[73] A. S. Kadyrov et al., *Phys. Rev. Lett.* **114**, 183201 (2015).

[74] C. M. Rawlins et al., *Phys. Rev. A* **93**, 012709 (2015).

[75] M. L. Wall, C. S. Norton, and F. Robicheaux, *Phys. Rev. A* **72**, 052702 (2005).

[76] S. Aghion et al. (AEGIS Collaboration), *Nucl. Instr. Meth. B* **407**, 55-66 (2017).

[77] C.P. Reeve, NIST, Gaitherburg, MD, routine RDELLS, 1990

[78] C. Evans, ICNFP 2017 Conference, Crete, Greece, 2017

[79] G. Consolati, 12th conference on positron and positronium chemistry, Lublin, 2017

[80] S. Aghion et al. (AEGIS Collaboration), *Nature Comm.* **5**, 4538 (2014).

[81] E. Gibney, *Nature* **548**, 20 (2017)

[82] http://aegis.web.cern.ch/aegis/

[83] A. Kellerbauer et al. (AEGIS Collaboration), *Nucl. Instrum. Methods Phys. Res. Sect. B* **266**, 351 (2008)

[84] L. Spitzer, *Physics of fully ionized gases*, Interscience Publisher, New York (1962).

[85] L.D.Landau and E.M.Lifsic, *Kvantovaja mehanika: nereljativistskaja teorija, vol. 3 of Teoreticeskaja fizika*, 4th ed., Nauka Moskva (1989).

[86] S. Sala, F. Castelli, M. Giammarchi, S. Siccardi and S. Olivares, *Journal of Physics B* **48**, 195002 (2015).

[87] A. Rich, *Rev. Mod. Phys.* **53**, 127 (1981).

[88] A. Dupasquier, in *Proceedings of the International School of Physics Enrico Fermi, Course 83, Varenna, Italy*, edited by W. Brandt and A. Dupasquier, North-Holland, Amsterdam (1983).

[89] A.S. Kadyrov et al.,*Nature Communications* **8**, 1544 (2017)

[90] E.P. Wigner, *Phys. Rev.* **73**, 1002-1009 (1948)

List of Publications

Refereed publications

- "Antihydrogen Physics, gravitation and spectroscopy in AEgIS", R. Ferragut et al. (AEGIS Collaboration), *Can. J. Physics* **89**, (2011).

- "Exploring the WEP with a pulsed cold beam of antihydrogen", M. Doser et al. (AEGIS Collaboration), *Class. Quantum Grav.* **29**, 184009 (2012).

- "The AEGIS experiment at CERN Measuring the free fall of antihydrogen", A. Kellerbauer et al. (AEGIS Collaboration), *Hyperfine Interactions* **209**, 43–49 (2012).

- "Positron bunching and electrostatic transport system for the production and emission of dense positronium clouds into vacuum", S. Aghion et al. (AEGIS Collaboration), *Nucl. Instr. Meth.* **B362**, 86 (2015).

- "Laser excitation of the n = 3 level of positronium for antihydrogen production", S. Aghion et al. (AEGIS Collaboration), *Phys. Rev. A* **94**, 012507 (2016).

- "Measurement of antiproton annihilation on Cu, Ag and Au with emulsion films", S. Aghion et al. (AEGIS Collaboration), *Jinst* **12**, 04021 (2017).

- "Characterization of a transmission positron/positronium converter for antihydrogen production", S. Aghion et al., (AEGIS Collaboration), *Nucl. Instr. Meth. B* **407**, 55-66 (2017).

Publications in conference proceedings

- "Measuring the fall of antihydrogen: the AEgIS experiment at CERN", M. Doser et al. (AEGIS Collaboration), *Physics Procedia* **17**, 49 (2011).

- "AEGIS at CERN: Measuring antihydrogen fall", M. Giammarchi et al. (AEGIS Collaboration), In V. A. Kostelecký (ed.), *Proceedings of the Fifth Meeting on CPT and Lorentz Symmetry*, World Scientific Publishing. Singapore (2011).

- "Probing antimatter gravity – The AEGIS experiment at CERN", A. Kellerbauer et. al. (AEGIS Collaboration), *Proceedings of the 4th International Conference on New Frontiers in Physics* (ICNFP 2015)

- "Experiments with low-energy antimatter", G. Consolati et al. (AEGIS Collaboration), *EPJ Web of Conferences* **96**, 01007 (2015).

- "Testing the Weak Equivalence Principle with an antimatter beam at CERN", M. Kimura et al. (AEGIS Collaboration), *Journal of Physics Conference Series* **631**, 012047 (2015).

- "Towards a gravity measurement on cold antimatter atoms", R. Caravita et al. (AEGIS Collaboration), *Nuovo Cimento C* **39**, 237 (2016).

- "Direct detection of antiprotons with the Timepix3 in a new electrostatic selection beamline", N. Pacifico et al. (AEGIS Collaboration), *Nuclear Instruments and Methods in Physics Research* **A831** proceedings, 12 (2016).

- "The AEgIS experiment at CERN: measuring antihydrogen free-fall in earth's gravitational field to test WEP with antimatter", R. S. Brusa et al. (AEGIS Collaboration), 14th International Workshop on Slow Positron Beam Techniques & Applications, IOP Conf. Series: *Journal of Physics: Conf. "Series* **791** 012014 (2017).

- "Overview of Recent Work on Laser Excitation of Positronium for the Formation of Antihydrogen", P. Yzombard et al. (AEGIS Collaboration), Proc. 12th Int. Conf. Low Energy Antiproton Physics, *JPS Conf. Proc.* **18** 011026 (2017)

Acknowledgments

I must first thank Marco Giammarchi for having convinced me to work on the Aegis experiment and to apply for the Phd course three times despite my age and the many years passed between my thesis in 1973 and my renewed interest in Physics in 2008.

My supervisor Fabrizio Castelli has constantly supported me in the mathematical and physical calculations which I could have never completed after so many years spent in information systems for banks and has accurately revised my thesis.

Davide Trezzi, at the time Phd student, explained the experiment to me in such an enthusiastic way to make me think it was worthwhile to help Marco and the rest of the AEGIS Milan team.

Ettore Fiorini, my thesis supervisor in 1973, told me in 1975 that my abandonment of physics was a serious mistake; his opinion always remained in my mind and pushed me to start again in this field. He also helped me with a very supportive referee letter in my unfortunate application to the Phd course in 2013.

The late Mico Rollier, my supervisor when I was a summer student at Cern in 1972, helped me with my first Monte Carlo program, called Nemo, to simulate the neutrino beam of the SPS accelerator.

My wife Marjorie and my son Pierfrancesco always supported my return to Physics even if they don't understand much of this subject.

My young colleague Simone Sala has given me an invaluable help with the C++ program for the cross-section calculation.

I appreciate the fact that the Phd admission commission in 2014 and particularly the chairman Prof. Perini thought that I would not lower the quality of the Phd course of Milan University with my presence and I would not take away a place from a young researcher.

Ten years have passed since I have started again studying Physics; this part of my life has been very important to me and I thank the colleagues of the AEGIS experiment, and especially Rafael Ferragut for their support. I hope to have contributed in some way to the advance of science in this sector.

I thank Giancarlo Maero e Massimiliano Rome for the support in Simion use.

A particular thank is due to Charles P. Reeve, who has helped me to understand and use the routine RDELLS he wrote in 1990 when he was at the National Institute of Standards and Technology (NIST).

I thank CINECA help-desk for the support to my Montecarlo calculations.

I thank Andrea Zanzani for his help in all the bureaucratic procedures of the doctorate school and for being a friend in many difficult occasions.

And finally I must thank my older brother Giorgio for having told me that our father Piero, who died in 1966, said when I was young that I would be very successful in Physics in the future.